UNIVERSITÉ DE STRASBOURG

ÉCOLE DOCTORALE DE PHYSIQUE ET CHIMIE-PHYSIQUE

Institut Charles Sadron

THÈSE présentée par :

Mattia MORANDI

soutenue le : **15 Decembre 2017**

pour obtenir le grade de : **Docteur de l'université de Strasbourg**

Discipline/ Spécialité : Physique

Disruption of model membranes' phase behavior upon interaction with hydrophilic/hydrophobic molecules

THÈSE dirigée par :	
[Dr. MARQUES Carlos]	Directeur de thèse, University of Strasbourg
RAPPORTEURS :	
[Dr. DIMOVA Rumiana]	Rapporteur externe, Max-Planck Institute
[Prof. Dr. SOMMER Jens-Uwe]	Rapporteur externe, Leibniz Institute for polymer science
AUTRES MEMBRES DU JURY :	
[Prof. MELY Yves]	Examinateur interne, University of Strasbourg
[Dr. FRAGNETO Giovanna]	Examinateur externe, ILL
[Prof. Dr. VERMANT Jan]	Examinateur externe, ETH
INVITE :	
[Dr. SCHRODER André]	Invité, University of Strasbourg

"To absent friends, lost loves, old gods, and the season of mists; and may each and every one of us always give the devil his due."

Neil Gaiman, *Sandman*

Acknowledgements

First and foremost, I would like to express my gratitude to the MCube team and all the colleagues of the Institut Charles Sadron. My three years at the institute have been constantly filled with research, learning and human relationships, and I have spent a wonderful time doing what I love.

I would like to thank Carlos for being a wonderful supervisor, with a keen insight on the smallest detail. His mentorship in many aspects of soft matter physics and biophysics that I was lacking was only matched by his support on the many experimental idea I had, no matter how bizzarre.

André for giving me a deeper knowledge of the experimental part of my work, and always providing a practical side and feedback to all my idea and elucubrations, and always have time to discuss microscopy.

Fabrice for the patience during our discussion on theory and thermodynamics, and for its constant input in my experimental work via papers, ideas and knowledge.

And of course all the members of the Mcube team: Thierry, Pierre, Tatiana, Marc, Othmene, Tiago and Salvatore for being a great team and always being there to talk science or anything.

A great thank you goes to all the people I had the chance to meet at the ICS, who made for a wonderful environment: Arthur, Amer, Laure, Morgane, François, Marc, Rigoberto, Flavio, Marvin.

The rugby team of the CNRS campus, and in particular Arthur and Thierry, who made me discover and love this great sport.

The whole ITN SNAL network, a group of fantastic people who made not only for great colleagues and fellows PhD candidates, but also for great company and fun during any conference: Alex, Daniela, Anna Sofia, Shiqi, Chan Fei, Berardo and Adrien.

In particular I want to thank Monika, for helping throughout my work at ICS, performing complementary experiments and being such an invaluable friend.

Finally, I want to thank all my friends, both geographically far away and not, who have always been close to me: Gianmarco, Andrea, Laurence, Marco, Alessandro, Robert, Rita, Matteo, Simone, Eleonora, Francesco, Alessio, Gilles, Girolamo, Stefano, Francesco, Francesco, Tony, Salvatore, and all the guys from Quintet. You make me feel at home even when I am not there.

A last and important acknowledgement goes to my family, who has supported me all these years and pushed my desire to pursue a scientific career. All I have achieved so far it is also because and thanks to them.

Contents

Acknowledgements **vii**

Preface **xvii**

1 Introduction **1**

- 1.1 The plasma membrane 1
  - 1.1.1 Membrane lipids 2
  - 1.1.2 Model membranes 5
- 1.2 Phase behavior of lipid bilayer 6
  - 1.2.1 Multicomponent bilayers 7
  - 1.2.2 Cholesterol 9
- 1.3 Concluding remarks 12

2 Materials and Methods **13**

- 2.1 Differential scanning calorimetry 13
- 2.2 SANS 15
  - 2.2.1 Scattering lengh and scattering lengh density 17
    - Contrast variation technique 18
  - 2.2.2 Data analysis 19
    - Guinier analysis 19
    - Kratky-Porod analysis 20
- 2.3 Fluorescence, microscopy and environment-sensitive fluorescent probes 20
  - 2.3.1 Microscopy 21
    - Laser scanning confocal microscope 23
  - 2.3.2 Laurdan and other environment-sensitive probes 25
    - Structure 26
    - Emission spectra 27
    - Di-4-ANEPPDHQ 30

2.4 Concluding remarks 31

3 **Polystyrene in a single component lipid bilayer** **33**
3.1 Results and discussion 34
3.1.1 Estimation of the polymer lateral distibution 35
3.1.2 SANS 37
Contrast matching 38
3.1.3 Cryo-TEM 41
3.1.4 Laurdan emission spectra 43
General polarization 44
Spectral decomposition 45
Chain length effect 46
3.1.5 DSC 48
3.1.6 GUV 52
3.2 Conclusions 54
3.3 Materials and methods 54

4 **Changes in multi-component lipid bilayers upon incorporation of polystyrene** **59**
4.1 Results and discussion 60
4.1.1 Binary mixtures 60
Laurdan emission spectra 60
GP 61
Excitation wavelength dependence 62
Domains coverage in GUVS 64
DOPC:DPPC phase diagram 65
4.1.2 Systems containing cholesterol 68
4.2 Conclusions 72
4.3 Materials and methods 73

5 **DPPC bilayers in solution of high sucrose content** **75**
5.1 Results and discussion 76
5.1.1 Laurdan emission spectra 76
5.1.2 Differential scanning calorimetry 80
5.1.3 Giant unilamellar vesicles 83
5.1.4 Thermodynamics model 85
5.2 Conclusions 89
5.3 Materials and methods 89

6 **Interaction of cholesterol grafted polymer with lipid membranes** **93**
6.1 Results and discussion 94
6.1.1 Polymer conformation at different pH conditions 94
6.1.2 GUVs formed in PPCHOL solution 95

6.2 Conclusions 98
6.3 Materials and methods 98

7 Conclusions and future outlook 101

**A Supplementary material for:
Polystyrene in a single component lipid bilayer 105**
A.1 Supplementary figures 105
A.2 SANS disk model 111
A.3 SANS lamellar model 112

**B Changes in multi-component phase diagrams
upon incorporation of polystyrene 113**
B.1 Estimation of gel domains area coverage in GUV 113
  B.1.1 Approximation A: determination of arc length 113
  B.1.2 Approximation B: determination of solid angle 114

**C Supplementary material for:
DPPC bilayers in solution of high sucrose content 117**
C.1 Derivation of thermodynamics model for sucrose-lipid interaction . . . 118
  C.1.1 Cooperativity in the lipid main transition 118
C.2 Phenomenology of the lipid main transition 119
C.3 Influence of the sucrose on the gel transition 122
  C.3.1 Connection with previous work and correspondence with the usual Ising model 124

List of Figures

1.1 A schematic of the cell plasma membrane. 2
1.2 A schematic of the lipid molecule and packing parameter. 3
1.3 Membrane lipids categories 4
1.4 Solid ordered and liquid disordered structure 6
1.5 Phase diagram of L_α-S_o lipid bilayer. 8
1.6 Morphologies of solid ordered domains 9
1.7 Structure of liquid ordered phase 10
1.8 Phase diagram of ternary system containing cholesterol 11
1.9 Example of quaternary mixture phase diagram. 11

2.1 Schematic of DSC apparatus 14
2.2 Example of DSC thermograph 14
2.3 Schematics of a SANS experimental apparatus 16
2.4 Regions of a scattering curve for lipid bilayer 19
2.5 Example of Jablonski diagram and Stokes shift. 21
2.6 Schematic diagram of an epifluorescence microscope. 22
2.7 Typical fluorescence images of lipid membranes in epifluorescence microscope. 23
2.8 Schematics of a confocal microscope apparatus. 24
2.9 Comparison between conventional and confocal microscope. 25
2.10 Laurdan - chemical structure and Jablosnki diagram. 26
2.11 Laurdan position within the bilayer and dipole moment in different phases. 26
2.12 Example of Laurdan general polarization. 28
2.13 Dependence of GP on the excitation wavelength. 29
2.14 Example of Gaussian decomposition of Laurdan. 29
2.15 Chemical structure of Di-4-ANEPPDHQ. 30
2.16 Example of confocal spectral imaging of Di-4. 31

3.1 Prjected areas of polymer in 2-D confinement 35
3.2 Schematics of the polymer distribution within the lipid bilayer 36
3.3 SANS scattering curves for h-DPPC and h-dPPC:PS liposomes in D_2O 37
3.4 Schematics of matching contrast conditions 39
3.5 SANS scattering curves for d62-DPPC and d62-dPPC:PS liposomes in lipid matched solvent 39
3.6 SANS fitting of d62-DPPC:PS in lipid matched solvent 40
3.7 Cryo-TEM images of DOPC and DOPC:PS 40:60 liposomes 41
3.8 Cryo-TEM images of mixed DOPC/DOPC:PS 40:60 liposomes 42
3.9 Bilayer intensity profiles of mixed DOPC/DOPC:PS 40:60 liposomes . 43
3.10 Laurdan emission spectra for DPPC at different polystyrene molar fractions 44
3.11 Laurdan GP plot for DPPC at different polystyrene molar fractions . . 45
3.12 Laurdan high energy band fraction for DPPC liposomes containing polystyrene 46
3.13 Dependence of GP variation over polystyrene molar fraction 47
3.14 DSC thermographs of DPPC bilayers at different polystyrene molar fractions 49
3.15 Normalized ΔH and T_m for DMPC, DPPC and DSPC 50
3.16 Dependence of the interaction parameter k on the bilayer thicknes . . . 51
3.17 DMPC and DMPC:PS GUVs at different temperatures 53
3.18 Statistics of DMPC GUVs phase separation at different polystyrene molar fractions 53

4.1 Laurdan emission spectra for DOPC:DPPC and DOPC:DPPC:PS 61
4.2 Laurdan GP plot for DOPC:DPPC containing polystyrene 62
4.3 Laurdan GP plot for DOPC:DPPC at different λ_{exc} 63
4.4 GUVs of DOPC:DPPC at different DPPC fraction with and without polystyrene 64
4.5 Comparison between experimental data points and DOPC:DPPC phase diagram 65
4.6 Comparison between theoretical DOPC:DPPC phase diagram and experimental results 67
4.7 Location of analyzed sample in the DOPC:DPPC:Chol phase diagram . 68
4.8 Distribution of the number of domains in GUVs at 1h and 36h stabilization 69
4.9 GUVs of DOPC:DPPC:Chol and DOPC:DPPC:Chol:PS after 1 h and 36 h of stabilization 70
4.10 Emission maxima of Di-4 in ternary GUVs containing polystyrene . . . 71

5.1 Comparison of Laurdan emission spectra of DPPC at 20°C and 60°C . 77
5.2 Laurdan GP plot for DPPC at different sucrose concentrations 78
5.3 DSC thermographs of DPPC bilayers at different sucrose concentrations 81

5.4 DMPC GUVs formed in water and sucrose at different temperatures . 83
5.5 Statistics of DMPC GUVs phase separation at different sucrose concentrations 84
5.6 Schematic representation of thermodynamics model 86
5.7 Comparison between experimental data and thermodynamics model . 88

6.1 Chemical structure of PPCHOL 94
6.2 Average diameter of PPCHOL over pH 95
6.3 GUVs of DOPC:DPPC in PBS and DOPC:DPPC in PPCHOL solution . 96
6.4 Variation of Di-4 emission spectra in presence of PPCHOL 97
6.5 Fitting of Di-4 emission spectra in presence of PPCHOL 97

A.1 Guinier and Kratky-Porod plots for h-DPPC and h-DPPC:PS in D_2O solvent 105
A.2 Guinier plot for d62-DPPC:PS in lipid matched solvent 106
A.3 Laurdan emission spectra for DMPC at different polystyrene molar fractions 106
A.4 Laurdan emission spectra for DSPC at different polystyrene molar fractions 107
A.5 Laurdan GP plot for DMPC at different polystyrene molar fractions . . 107
A.6 Laurdan GP plot for DSPC at different polystyrene molar fractions . . 108
A.7 Laurdan high energy band fraction for DMPC liposomes containing polystyrene 108
A.8 Laurdan high energy band fraction for DSPC liposomes containing polystyrene 109
A.9 GP values at different polystyrene content in gel and fluid phase 109
A.10 DSC thermographs of DMPC bilayers at different molar fractions of polystyrene 110
A.11 DSC thermographs of DSPC bilayers at different molar fractions of polystyrene 110

B.1 Arc length approximation for area coverage estimation 114
B.2 Solid angle approximation for area coverage estimation 115

C.1 Laurdan emission spectra for DPPC at different sucrose concentrations 117
C.2 Enthalpy variation with temperature at increasing σ 125
C.3 Resulting enthalpy change vs $1-\sigma$ 125
C.4 Variation of the apparent T_m 125

List of Tables

2.1 Calculated scattering length densities 18

3.1 Calculated polystyrene area coverage for extended and coiled conformations. Dotted line represent crossing point to overlapping chains. . 36
3.2 Bilayer structural parameters for h-DPPC and h-DPPC:PS in D_2O . . . 38
3.3 Calculated ΔH, T_m and $T_{1/2}$ for DPPC with increasing molar fractions of polystyrene. 49

4.1 Summary of S_o area coverage for DOPC:DPPC GUVs at different composition. Each value represents average and standard deviation of two separate samples of 40 vesicles each. 66
4.2 Summary of average number of domains for ternary GUVs composed of DOPC:DPPC:Chol and DOPC:DPPC:Chol:PS. Each value represents average and standard deviation of two separate samples of 70 vesicles each. 69
4.3 Emission maxima of Di-4 in ternary lipid membrane and ternary lipid membranes containing cholesterol. Each value represents average and standard deviation of two separate samples of 70 vesicles each. . . 71

5.1 Summary of DSC results for DPPC liposomes in sucrose solution . . . 82

A.1 Calculated ΔH, T_m and $T_{1/2}$ for DMPC with increasing molar fractions of polystyrene. 111
A.2 Calculated ΔH, T_m and $T_{1/2}$ for DSPC with increasing molar fractions of polystyrene. 111

List of Abbreviations

DOPC = 1,2-dioleoyl-sn-glycero-3-phosphocholine
DMPC = 1,2-Dimyristoyl-sn-glycero-3-phosphocholine
DPPC = 1,2-dipalmitoyl-sn-glycero-3-phosphocholine
DSPC = 1,2-Distearoyl-sn-glycero-3-phosphocholine
d62-DPPC = deuterated 1,2-dipalmitoyl-sn-glycero-3-phosphocholine
Chol = Cholesterol
PS = polystyrene
Laurdan = 6-Dodecanoyl-2-Dimethylaminonaphthalene
DiI = 1,1′-dioctadecyl-3,3,3′,3′-tetramethylindocarbocyanine
SANS = Small angle neutron scattering
DSC = Differential scanning calorimetry
GP = general polarization
Cryo-TEM = Cryo-transmission electron microscopy
LSCM = Laser scanning confocal microscopy
PLP = Poly (L-lysine isophthalamide)
PPCHOL = Cholesterol grafted PLP

Preface

The complexity of the cellular membrane has motivated the development of minimal model systems to investigate the role of lipids in cellular mechanisms. Over the years the role of phospholipids has been reevaluated by the scientific community as studies unraveled their crucial role in membrane signalling and functionality. In particular the phase behavior of lipid bilayers has been extensively investigated and allowed to understand the significance of composition and cholesterol in modulating membrane proteins activity and membrane fluidity. The hypothesis of membrane "rafts", domains with laterally different composition and properties, also came to prominence as these studies progressed. Therefore, the study of the effects of a molecule or nanobject on the phase behavior of lipid model membranes is significant in understanding the interplay between interactions and behaviors, and in assessing any possible hazardous effects on biological membranes.

This thesis is the result of a three year project conducted at the Institut Charles Sadron (ICS) in Strasbourg, France, under the supervision of Dr. Carlos Marques and Dr. André Schroder, as a part of the european funded Initial Training Network Smart Nanoobjects Altering the Lipid bilayer (SNAL). The aim of the ITN consortium was to understand and investigate at different levels the interaction between nanoobjects and lipid membranes, with the aim of developing better drug delivery systems, by studying from the theoretical and experimental point of views both model and biological systems. The network developed by the ITN allowed fnot only for a fruitful collaboration and scientific discussion among members but as well for the participation in conferences and workshops to divulgate the results.

At ICS, the interaction between ITN members was also of great benefit for this work, as for instance for the joint work on Cryo-TEM and neutron scattering developed with Monika Kluzek and Marc Schmutz for the elucidation of membrane polystyrene interactions, or for the contribution and theoretical support provided by Fabrice Thalmann for the chapter on membrane sucrose interaction, and by Jean Wolff for the binary phase diagrams of membranes containing polystyrene.

The manuscript falls in the field of membrane biophysics, and focuses on the alterations of the phase behavior of lipid bilayers induced by small molecules, and on the role of the different degrees of hydrophobicity/hydrophilicity on the interplay taking place.

Chapter 1 is an introduction to the lipid membrane and its physical-chemical properties, and to the changes in its phase behavior depending on composition and external factors.

In **Chapter 2** a description of the techniques employed in the thesis is presented, with particular focus on data analysis and presentation of characteristic fluorescent probes sensitive to their surroundings.

Chapter 3 focuses on the changes in model membranes composed of unsaturated lipids upon incorporation of polystyrene oligomers.

Chapter 4 continues the investigation of polystyrene assessing its effects on more biologically relevant membranes, i.e. membrane displaying phase separation or containing cholesterol.

Chapter 5 is devoted to the effects of high concentration of sucrose on the phase transition of DPPC bilayers, motivated by the relevance of sugar in cryo- and biopreservation. The work is the result of a two months internship programme with a third year Bachelor Degree student, Matthieu Sommer, who performed part of the experiments under supervision.

Chapter 6 presents the preliminary results obtained in studying the effects of a cholesterol grafted amphiphilic polymer on phase separated lipid membranes. The polymer, synthesized and provided by the ITN SNAL member Alex Chen from the University of Cambridge, was developed as a possible lipid altering agent and provided an interesting and novel idea to pursue.

Finally, **Chapter 7** summarises the results obtained and provides future directions to pursue based on the experimental results.

Mattia Morandi, November 2017

Resumé de these en français

Introduction

La complexité de la membrane cellulaire a motivé le développement de systèmes modèles minimaux pour étudier le rôle des lipides dans les mécanismes cellulaires. Au fil des années, le rôle des phospholipides a été réévalué par la communauté scientifique alors que les études ont révélé leur rôle crucial dans la signalisation membranaire et la fonctionnalité. En particulier, le comportement en phase des bicouches lipidiques a été largement étudié et permis de comprendre l'importance de la composition et du cholestérol dans la modulation de l'activité des protéines membranaires et de la fluidité de la membrane. L'hypothèse de «radeaux» membranaires, domaines avec une composition et des propriétés latéralement différentes, est également apparue au fur et à mesure que ces études progressaient. Par conséquent, l'étude des effets d'une molécule ou d'un nanobjet sur le comportement de phase des membranes modèles lipidiques est significative pour comprendre l'interaction entre les interactions et les comportements, et pour évaluer les éventuels effets dangereux sur les membranes biologiques.

Accumulation des oligomères de polystyrene dans la bicouche lipidique

La quantité croissante de plastique présente dans les eaux océaniques est devenue un problème majeur ces dernières années, avec des préoccupations croissantes concernant les effets potentiellement dangereux qu'elle peut avoir sur les systèmes vivants. La production annuelle de plastique a atteint près de 300 millions de tonnes par an, dont on estime que 5 à 13 millions de tonnes atteindraient les eaux océaniques par différents moyens. Bien qu'initialement présent en grande taille, des facteurs environnementaux externes tels que la température, le rayonnement oxydant et la dégradation bactérienne peuvent réduire le plastique en fragments micrométriques et nanométriques. Les objets de cette échelle peuvent facilement entrer dans la chaîne alimentaire par digestion et il y a de plus en plus de preuves de micro-objets en plastique trouvés dans les formes de vie marine.

La présence de nano-objets n'a pas encore été signalée, mais le manque de preuves peut être associé à des difficultés à détecter de tels objets plutôt qu'à leur absence. Outre la dégradation plastique, des particules de polymère de taille nanométrique sont également produites industriellement pour des applications spécifiques de recherche et de technologie, telles que l'imagerie, la détection et la préparation de nanocomposites. La présence de plastiques nanométriques dans les laboratoires de recherche, l'industrie et l'environnement soulève des questions sur leur toxicité potentielle.

La membrane cellulaire est la première barrière rencontrée par n'importe quel corps étranger entrant dans un organisme, et est donc le principal candidat d'investigation dans l'évaluation de la toxicité possible des nanoparticules de plastique. En particulier, le comportement de la phase membranaire joue un rôle crucial dans le maintien de la fonctionnalité cellulaire, et même de légères modifications des propriétés de la membrane peuvent entraîner une menace potentielle pour l'organisme.

Dans ce travail, nous effectuons une étude systématique sur les effets des oligomères de polystyrène (M_n = 500 Da) sur la transition de phase des lipides non-saturés. Nous avons étudié les changements de transition en utilisant la diffusion de neutrons aux petits angles, la calorimétrie différentiel et les spectres de fluorescence de Laurdan pour extraire des informations sur la structure et la thermodynamique. De plus, nous avons directement visualisé les changements sur la membrane à différentes longueurs d'échelle en utilisant la microscopie Cryo-TEM et la microscopie a epifluorescence.

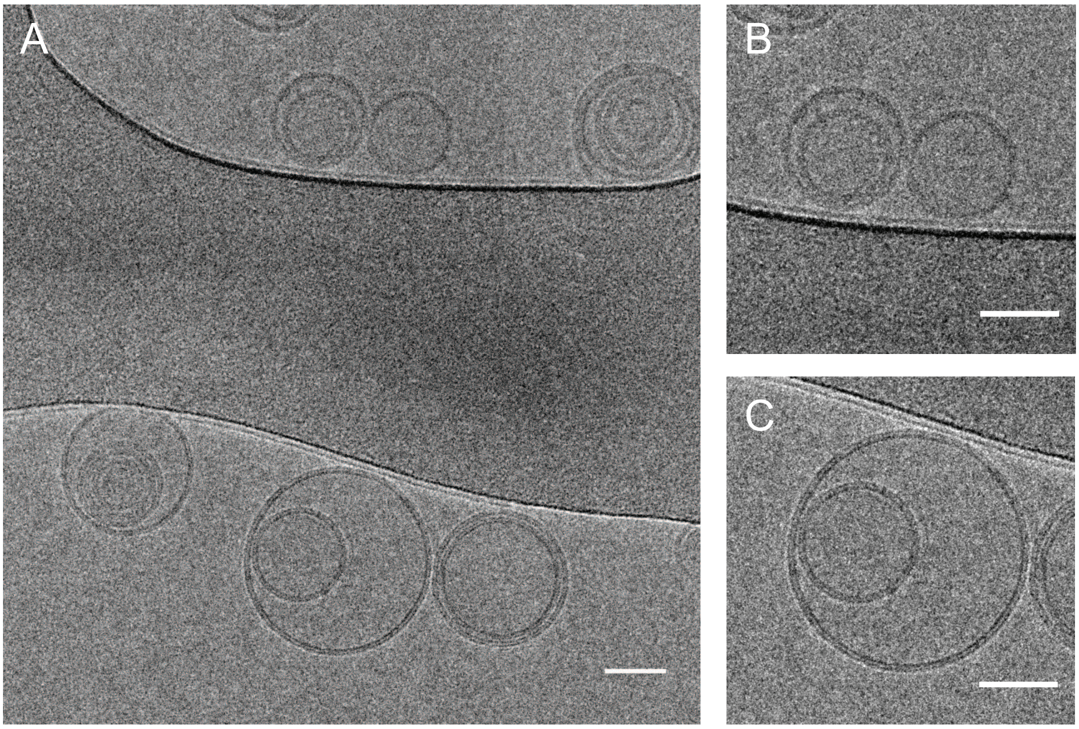

FIGURE 1: (A) Cryo-TEM image d'un échantillon mixte de DOPC / DOPC: PS 40:60, montrant la coexistence de vésicule avec bicouche bien contrastée et vésicules avec flou contraste. (B) Détail du liposome affichant un contraste inférieur. (C) Détail de liposome affichant un contraste élevé. Barre d'échelle 50 nm.

Nos résultats indiquent que le polystyrène de faible poids moléculaire incorporé dans la région hydrophobe d'une bicouche lipidique a une distribution différente entre les deux phases. Pour la phase S_o, le polystyrène est séparé dans le plan médian de la membrane, comme indiqué par les courbes de diffusion SANS et les spectres d'émission de Laurdan. Ce confinement est dû à la mauvaise solubilité du polymère à la hauteur des chaînes alkyles qui sont fortement structurées. À mesure que la bicouche fond à la phase L_α, la distribution du polymère devient plus uniforme, comme sondé par l'imagerie Cryo-TEM, et s'intercale entre les chaînes alkyle vers l'interface de l'eau. La forte variation de la GP dans la phase fluide, ainsi que la dépendance linéaire de l'émission de Laurdan et de l'enthalpie de transition avec les changements de la teneur en polymère soutiennent fortement ce scénario.

On a également trouvé que l'incorporation du polymère modifiait la transition principale gel-liquide et l'ordre lipidique de la membrane dans la phase fluide, comme indiqué par les spectres d'émission de Laurdan. Ces changements peuvent etre attribues de façon générale a une interaction hydrophobe / membrane dans laquelle le polymère se répartit préférentiellement dans la phase liquide, réduisant ainsi la température de fusion de la bicouche lipidique. Les différences de garnissage entre la membrane sans polymère et une membrane contenant le polystyrène peuvent être expliquées par les changements de la contribution enthalpique dans la transition gel-liquide.

Nos résultats sont en bon accord avec les données précédemment rapportées concernant la répartition préférentielle du polystyrène et la distribution du polymère dans la bicouche lipidique fluide, et avec les tendances thermodynamiques observées pour d'autres composés hydrophobes. L'incorporation du polymère a montré une nette diminution de la contribution enthalpique, comme observé par DSC, couplée à une petite variation de la température de fusion. L'analyse des spectres d'émission de Laurdan a montré une augmentation de l'ordre de la bicouche avec l'augmentation du fraction molaire du polymère. L'information sur la bicouche a été complétée par des mesures SANS et l'imagerie Cryo-TEM, qui ont démontré que le polystyrène est plus ségrégué dans la phase S_o, et alors que lors de la transition de phase il se distribue de maniere homogene dans la bicouche lipidique. La distribution uniforme du polymère dans la membrane produit un tassement plus serré des lipides dû à l'intercalation du polymère entre les chaînes alkyle.

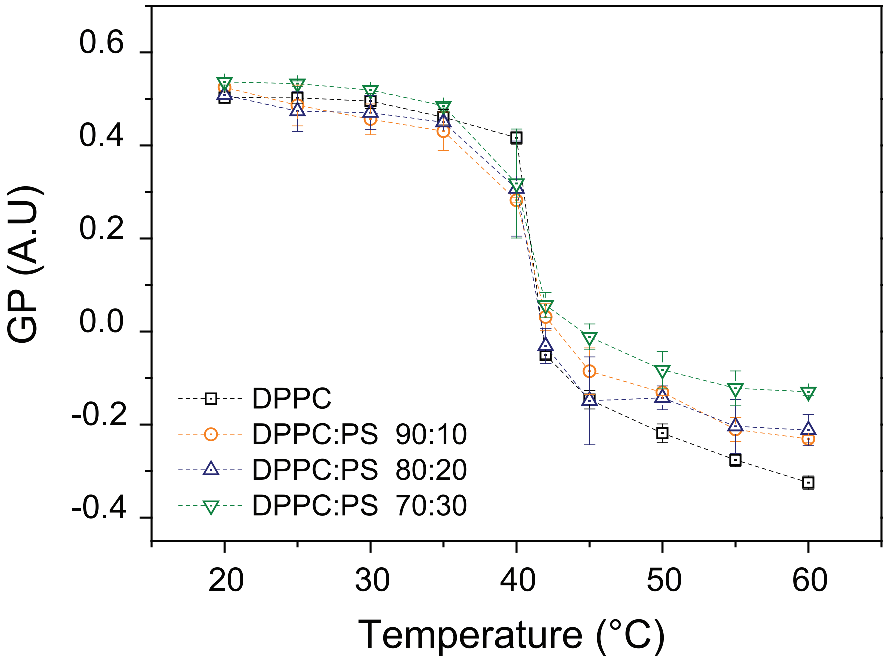

FIGURE 2: Variation de la polarisation générale (GP) avec la température pour les liposomes multilamellaires de DPPC formés dans l'eau à 0 (carrés noirs), 10 % (cercles orange), 20 % (triangles bleus) et 30 % (triangles verts inversés) fraction molaire du polystyrène.

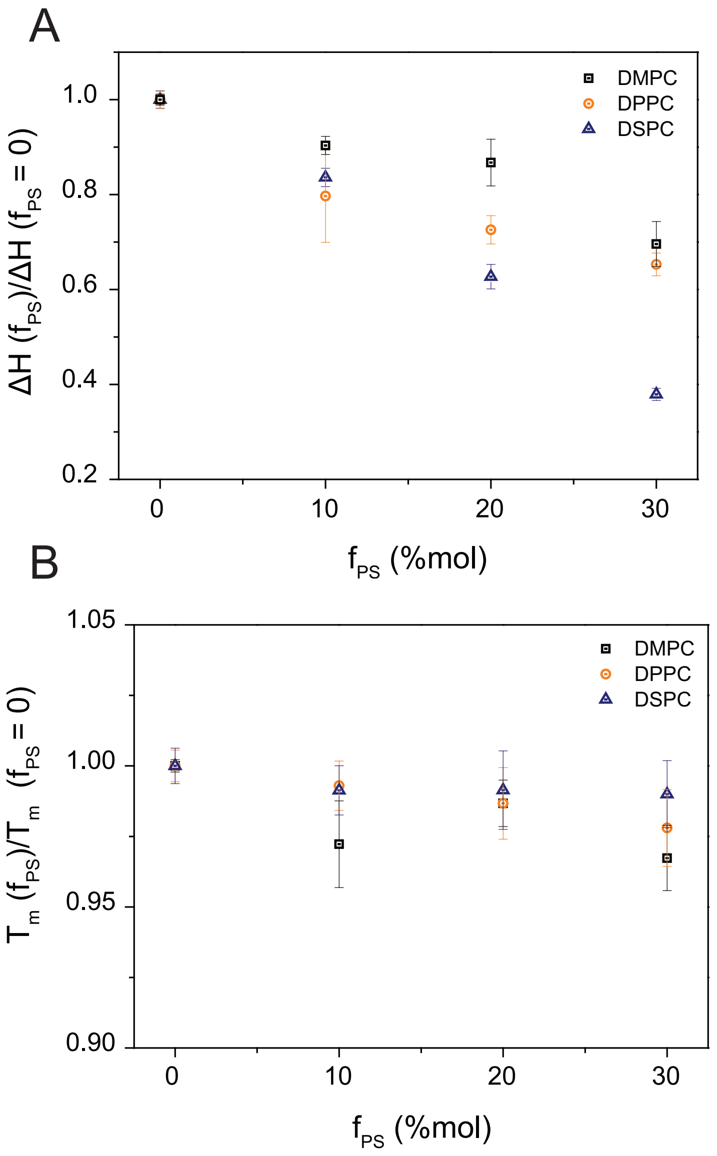

FIGURE 3: (A) $\Delta H(f_{PS})/\Delta H(f_{PS} = 0)$ calculé à partir des thermographes DSC pour DMPC (carrés noirs), DPPC (cercles orange) et DSPC (triangles bleus). (B) $T_m(f_{PS})/T_m(f_{PS} = 0)$ calculé à partir des thermographes DSC pour DMPC (carrés noirs), DPPC (cercles orange) et DSPC (triangles bleus). Chaque point de données est la moyenne de 2 échantillons sur 3 cycles de chauffage / refroidissement.

Nous avons aussi observé que le polystyrène modifie significativement le comportement de phase des bicouches lipidiques à plusieurs composants avec un effet different en presence de cholesterol.

Dans le cas du système binaire, la présence de polymère déplace la miscibilité S_o et L_α vers des températures plus basses, en raison de l'ordre similaire entre les deux phases induites par le polystyrène. Ce comportement est similaire a l'alteration du comportement en phase rapportee dans le cas de molecules hydrophobes incorporées dans la région hydrophobe de la bicouche lipidique qui, en se répartissant préférentiellement dans la phase fluide, élargit la transition de phase principale et réduit la température de fusion. Nos résultats sont en bon accord avec l'inhibition de la coexistence de la phase membranaire précédemment rapportée. Cependant, dans notre cas, l'insertion de PS ne modifie pas la température de transition des membranes lipidiques à un composant.

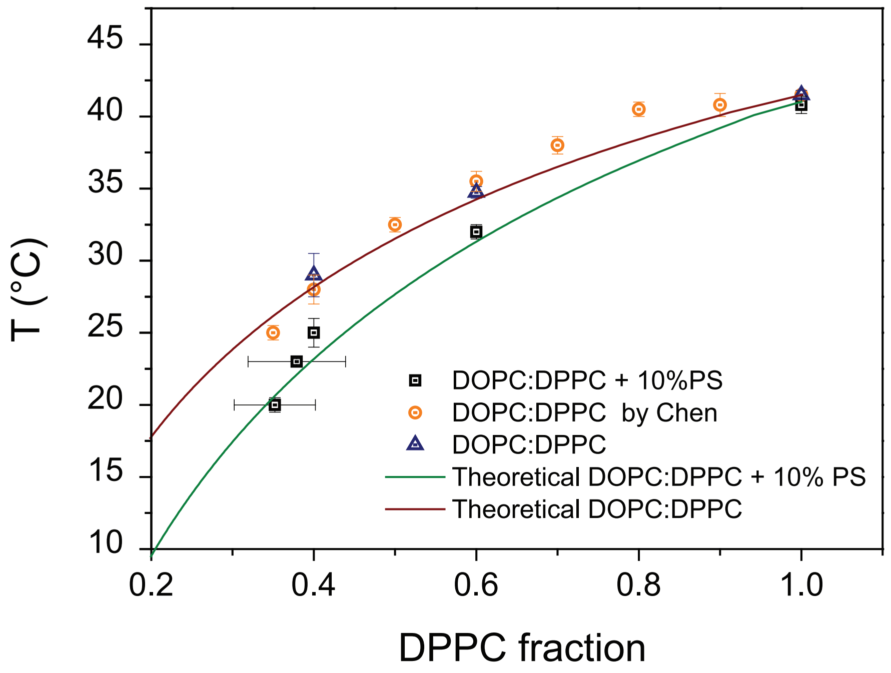

FIGURE 4: Comparaison entre point de données expérimentales pour la lignée de liquidus obtenue par autre etudes (orange), point de données expérimentales pour DOPC:DPPC (triangles bleus) et DOPC:DPPC:PS (carrés noirs) obtenus à partir des spectres d'émission de Laurdan, et prédictions théoriques des lignes liquides pour DOPC:DPPC (rouge) et DOPC:DPPC + 10 % PS (vert).

De plus, nous avons observe que le polystyrene se partitionne preferentiellement dans la phase desordonnee liquide avec moins de cholesterol, de maniere coherente avec des simulations moleculaires et des etudes experimentales sur des molecules hydrophobes incorporees dans la membrane contenant du cholesterol. La présence du polymère dans des membranes présentant des domaines ordonnés liquides stabilise la ségrégation de phase latérale et empêche la coalescence des domaines.

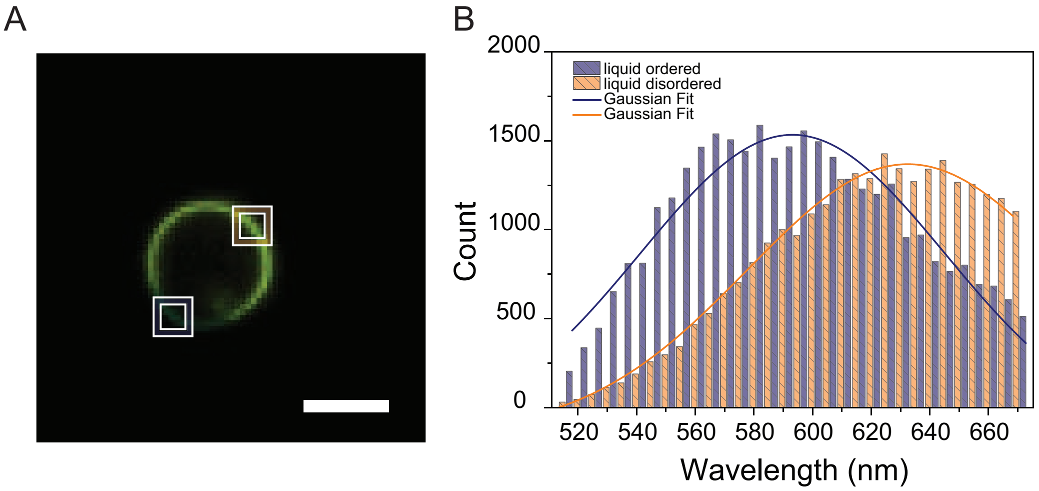

FIGURE 5: (A) Exemple d'imagerie spectrale du Di-4 dans des vesicules geantes de DOPC:DPPC:Chol. Il est possible de visualiser simultanément les phases L_d (carré orange) et L_o (carré bleu) et (B) d'extraire les spectres d'émission locaux.

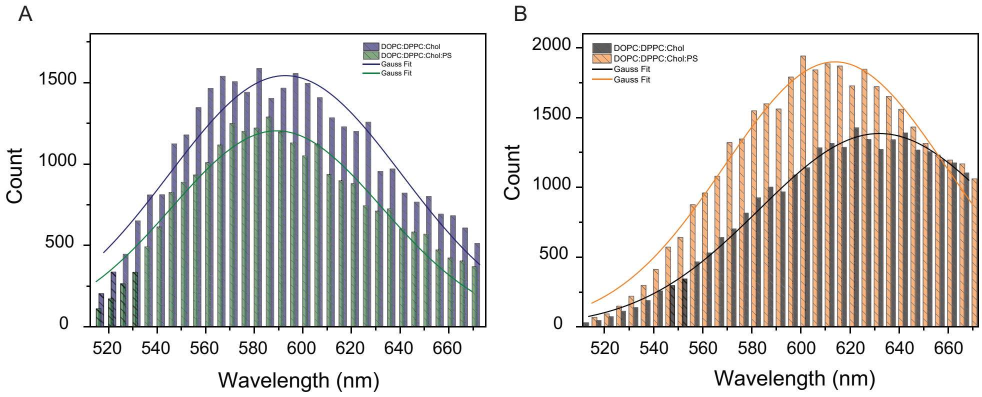

FIGURE 6: (A) Spectres d'émission typiques de Di-4 pour la phase liquide ordonnée pour les GUV composés de DOPC:DPPC:Chol 45:30:25 (bleu) et DOPC:DPPC:Chol:PS 36:24:20:20 (vert). (B) Spectres d'émission typiques de Di-4 pour la phase désordonnée liquide pour GUVs composé de DOPC:DPPC:Chol 45:30:25 (bleu) et DOPC:DPPC:Chol:PS 36:24:20:20 (vert). Les lignes représentent l'ajustement gaussien de la distribution.

Comportement de phase au haut concentration du saccharose

En général, les disaccharides et les sucres jouent un rôle clé dans la préservation de la structure et de la fonctionnalité des membranes biologiques pendant la période de stress environnemental. De nombreux rapports ont montré que les structures membraneuses sont particulièrement stabilisées par de petits sucres. Outre leur rôle important dans la régulation cellulaire, les glucides ont également une large gamme d'applications en biophysique et en recherche industrielle, en particulier dans le domaine de la biopréservation et de la cryoconservation. Leurs interactions avec les membranes ont donc fait l'objet de nombreuses études.

Certains sucres tels que le saccharose et le tréhalose sont des cryoprotecteurs très efficaces. Ils ont montré qu'ils réduisaient facilement la température de transition liquide-gel dans des bicouches lipidiques hautement déshydratées, et augmentaient la capacité de survie de la membrane subissant des processus de congélation / décongélation. Alors que ce mécanisme était initialement associé à la capacité des disaccharides à s'insérer entre les groupes de tête lipidiques adjacents pendant la déshydratation et la liaison hydrogène, un autre modèle a été proposé pour expliquer les effets observés en termes de changements de sucres sur la répulsion d'hydratation.

Malgré les nombreux effets des sucres sur les bicouches sèches, semi-sèches et hydratées, relativement peu d'études ont été menées afin de comprendre l'effet principal du disaccharide sur la transition lipidique bicouche et les mécanismes d'interaction restent à comprendre. Bien qu'il y ait un accord sur le fait qu'une forte concentration de sucre augmente la température de transition de la fusion bicouche, l'effet sur la contribution enthalpique est assez discordant, rapportant dans certains cas aucun effet sur l'enthalpie de la transition, et dans d'autres études une diminution significative de la l'énergie.

Dans ce travail nous avons exposeé des bicouches bien hydratées de DPPC à des concentrations élevées de saccharose et étudions les effets sur le comportement de la membrane de l'augmentation de la concentration de saccharose en utilisant une combinaison de calorimétrie différentielle et de spectres d'émission de Laurdan pour obtenir des informations structurales et thermodynamiques. Nous utilisons également des vésicules unilamellaires géantes pour visualiser les changements de comportement de phase et de cinétique de transition. Sur la base de notre observation expérimentale, nous proposons un un modele thermodynamique de l'interaction bicouche lipidique - sucre pour expliquer nos résultats et ceux rapportés par des études antérieures.

Nos observations expérimentales suggèrent que le saccharose peut induire une déshydratation de la bicouche, telle qu'elle est enregistrée par les spectres d'émission de Laurdan. L'élimination des molécules d'eau, couplée à la formation de grappes lipide-saccharose, réduit l'enthalpie globale de la transition et augmente la température de transition, telle que mesurée par DSC. Nous avons décrit avec succès l'interaction à l'aide d'un modèle thermodynamique et effectué des simulations numériques en bon accord avec nos données expérimentales. Nos résultats fournissent une interprétation novatrice de l'interaction sucrose / lipide et sont pertinents pour comprendre les interactions avec d'autres molécules hydrophiles.

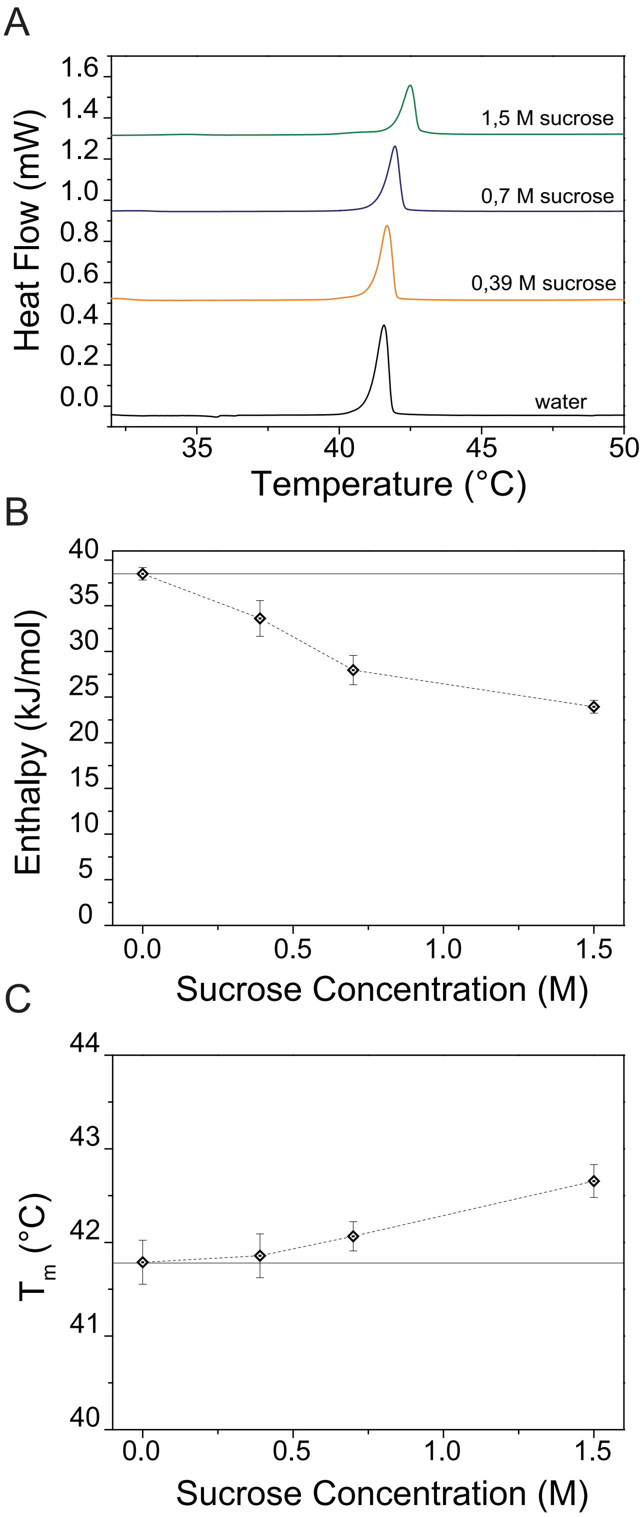

FIGURE 7: (A) Signal calorimétrique DSC (B) Variation de T $_m$ par rapport à la concentration en saccharose (C) Diminution de l'enthalpie à différentes concentrations de saccharose. Dans B) et C) la ligne droite représente la valeur initiale dans l'eau pure.

Cette interaction est décrite avec succès par un modèle thermodynamique simple qui prend en compte les deux populations qui subissent une transition de phase à différentes températures, et fournit un excellent accord avec nos données expérimentales.

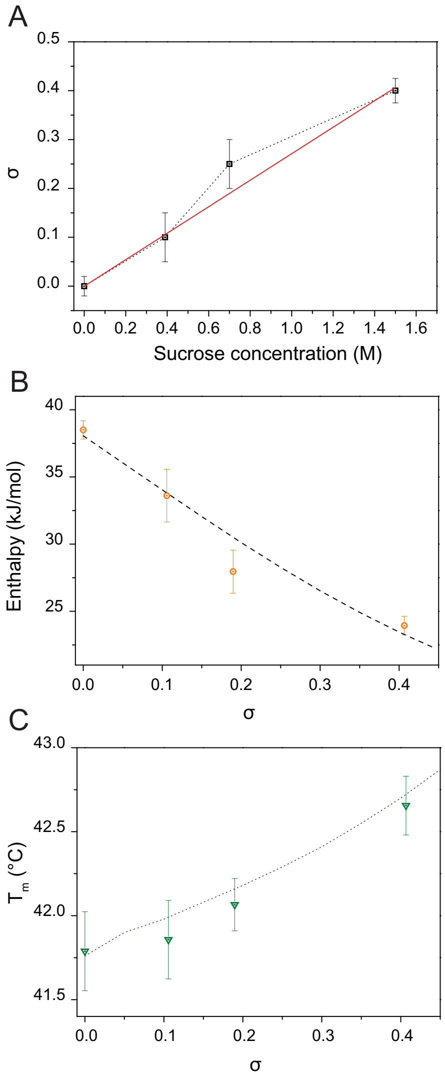

FIGURE 8: (A) Dépendance de la couverture de saccharose σ sur la concentration en saccharose (carrés noirs) et l'ajustement linéaire (ligne rouge). (B) Valeurs expérimentales de ΔH pour la transition gel-liquide DPPC à différentes concentrations de saccharose (cercles orange), avec les prédictions théoriques du modèle thermodynamique (ligne pointillée noire). (B) Valeurs expérimentales de T_m pour la transition gel-liquide de DPPC à différentes concentrations de saccharose (vert), avec les prédictions théoriques du modèle thermodynamique (ligne pointillée bleue).

Interaction d'un polymére greffé de cholestérol avec des membranes modéles

Les thérapies anticancéreuses traditionnelles sont conçues pour interagir avec les protéines et les acides nucléiques pour traiter les cellules tumorales. Cependant, ces dernières années, le développement d'outils scientifiques concernant les lipides et le métabolisme lipidique ouvert de nouvelles voies vers la comprehension des cellules tumorales, indiquant des différences possibles dans la composition lipidique et la fonction membranaire des cellules tumorales comparées aux cellules saines. Le développement de la lipidomique a donc postulé que la modulation ou l'interaction avec les lipides pourrait modifier la composition lipidique, les propriétés membranaires ou altérer les propriétés des cellules tumorales pour interférer spécifiquement avec les membranes des cellules cancéreuses.

Nous avons étudié les effets du polymère greffé de cholestérol sur le comportement en phase de vésicules unilamellaires géantes présentant une coexistence de phase gel-liquide en utilisant l'imagerie spectrale confocale des spectres d'émission DI-4-ANEPPDHQ.

Nos résultats montrent que la présence du polymère greffé de cholesterol perturbe significativement le comportement de phase des membranes composé de DOPC:DPPC, induisant un mélange entre les deux lipides soit par intercalation de chaînes de cholestérol ou de polymère. Les spectres d'emission obtenus montrent que bien que le mélange se produise à l'échelle optique, Il existe deux populations proches des L_o et L_d observées pour les membranes lipidiques contenant du cholestérol.

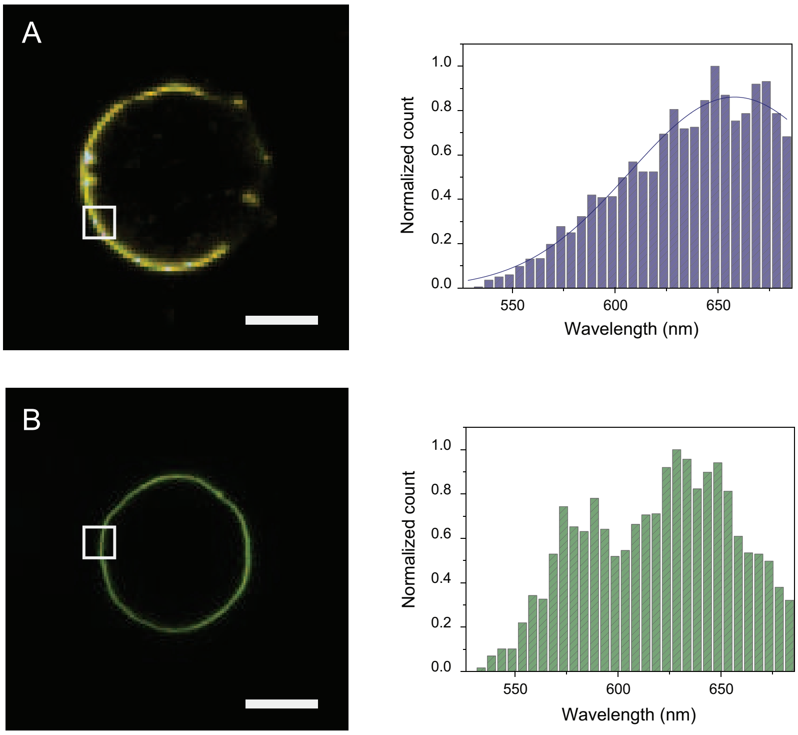

FIGURE 9: (A) GUV typiques composés de DOPC:DPPC 6:4 formés dans PBS à pH 7,4 et des spectres d'émission Di-4 locaux relatifs. (B) GUV typiques composés de DOPC:DPPC 6:4 formé dans une solution de PPCHOL à 500 μ g / mL dans du PBS à pH 7,4 et des spectres d'émission Di-4 locaux relatifs. Barre d'échelle 10 μ m.

Bien que préliminaires, nos données suggèrent que la greffe de molécules altérant la membrane sur l'épine dorsale des polymères est une approche viable dans le développement de stratégies thérapeutiques pour faire varier les propriétés des membranes cellulaires.

Conclusions

Dans ce travail, nous avons étudié avec succès les effets de molécules simples hydrophiles et hydrophobes sur le comportement en phase des membranes modèles lipidiques. En utilisant une combinaison de fluorescence en régime permanent, de calorimétrie différentielle (DSC) et de microscopie à fluorescence, nous avons extrait des informations structurelles de la membrane, ainsi que sur la thermodynamique de la transition de phase, en interaction avec différentes molécules. L'utilisation de sondes fluorescentes sensibles à l'environnement pour extraire des informations pertinentes aux échelles de longueur nanométrique et micrométrique est également un aspect clé de ce travail. De plus, en utilisant l'état de l'art Cryo-TEM et la diffusion des neutrons, nous avons obtenu une image complète de l'interaction au niveau nanométrique.

En conclusion, cette these de doctorat présente une étude complète des effets des molécules hydrophobes / hydrophiles sur le comportement en phase de la membrane lipidique.Nous avons demontre que la combinaison de sondes fluorescentes sensibles a l'environnement, de la calorimetrie et de l'imagerie confocale forme un puissant ensemble d'outils pour caracteriser les variations de comportement de phase, fournissant ainsi une image plus claire des interactions qui s'établissent dans ces systèmes complexes.

1

Introduction

The cell membrane is the gateway of the cell with the exterior, providing not only for compartmentalization, but also regulating its interactions and the signalling processes with the exterior.

In early stages of research on plasma membranes, proteins were the focus, being ascribed as responsible for the majority of recognition and functional processes. In later years, however, lipids have come under the spotlight [1, 2], due to the hypothesis of lipid rafts — nano and micrometric domains which modulate several processes, including intracellular trafficking [3, 4]. The existence of rafts strongly implies that the lipid bilayer is not just a matrix for saccharides and proteins, but a functional component whose phase behaviour and composition is vital for cellular activity. However, developing experimental studies on the biological membrane and on its interaction with other molecules is a difficult task, due to the high complexity of the membrane.

Model membranes provide an optimal platform to study phase behavior of lipids under different conditions, and many studies confirmed indeed that composition regulates the existence of domains in model lipids bilayers [5].

In this chapter we will outline the main processes involved in lipid bilayer' phase behaviour and the feature arising when one or two more component self-assemble into a membrane.

1.1 The plasma membrane

The cell membrane (or plasma membrane) envelops the cytoplasm, separating the interior of the cell and its components from the external environment. It has also the role, together with cytoskeleton, to provide the shape of the cell and by attaching to the extracellular matrix to form cell junctions. Being selectively permeable to ions and other molecules, it regulates the transport of nutrients and metabolic products between cells and extracellular environments. Other processes crucial to cellular activities, such as recognition, immunological response are regulated or performed by the plasma membrane.

The plasma membrane is composed by three main elements: lipids, proteins and sugars (Fig 1.1). The relative rates of these components vary between species and there is also variability in composition in eukaryotic cell. Another important property of the plasma membranes of human and animal cells is that they exhibit transverse lipid compositional asymmetry, i.e.the lipid composition of the outer and inner monolayers or leaflets of the lipid bilayer are different. The structure of the plasma membrane has been studied extensively, and in 2017 the first scattering image of the live cell was reported [6].

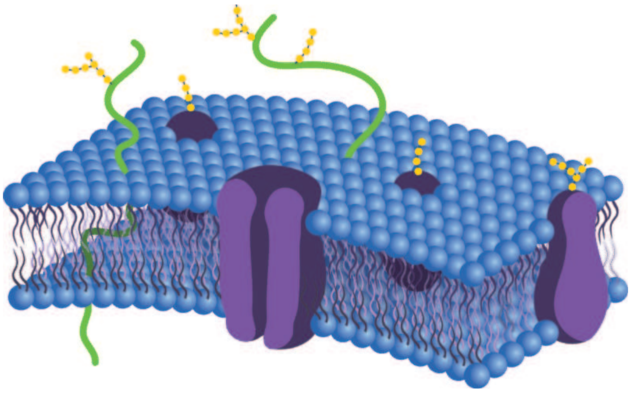

FIGURE 1.1: A schematic represeantion of the plasma membrane of a cell, displaying the lipid bilayer, saccharides and membrane proteins

.

Most plasma membranes consist of approximately 50% lipid and 50% protein by weight, with the carbohydrate portions of glycolipids and glycoproteins constituting 5 to 10% of the membrane mass. While lipids are the fundamental structural elements of membranes, carbohydrates and proteins are responsible for carrying out specific membrane functions. Membrane carbohydrates form a coat around the cell called glycocalyx and are receptors for biological agents. Membrane proteins also acts as receptors for membrane signalling, and protein channels regulate the cell ionic content and metabolism.

1.1.1 Membrane lipids

Lipids are amphiphilic molecules that contain a hydrophobic tail and a hydrophilic polar headgroup (Fig 1.2), which readily interacts with water. The nature of the polar head group (charged or uncharged) as well as the acyl chain (saturated or unsaturated and number of carbon atoms) will determine their localization and function in the body.

Lipids, as many amphiphiles, can self-assemble in aqueous medium into a variety of structures. The main driving force of self-assembly is the hydrophobic effect, which induces self-association of the hydrophobic domains to minimize the total surface that is in contact with water, resulting in an entropy-driven relaxation of water structure and an energy minimum for the self-associated molecular organization [7]. The polar domains of lipids interact with water and other head groups and are therefore energetically stable in an aqueous environment [8].

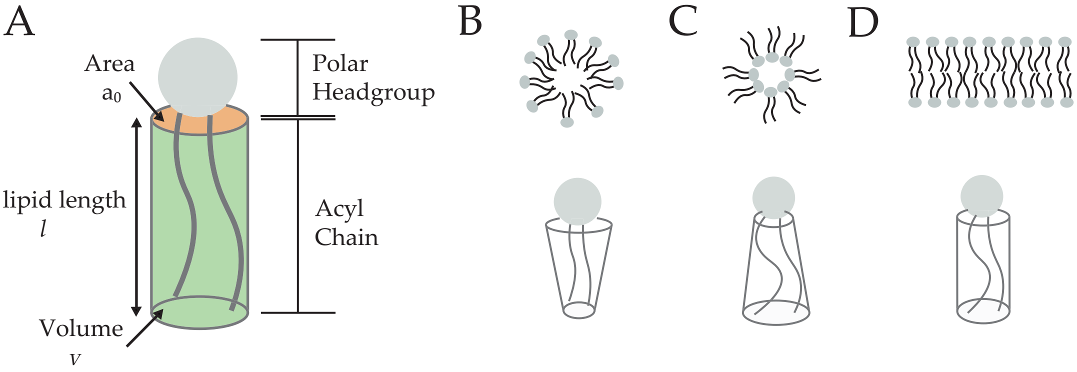

FIGURE 1.2: (A) Schematics of the lipid structure with the main geometrical parameters. Typical self-assemblies depend on the packing parameter. In case of an inverted cone geometry, internal assemblies like micelles or heaxagonal phases arise (B). When the geometry is conical (C), it self-assembles into an inverted structure. In the case of cylindrical packing (D), the assembly is lamellar.

The structure of the formed assemblies is dictated by the chemical nature of the amphipathic lipid as well by the self-assembling environment. One of the major parameters that determines the final conformation is a geometric factor referred to as the packing parameter, P. This dimensionless parameter is given as the ratio of the hydrocarbon volume (v) to the product of the area of the polar head group (a_0) and the critical acyl chain length (l) beyond which the chain can no longer be considered fluid.

$$P = \frac{v}{a_0 \cdot l} \tag{1.1}$$

If the value of P is less than $1/3$ then the amphipathic molecules are expected to form spherical micellar structures. If the value is above $1/3$ but below $1/2$ it may form non-spherical micellar structures while P values >1 favour inverted assemblies. However, this prediction is applicable only when a single amphipathic molecule is involved in the self-assembly process. When more than one component is involved, due to the complex interactions involving electrostatic interactions, hydrogen bonding and/or van der Waals forces between the constituent molecules, deviations from the predicted structures are expected.

Lipids that can be found in mammalian plasma membranes fall into three main classes of lipids: i) glycerophospholipids (called phospholipids, PL), ii) sphingolipids (SLs) and iii) sterols (Figure 1.3).

Phospholipids have a chemical structure based on glycerol backbone with attached fatty acid hydrocarbon chains in adjacent positions. A phosphate linked to an alcohol(choline, ethalonamine or serine) occupies generally the sn3 position. There is also a large variability in the fatty chains in terms of chain length and degree of unsaturation, which contributes greatly to the lipid physico chemical properties.

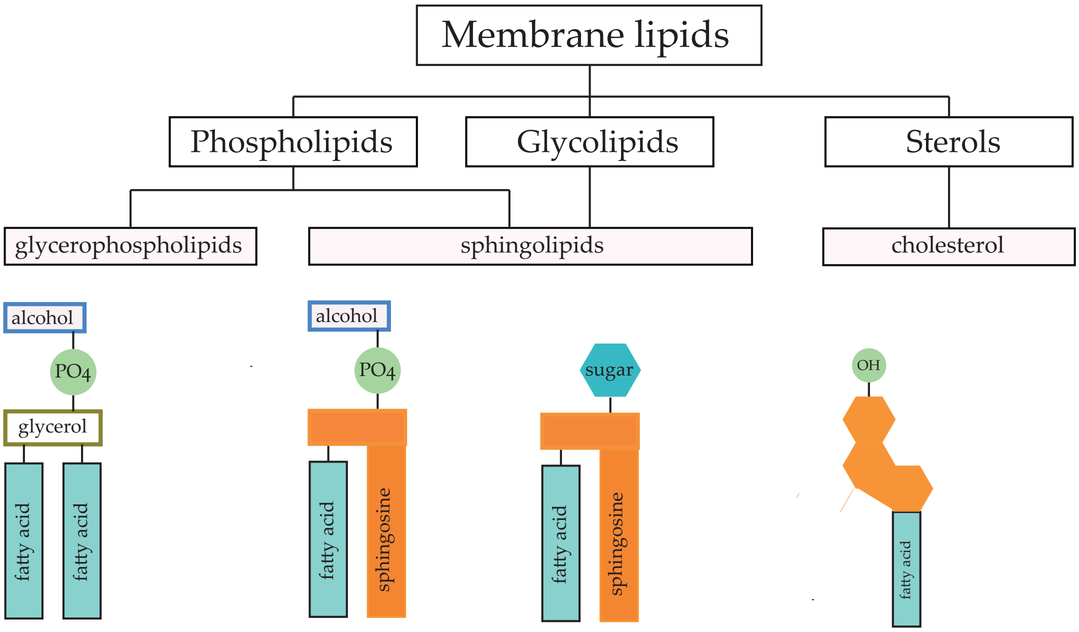
Membrane lipids
Phospholipids
Glycolipids
Sterols
glycerophospholipids
sphingolipids
cholesterol
alcohol
PO4
glycerol
fatty acid
fatty acid
alcohol
PO4
fatty acid
sphingosine
sugar
fatty acid
sphingosine
OH
fatty acid

FIGURE 1.3: Plasma membrane lipid species. Glycerophospholipids are glycerol-backboned molecules with variable fatty acid hydrocarbon chains attached in one side, and different types of headgroup in the other. Sphingolipids have fatty acid chains attached to sphingosine, which is also coupled to either phosphate-alcohol, or to sugar moieties. Cholesterol is a sterol, with four-ring hydrocarbon body and attached short hydrocarbon chain. The polar headgroup of cholesterol is a single hydroxyl group.

SLs, another important group of structural lipids, are derivatives of sphingosine, which is a long chain amino alcohol with attached hydrocarbon chain. The most common sphingolipids are sphingomyelins: sphingophospholipids with either phosphocholine or phosphoethanolamine headgroups. The structural features of sphingolipids allows them to pack tightly together through the van der Waals interactions explaining the physicochemical properties of these lipids in biological membranes.

Sterols are lipid-like molecules, but with different hydrophobic chains and smaller headgroups. Cholesterol is the main sterol and is present in all eukaryotic cells, but absent in prokaryotic membranes. It possesses a rigid four ring hydrocarbon structure with a short hydrocarbon chain attached and a hydroxyl group as a hydrophilic headgroup.

Cholesterol, which is present in the cell membrane plays an important role in membrane phase behaviour and, as first hypothized by Ikonen [9] in 1997, the interaction with sphingolipids is important in the formation of rafts.

The lipid composition of the outer and inner monolayers or leaflets of the lipid bilayer are different. Specifically, the zwitterionic glycerophospholipid phosphatidylcholine (PC) and the zwitterionic phosphosphingolipid sphingomyelin (SM) are enriched in the outer monolayer, while the zwitterionic glycerophospholipid phosphatidylethanolamine (PE) and the anionic glycerophospholipid phosphatidylserine (PS) are enriched in or restricted to, the inner leaflet of the plasma membrane composition.

1.1.2 Model membranes

Many phenomena occurring in biological membranes can be extrapolated or reproduced using model lipid bilayers, which are membranes assembled from a known lipid composition. Lipid bilayers exhibit many interesting properties arising from the cooperative interaction between lipid molecules. Several self-assembled bilayers are therefore used as biomimetic models of cell membranes. Several structures have been developed for biophysical studies and the intrinsic properties of bilayer as well as their interaction with other molecules have been investigated. Depending on the length scale of the mechanism at study, different models exist, ranging from unilamellar and multilamellar vesicles, supported lipid bilayers, nanodiscs and others.

The advantage of working with model lipid bilayers is the ability to precisely control the composition and conditions of the membrane, which is of great utility when studying phase behaviour. Lipid vesicles, also known as liposomes, were first introduced by Bangham [10] in the 1960s and are structural homologues of biological membranes. Liposomes can be produced with a large range of sizes (from 30 nm to 100 um) and their size can be controlled with great precision. Liposomes have been used on spectroscopic and calorimetric studies to investigate phase behavior [11–13].

The development of giant unilamellar vesicles (GUVs) [14, 15] has allowed the study of many macroscopic and mesoscopic lipid bilayer systems using optical and fluorescence microscopy techniques. These vesicles have sizes in the micrometric range and are particularly suited for studying mechanical properties like viscosity, rigidity, and also phase separation and domain morphology in lipid membranes [16]. Moreover their size allows for studies of membrane shape deformation and membrane related processes of biological cells. Micropipette manipulation of GUVs has been successfully used to inject substances within the interior of the vesicle without damaging the membrane, probe the membrane permeability [17], bending rigidity [18], and incorporation of molecules within the lumen or within the hydrophobic core of the bilayer. In the study of phase behaviour of lipid membranes they have been useful in determining changes in domain morphology in response to changes in membrane curvature, tension, composition and presence of polymers or other molecules.

1.2 Phase behavior of lipid bilayer

A characteristic feature of the lipid bilayer is the changes in the mobility of individual lipid molecules with variation of temperature and lipid species. In eukaryotic cell membranes the hypothized rafts arise from changes in the lipid phase behavior and therefore the investigation of lipid phase behavior in single and multicomponent bilayers has been a focus in soft matter physics over the last decades.

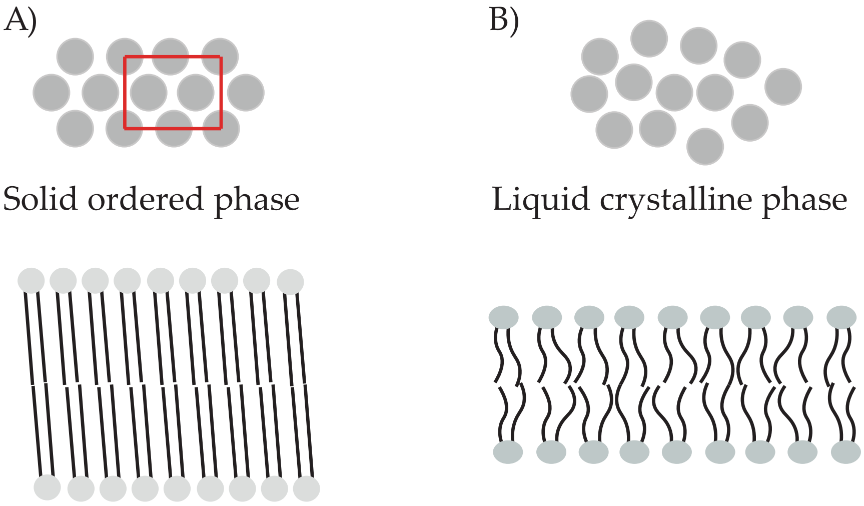

FIGURE 1.4: (A) Structure of hydrated lipid bilayer in gel phase. The acyl chains are completely extended and packed in a rectangular lattice. The lipids can be either straight (L_β) or tilted ($L_{\beta'}$).(B) A fluid phase bilayer, with chains posessing trans- and gauche- conformations and lipids disorderly distributed.

Generally, when considering a lipid bilayer, the membrane can exist in two possible states: a solid or a liquid phase [19]. The solid phase (also called "gel" phase, S_o or L_β) is characterized by a tight packing of the lipid molecules. Hydrocarbon chains are in the fully extended all-trans conformation, the cross-sectional area of the phospholipid molecules is minimal, the thickness of the phospholipid bilayer is maximal, and both intra- and intermolecular motion are severely restricted [20–23].

The fluid phase (also referred to as L_α phase), on the other hand, has highly disordered chains, the phospholipid hydrocarbon chains contain a number of gauche rotational conformers, the cross-sectional area of the lipid molecules increases considerably, the phospholipid bilayer thins substantially [24], and relatively high rates of both intra- and intermolecular motion are present [20, 25–27].

Many physical properties of the membrane change with respect to the phase, ranging from cross sectional area to bending rigidity and permeability [20].

The transition from gel to fluid, and vice versa, is a cooperative phenomenon that occurs when the temperature of the system goes above (or below) the characteristic temperature of the lipid [28, 29]. The transition temperature T_m, among other parameters, is strongly influenced by the length and degree of unsaturation of acyl chains, head group size and charge, etc [30, 31]. Assuming a first order transition for the L_β to L_α phase change, it is possible to write:

$$\frac{P_{L_\alpha}(T_m)}{P_{So}(T_m)} = K \cdot T_m = e^{-\frac{\Delta G}{k_B T_m}} = 1 \tag{1.2}$$

where P_{L_α} is the probability for a single lipid to be in the fluid phase and P_{So} the probability of being in the gel phase, and ΔG is the Gibbs free energy difference. At the transition, it is possible to describe T_m as:

$$\begin{gathered}\Delta G = \Delta H - T_m \Delta S = 0 \\ T_m = \frac{\Delta H}{\Delta S}\end{gathered} \tag{1.3}$$

where ΔH is the enthalpy and ΔS is the entropy of melting. Enthalpic and entropic contributions values strongly depend on the length and saturation of lipid tails [20], and thus the value of the transition temperature. Other factors, however, such as cations (divalent ions) [32, 33], membrane hydration [34, 35], membrane curvature, and pH [33, 36] can affect the transition temperature and the Gibbs free energy.

1.2.1 Multicomponent bilayers

When the bilayer is composed of two or more lipid species, complex phase behavior arises due to the combination of each lipid transition. For a binary system composed of high melting lipid (like DPPC) and low temperature melting lipid (like DOPC), three distinct regions exist [37, 38].

When the temperature is below both lipid T_m, the bilayer is in a S_o phase. Conversely, when temperature is above both T_m the membrane is in a fluid phase.

In the intermediate region between the two lipid T_m phase separation appears, and we observe a coexistence of S_o and L_α phase within the membrane. The relative amount of each phase is dependent on the temperature and molar ratio of the two components (Fig. 1.5). The behavior of phase separation can be affected by many factors, like temperature [33], charge [39], pH [33], interaction with molecules and types of lipids [40].

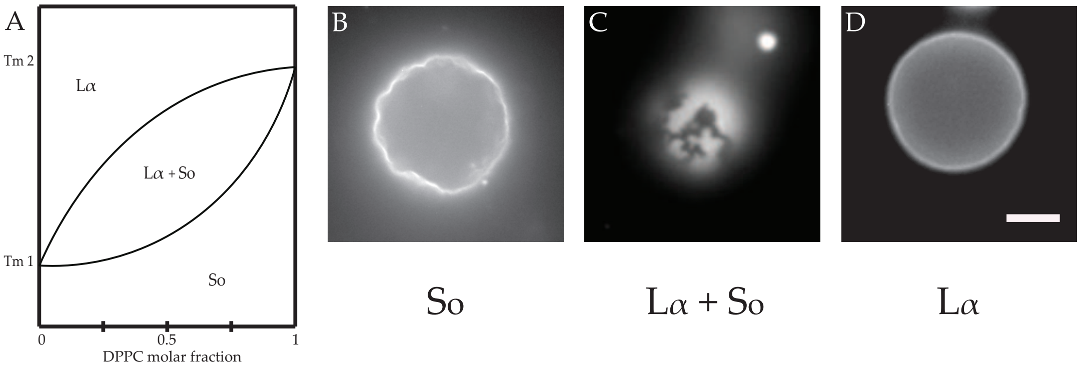

FIGURE 1.5: (A) Typical phase diagram of a binary lipid system composed of a low-melting and high-melting lipid. (B) Typical micrometric behavior for GUV composed of DOPC:DPPC 75:25 at 15°C showing pure S_o phase. (C) 20°C with L_α-S_o coexistence and (D) and at 35°C with bilayer in L_α state. Scale bar 20 μm.

The phase separation process plays an important role in biological membranes due to the formation of compositionally distinct domains, implying the creation of regions of different bilayer hydrophobic thickness. It is reported that many membrane proteins partition preferentially in one of the domains and the activity of some membrane proteins depend on the hydrophobic mismatch created by phase separation [41].

Domains exist both at the nanoscopic and micrometric length scale. Nanoscopic domains have been studied using neutron scattering techniques and AFM imaging [42], and have been reported to exist, together with percolative structures, in the two-phase coexistence region.

The properties and behavior of micrometric domains have been extensively investigated using two-photon microscopy [43] and confocal microscopy [44]. Solid ordered domains appear in many morphologies, as illustrated in Fig 1.6 and several factors contribute to the typology of the domains observed, including membrane tension, temperature rate, and ionic strength [45]. Aside from liquid-solid coexistence, solid-solid coexistence has also been observed in systems composed of lipids with high chain length mismatch.

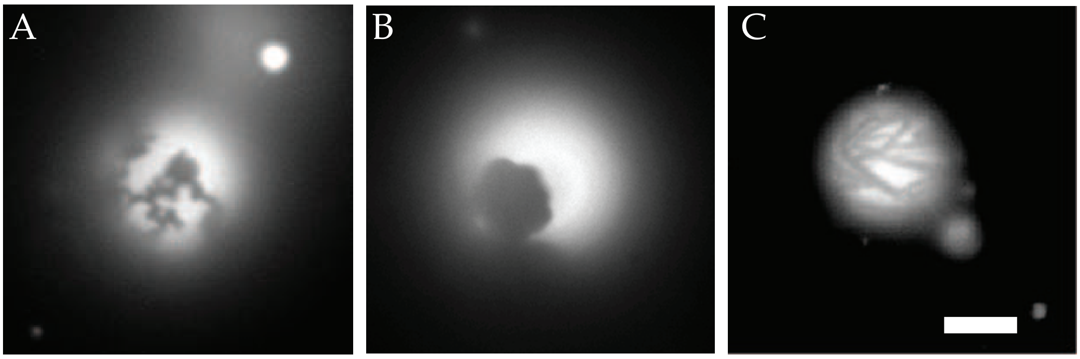

FIGURE 1.6: Different type of S_o domains that can be observed, depending on membrane tension and heating rate. (A) irregular shape (B) hexagonal domains and (C) striped domains. Scale bar 10 μm.

1.2.2 Cholesterol

Eukaryotic plasma membranes can contain up to 30% of cholesterol [46], therefore it is not surprising that the effect of the molecule on the membrane properties is very significant. Cholesterol has been identified as one of the main components of the cellular rafts, due to its ability to modulate diffusion and phase behaviour. It was initially proposed that cholesterol's main role is to reduce the intrinsic phase separation in cellular membranes due to the lipid composition. Hao *et al.* [47] proved that indeed a cellular membrane depleted of cholesterol exhibits phase coexistence.

In model lipid bilayers the effects of cholesterol have been studied extensively using DSC [48], AFM, fluorescence microscopy [49, 50], spectrometry [51, 52], NMR [48, 49, 53] and X-ray scattering. Addition of cholesterol to the bilayer has been shown to reduce the enthalpy of the L_α—S_o transition in DPPC bilayers (eliminating it almost completely at 50% mol), alter the bilayer permeability [54, 55] and the lipid lateral diffusion [56]. Moreover cholesterol-rich bilayers have smaller cross sectional area [57, 58], larger membrane thickness than L_α phase bilayers and different acyl chain order in both gel and liquid phase [59].

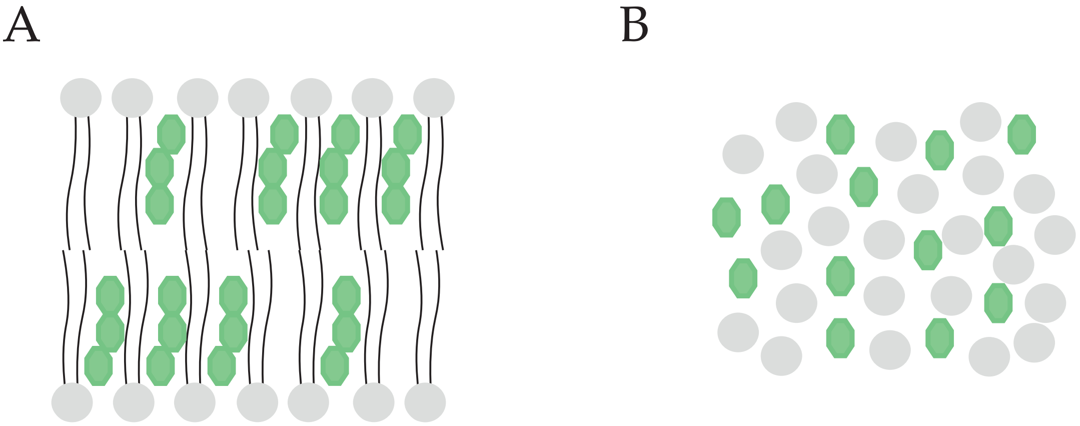

FIGURE 1.7: Structure of liquid ordered phase (L_o) of lipid bilayer. The sterol rings prevent the hydrocarbon chains of the lipid from strongly interacting together, but also block the total expansion of the lipid upon melting (A). The packing of the bilayer is almost as tight as in the S_o phase, however there is no packing lattice and lipids have a higher diffusivity (B).

All the changes in the physical properties of the bilayer in presence of cholesterol point to an intermediate phase between gel and liquid. This state of the cholesterol rich bilayer, also called liquid ordered (L_o) phase [59], retains the tight packing and rigidity of the gel phase, but the fluidity of the liquid phase [46, 60]. Conversely, fluid membrane in presence of cholesterol is called liquid disordered (L_d) phase.

Perhaps one of the most striking features of the cholesterol is the changes it induces in phase diagrams when incorporated in single or multi component membranes. For single lipid bilayers, the presence of cholesterol at 7% already induces a phase separation between the S_o and L_o phases [61]. As the temperature rises, phase coexistence still remains, but between L_d and L_o phases [62, 63].

Similar behavior can be observed in ternary phase diagrams composed of low-melting lipid, high melting lipid and cholesterol (Fig 1.8) [64]. For relatively low molar fractions of cholesterol the system still is in a L_d-S_o coexistence region, however as cholesterol content increases the system goes trhough a ternary coexistence (L_d+S_o+L_o) and eventually reaches a liquid phase coexistence of L_d-L_o. Above $X_{chol} \sim 0.4$ mole fraction (and below $X_{chol} \sim 0.67$ mole fraction where cholesterol monohydrate crystals precipitate) a single phase exists. Highly non-random mixing occurs in this single phase, i.e. extensive clustering of some components. This one phase region changes continuously from L_o to L_d as composition is varied.

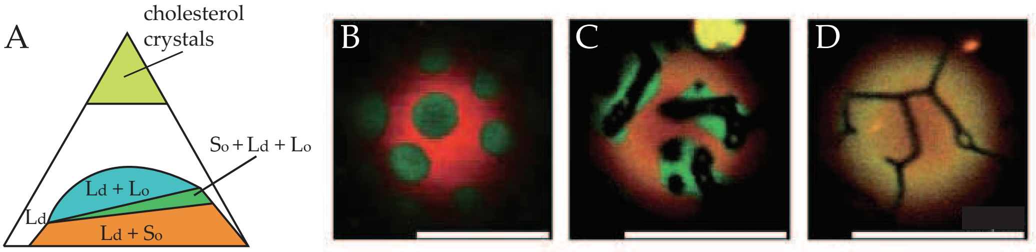

FIGURE 1.8: (A) Typical phase diagram of ternary lipid mixtures composed of low-melting lipid, high-melting lipid and cholesterol. (B) Characteristic micrometric domains of ternary phase separation (extracted from ref. [39]) displaying L_d-L_o. (C) L_d-L_o-S_o three phase coexistence and (D) L_d-S_o coexistence. Scale bar 20 μm.

Studies on micrometric liquid ordered phase have been performed on GUVs and planar membranes [65–68]. These domains are generally circular, due to line tension driving the phase domains toward the minimum perimeter, and coalesce upon collision to form larger domains.

Similarly for binary systems, evidence of nanometric liquid domains has been reported [69]. In some cases, submicron lipid organization is reported in vesicles that never exhibit large scale liquid immiscibility [48, 70], and in other cases, the same vesicle system can produce both small and large-scale features, but at different compositions and temperatures [49, 52, 71].

Beyond ternary systems, Konyakhina *et al.* [72] explored the phase behaviour even further by studying the effects of cholesterol in quaternary systems, and reported the presence of modulated domains with very distinctive domain patterns (Fig 1.9).

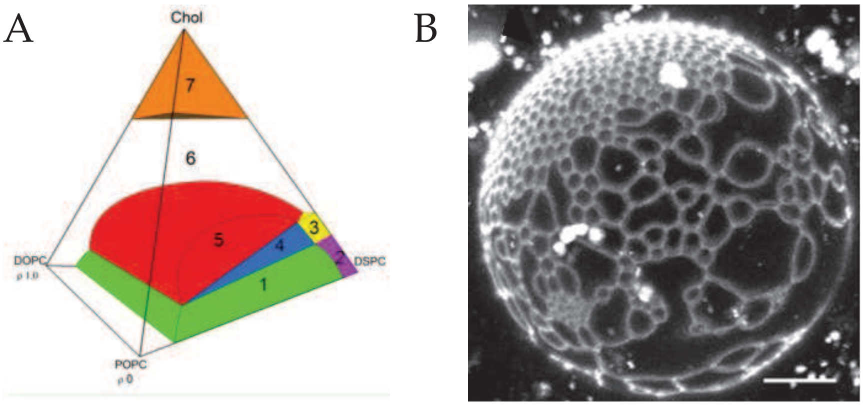

FIGURE 1.9: (A) Example of a four component mixture phase diagram (DOPC:POPC:DSPC:Chol) highlighting normal coexistence regions and modulated phase separation region. (B) Image of GUV in the modulated phase region exhibiting disitinctive domains. Both images are from ref. [72]. Scale bar 10 μm.

.

1.3 Concluding remarks

The possibility to replicate or probe biologically relevant phase behavior has made model lipid membranes an invaluable tool in biophysics. Indeed, many cellular mechanisms of interaction have been elucidated using lipid bilayers and despite being a minimal system, they have allowed an understanding of the mechanism of interaction between drugs, nanoparticles or biomolecules with cell membranes.

2

Materials and Methods

In this chapter the main techniques employed during this Ph.D project will be described. A brief description of the working principle of each methodology will be outlined, followed by a more detailed explanation of the data analysis used in the experimental work. The use of fluorescent probes sensitive to the environment is a key element of this work, therefore an in-depth analysis of the differentt properties of the probes used will be presented. In particular, analysis of emission and excitation spectra of Laurdan and Di-4 and their relation to phase behavior of lipid bilayer will be described.

2.1 Differential scanning calorimetry

Differential scanning calorimetry (DSC) is a calorimetric technique that allows to quantitatively study phase transitions upon changes in temperature. This method has been used extensively to investigate the lipid bilayer gel to liquid transition and phase behavior in dry and hydrated membranes [73]. It has been succesfully used to probe the phase diagrams for binary and ternary mixtures with and without cholesterol, as well as the effects of micromolecules on the phase behavior of model lipid membranes [52, 74–80].

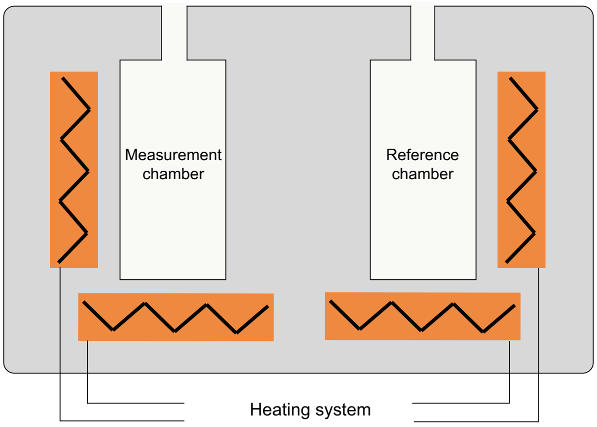

FIGURE 2.1: A schematic representation of a typical DSC apparatus. The measurement chamber contains the sample while the reference chamber is filled with solvent of reference. The feedback system mantains both cells at the same temperature while heating or cooling the chambers at the same rate.

The apparatus consists of an adiabatic chassis with two separate chambers: a measurement and a reference cell. Sample of lipid bilayer in solution is placed in the measurement cell while reference cell contains the same mass of pure solvent. The apparatus heats both cells at the same rate and records the energy provided to the system to keep both chambers at the same temperature. Because the phase transition of lipid bilayer requires adsorption or release of energy the resulting signal is a peak centered at T_m.

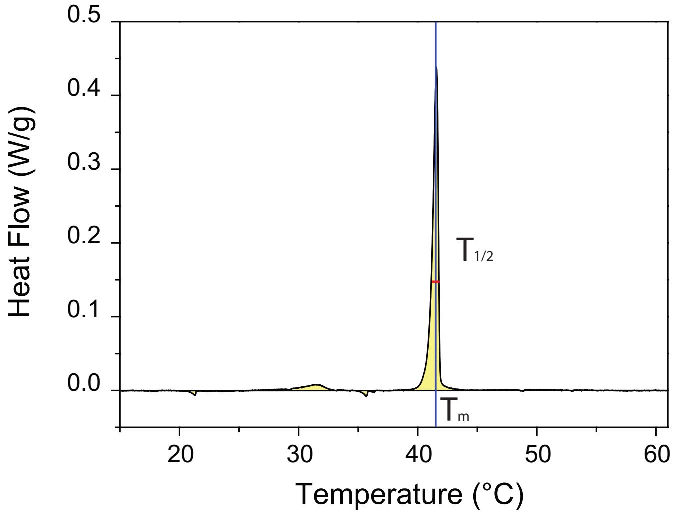

FIGURE 2.2: Example of a typical thermograph of liposomal suspension of DPPC in water. The mid point of the curve is defined as the transition temperature T_m, whereas the width at half maximum is $T_{1/2}$

For first order phase transitions such as the bilayer transition from gel to liquid-crystalline, the transition temperature, T_m, is where the heat capacity, C_p, reaches its maximum value. The value of the calorimetric enthalpy (ΔH_{cal}) for the phase transition is determined by integrating the area under the peak,

$$\Delta H_{cal} = \int C_p dT \tag{2.1}$$

and the entropy of the transition is extracted by using the simple relation:

$$\Delta S = \frac{\Delta H_{cal}}{T_m} \tag{2.2}$$

Comparison of ΔH_{cal}, ΔS and T_m shows the effect of a structural modification (e.g. chain length) on the thermodynamics of the phase transition.

Theoretically for pure lipid systems the transition should be completely symmetrical, however experimentally the thermograms of biological systems and lipid bilayer are asymmetrical. T_m is therefore no longer the midpoint of the transition and $T_{1/2}$, the width of the distribution, becomes an important parameter.

Analysis of the shape of the peak provides additional information about the melting process. The $T_{1/2}$ parameters, defined as the width at half height of the peak, is a valuable tool to estimate purity, protein-lipid interactions, as well as lipid-lipid interactions, and provides information about the cooperativity of the phase transition [81], as explained in Chapter 1.

The cooperativity of a pure lipid transition is in fact related to the shape and sharpness of the peak and is described by a cooperative unit (CU), the number of lipids involved in the transition [81]. The cooperative unit can be calculated by the ratio of $\Delta H_{vH}/\Delta H_{cal}$, where ΔH_{cal} is the enthalpy of the transition and ΔH_{vH} is the van't Hoff enthalpy [82].

$$\Delta H_{vH} = \frac{4RT_m^2}{T_{1/2}} \tag{2.3}$$

with R is the gas constant.

2.2 SANS

Although many techniques allow characterization of biological structures and interactions, scattering techniques, such as X-ray and neutron scattering, have allowed to probe objects at the nanometric level with great precision. Among the different methods using neutron scattering, small-angle neutron scattering (SANS) is one of the most implemented and has had a major impact in polymer science, biology and material science.

Particularly, in the field of membrane physics, neutron scattering data were used to investigate structural parameters of the lipid bilayer like thickness, hydration, area cross section, bending rigidity and domain size upon phase coexistence. The range of applicability and uses of scattering techniques were successfully employed to obtain the first structure of live bacterial membrane [6].

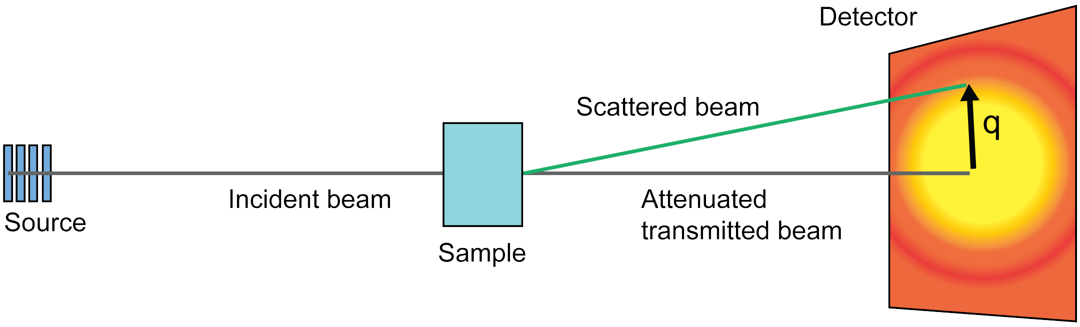

FIGURE 2.3: Schematics of a SANS experimental apparatus. The incident beam from the source impinges on the sample, resulting in a scattered beam and a transmitted beam that are collected by the detector.

During a SANS experiment a beam of neutrons is directed at a sample, which can be an aqueous solution, a solid, a powder, or a crystal (Fig. 2.3). The neutrons are elastically scattered by nuclear interaction with the nuclei or interaction with magnetic momentum of unpaired electrons. The detector measures the scattering intensity I(q) at varying angles as a function of the scattering variable q, defined a

$$q = \frac{4\pi}{\lambda}\frac{sin\phi}{2} \approx \frac{2\pi\phi}{\lambda} \tag{2.4}$$

where ϕ is scattering angle, λ the wavelength of neutron radiation. Taking account the detector distance, D, from sample, the scattered radiation striking the detector at distance, S, from its center defines the low limit of scattering angle. When D > S, the scattering wave vector equals

$$q = \frac{4\pi}{\lambda}\frac{sin\phi}{2} \approx \frac{4\pi}{\lambda}tan(\phi/2) = \frac{2\pi}{\lambda}\frac{S}{D} \tag{2.5}$$

The scattering of neutrons upon impinging on the sample is collected by a detector, and afterwards is corrected by detector efficiency, which is determined in separate measurement. The scattering cross section, $d\Sigma/d\Omega$, is related to the count rate I(q) measured by the detector

$$I(q) = I_0 AdT(\frac{d\Sigma(q)}{d\Omega})_{sample}\Delta\Omega\epsilon t \tag{2.6}$$

where $\Delta\Omega$ is a solid angle, A the area of the sample, d the sample thickness, ϵ the detector efficiency, t the counting time, and T the transmission efficiency of filled cell.

2.2.1 Scattering lengh and scattering lengh density

Scattering of a neutron is due to interaction between neutron and the atomic nucleus, therefore isotopes of the same atom scatter neutrons in different way. The intensities of scattered neutrons is proportional to the scattering lengh, b, which describes the scattering potential of a single atom. It can be shown that the intensity by the detector is related to b by the simple equation:

$$\begin{gathered} \frac{I_s}{I_0} = \frac{|b|^2 \cdot A}{D^2} = |b|^2\Delta\Omega \\ \frac{I_s}{d\Omega I_0} = |b|^2 \end{gathered} \tag{2.7}$$

Which gives the relative amount of scattered neutrons by sample towards the detector. To obtain the scattering into all directions, this quantity must be integrated over all solid angles:

$$\begin{gathered} \int_\Omega |b|^2 d\Omega = 4\pi|b|^2 = \sigma \\ \frac{d\sigma}{d\Omega} = |b|^2 \end{gathered} \tag{2.8}$$

where: σ- scattering cross section, $d\sigma/d\Omega$ differential scattering cross section.

Usually it is more convienient to describe the scattering potency of the sample as built up by atoms with an associated scattering length in a finite volume, called scattering length density (SLD) ρ.

$$\rho = \frac{\sum_i^n b_i}{V} \tag{2.9}$$

where V is the molecular volume.

The scattering intensity of sample in solution is a combination of scattering from particles and solvent. Assuming a homogenous scattering signal from the solvent, the excess scattering length density, $\Delta\rho$, of the particles compared to solvent gives:

$$\Delta\rho = \rho_{molecule} - \rho_{solvent} \tag{2.10}$$

Therefore intensity and shape of scattering curves is determind only by the scattering density deviations from the solvent. If the sample and solvent have the same SLD values, $\Delta\rho$ vanishes with no signal recorded by the detector. Thus, $\Delta\rho$ is usually referred to sample contrast.

In this thesis we used equation 2.9 to calculate the SLD of hydrogenated lipid head groups and fatty acids together with their deuterated analogs. Since we worked at two different temperatures, i.e. above and below T_m of DPPC the changes in SLD due to volume variations at different temperature were taken into account as well. The calculated SLD values of lipids and polymer used are collected in Table 2.1.

Molecule	Part of the molecule	Chemical formula	Temperature	Scattering length	Volume	Scattering length density
			[°C]	[10^{-5} Å]	[Å^3]	[10^{-6} Å^{-2}]
h-DPPC	Lipid	$C_{40}H_{80}NO_8P$	20	27.6	1144	0.24
h-DPPC	Lipid	$C_{40}H_{80}NO_8$	50	27.6	1232	0.22
d-DPPC	Lipid	$C_{40}H_{18}NO_8PD_{62}$	20	673	1152	5.84
d-DPPC	Lipid	$C_{40}H_{18}NO_8PD_{62}$	50	673	1242	5.42
h-DPPC	two tails (h)	$C_{30}H_{62}$	20	-32.5	825	-0.39
h-DPPC	two tails (h)	$C_{30}H_{62}$	50	-32.5	913	-0.36
d-DPPC	two tails (d)	$C_{30}D_{62}$	20	613	833	7.36
d-DPPC	two tails (d)	$C_{30}D_{62}$	50	613	923	6.64
DPPC	head group (h)	$C_{10}H_{18}NO_8P$		60.1	319	1.88
Water	all	H_2O	25	-1.7	30	-0.56
Heavy water	all	D_2O	25	19.2	30	6.44
Polystyrene	all	$(C_8H_8)_n$				1.41

TABLE 2.1: Neutron scattering lengths, molecular volumes, and corresponding scattering length densities of lipids used in this work.

Contrast variation technique

As mentioned in the last paragraph the scattering intensity depends solely on the contrast between the sample and the solvent. This allows, by selective deuteration of sample, to highlight parts of interests by matching the SLD of certain components by choosing the proper H_2O/D_2O ratio.

Contrast variation technique can improve the information extracted from sample, however special care should be taken. The incoherent scattering increases by adding extra H_2O and for weakly scattering samples, the resulting lower signal to noise ratio may mask structural signal.

2.2.2 Data analysis

A complete analysis of scattering curves generally requires the choice of a model with a form factor for the object and a size distribution of the sample. This analysis can be fairly difficult and very sensitive to the choice of parameters and scattering length densities. However, it is possible to analyse the scattering data and extract significant information on the structure of the sample by studying the behaviour of the scattering profiles in different regions (Fig. 2.4) [83]. In particular, for lipid bilayer the model free analys allows to estimate the average size of the object and the thickness of the bilayer.

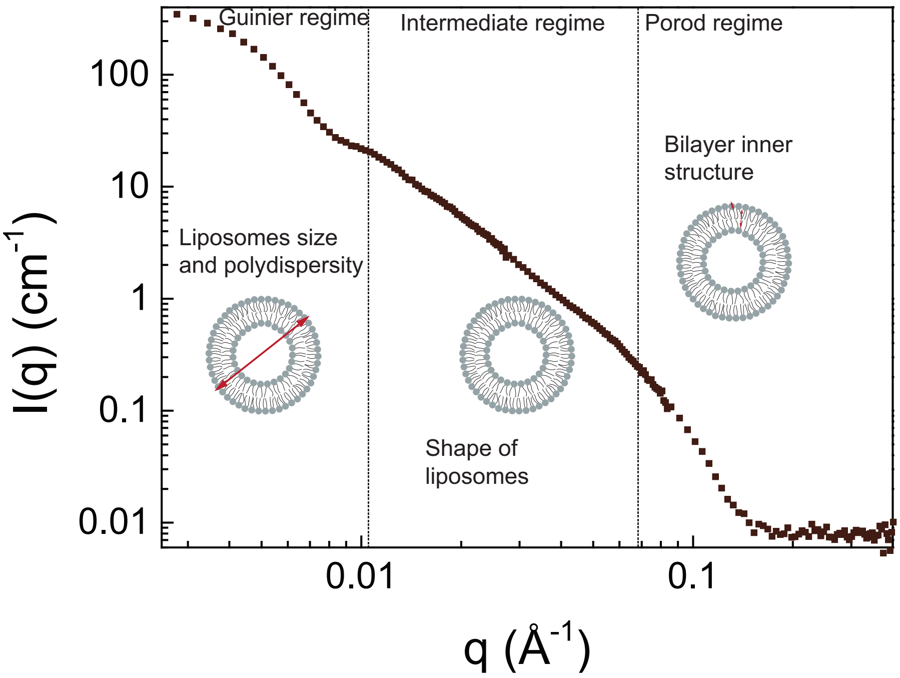

FIGURE 2.4: Example of a SANS scattering curve, highlighting the q to their corresponding bilayer structural information.

Guinier analysis

In the limit of q close to 0, for n orienteded particles, the scattered intensity can be approximated by, as first proposed by Guinier in 1939,

$$I(q) \propto exp(-q^2 R_g^2/3) \tag{2.11}$$

where R_g is the radius of gyration, which represents the effective size of the scattering "particle", whether it is a polymer chain, part of a protein, a micelle, or a domain in a multiphase system. This approximation provides a simple way to estimate R_g

of the measured system, by plotting $\ln[I(q)]$ vs q^2 in order to obtain the slope $R_G^2/3$. However, it has to taken into account that expression is valid only for $q \cdot R_g \leq 1$.

Kratky-Porod analysis

Although the Kratky-Porod plot is a powerful tool in probing the membrane thickness, it has to be stressed that this method is an average of the scattering density profile from the bilayer. Moreover the penetration of solvent molecules within the bilayer interface must be small enough to avoid changes in the SLD distribution.

In the intermediate q regime the signal corresponds to smaller lenght scales, where the bilayer appears as a sheet with given thickness d. By fitting linearly $\ln[I(q) \cdot q^2]$ vs q^2 and extracting the slope R, the corresponding value for the thickness can be written:

$$d = R\sqrt{2} \tag{2.12}$$

2.3 Fluorescence, microscopy and environment-sensitive fluorescent probes

Fluorescence is the property of a molecule or a material to absorb energy from incoming light, and emit it in form of light at a different wavelength. It occurs when an orbital electron of a molecule, atom, or nanostructure, relaxes to its ground state by emitting a photon from an excited singlet state.

As illustrated in the Jablonski diagram (Figure 2.5), a fluorophore absorbs light at λ_{exc} wavelength rising from the ground state to the first electronic state S_2. Subsequently it returns to the ground state emitting a photon at a higher wavelength λ_{em}. Emitted fluorescent light has a longer wavelength and lower energy than the absorbed light. This phenomenon, known as Stokes shift, is due to the internal energy loss between the time a photon is absorbed and when it is emitted (Fig. 2.5 B).

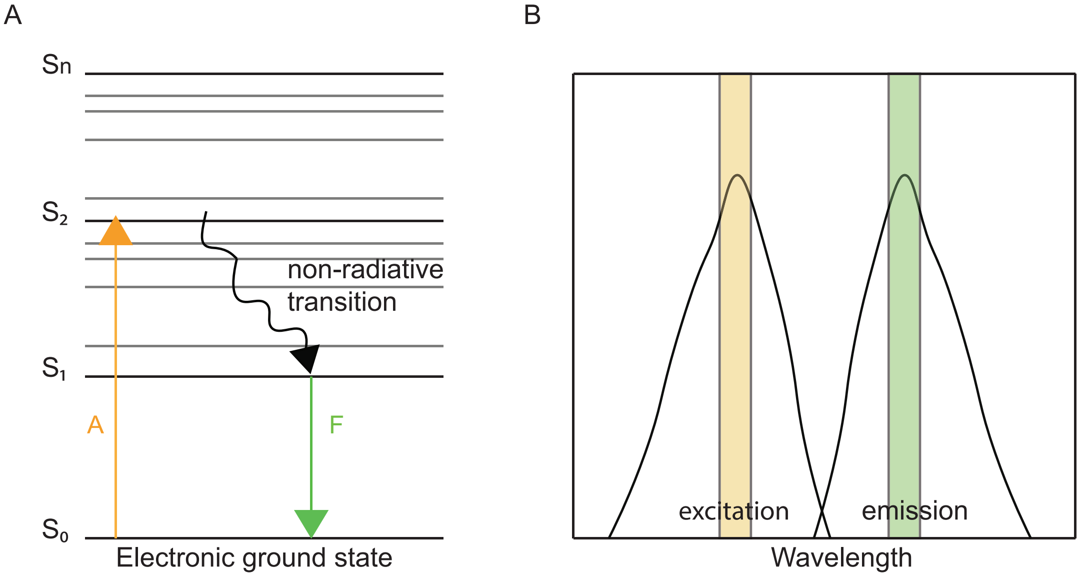

FIGURE 2.5:)A) A typical Jablonski diagram illustrating the main principle of fluorescence. Light at λ_{exc} is absorbed by the molecule, raising the electrons from the ground state S_0 to the excited state S_2. The electronic state relaxes back to ground state by emitting light at lower wavelength λ_{em}. (B) Schematics of Stokes shift, the difference between λ_{em} and λ_{exc}.

2.3.1 Microscopy

Microscopy has become over the years an indispensable tool in biological research, due its many applications and variants that allow to investigate different properties of cells, macromolecules and other organisms. Besides the traditional wide field optical microscope, which operates on white light, epifluorescence microscopy has rapidly taken over. The possibility to stain different biological components within the same cell with different fluorescent molecules has allowed to study the phase behaviour of cells and model membranes.

Conventional epi-fluorescence microscopy relies on the principle of fluorescence to obtain an image of an object, by exciting the fluorescent molecule using a light source and recording the emitted light from the sample with a camera.

A typical epi-fluorescence microscopy setup is illustrated in Fig. 2.6.

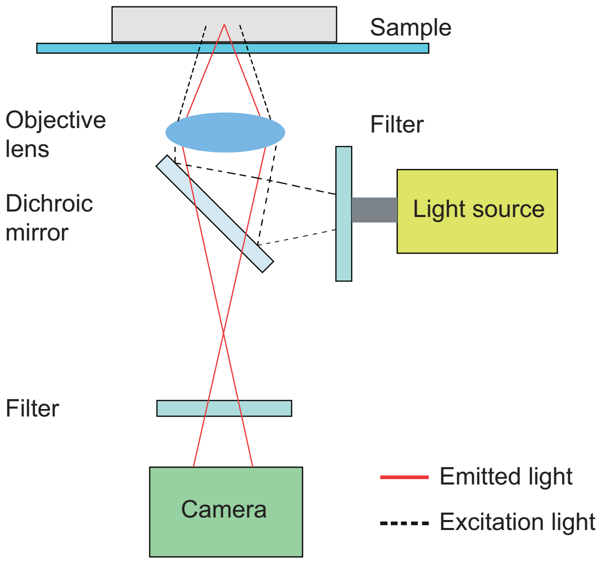

FIGURE 2.6: A schematic diagram of a conventional fluorescence microscope. The light source illuminates the sample at a specific λ_{exc} and the resulting fluorescence is filtered by the mirror and recorded by the camera.

The specimen is illuminated with light of the specific excitation wavelength. Typical light sources are xenon arc lamp or mercury-vapor; more advanced forms are high-power LEDs and lasers. The illumination light is separated from the much weaker emitted fluorescence through the use of a filter cube (which is composed by an excitation filter, a dichroic mirror and the emission filter). The filters and the dichroic beam splitter are chosen to match the spectral excitation and emission characteristics of the fluorophore used to label the specimen. In this manner, the distribution of a single fluorophore (color) is imaged at a time.

Epifluorescence microscopy is often used in combination with fluorescent probe that are incorporated within the lipid bilayer. The majority of these probes display a preferential partitioning towards a specific phase. When the membrane display phase coexistence, the probe accumulates in one of the two phases, therefore fluorescence is present only in a portion of the membrane. The resulting microscopy images show therefore one phase with fluorescence intensity and the other phase as darker areas (Fig 2.7 A).

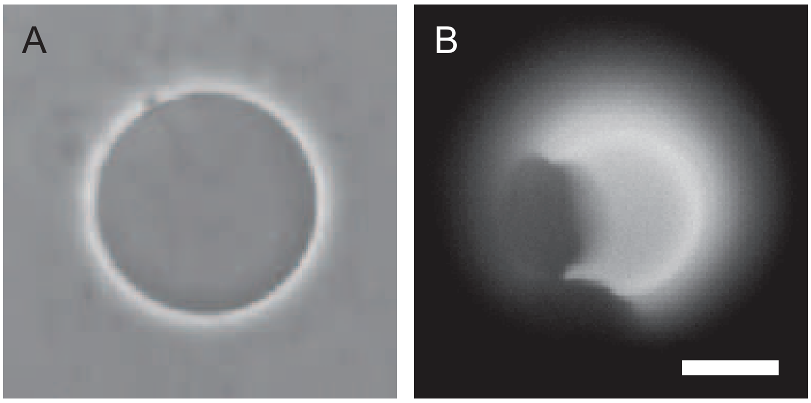

FIGURE 2.7: Typical images obtained by staining the lipid membrane with a fluorescent probe in case of vesicle displaying phase separation. (A) The membrane appears completely uniform in bright field, but when visualized using fluorescence (B) the different phases are visible due to the preferential partitioning of the dye towards one of the two phases. Scale bar 10 μm

Laser scanning confocal microscope

The confocal microscope is a variant of epi-fluorescence microscopy first developed by Minski in 1957 in order to overcome limitations of conventional microscopes in optical resolution and contrast. In epifluorescence microscope the entire specimen is flooded evenly in light from a light source. All parts of the specimen in the optical path are excited at the same time and the resulting fluorescence is detected by the microscope's photodetector or camera including a large unfocused background part.

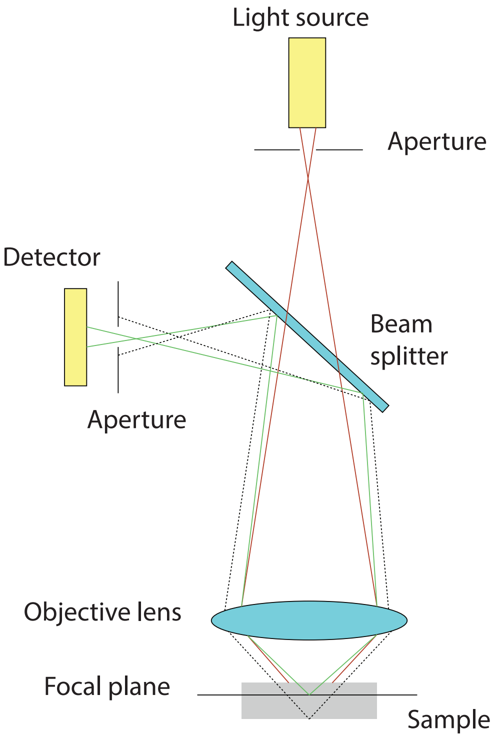

FIGURE 2.8: Simple schematic diagram of the optical pathways and basic components of a confocal microscope. Point light source is employed and generally obtained from the output of a laser coupled to an optical fiber or a laser passing through a pinhole aperture that is located in a conjugate plane with the focal point in the specimen. Dotted black line represents the emitted light from out of focal plane, which are then removed by confocal pinhole.

In contrast, a confocal microscope uses point illumination and a pinhole in an optically conjugated plane in front of the detector to eliminate out-of-focus signal – the name "confocal" stems from this configuration. Successive slices make up a 'z-stack' which can either be processed by softwares to create a 3D image, or it is merged into a 2D stack (predominately the maximum pixel intensity is taken, other common methods include using the standard deviation or summing the pixels).

Confocal microscopy provides better contrast with respect to a conventional epifluorescence microscope. Moreover, since the fluorescence intensity recorded comes only from the focal plane, it is possible to perform quantitative analysis on the fluorescent probe.

In the analysis of lipid bilayer phase behavior, confocal imaging provides indeed better contrast for visualization of domains, at the cost of direct imaging of phase coexistence. The ability to perform 3D reconstruction allows for better quantification of domains area coverage (Fig. 2.9).

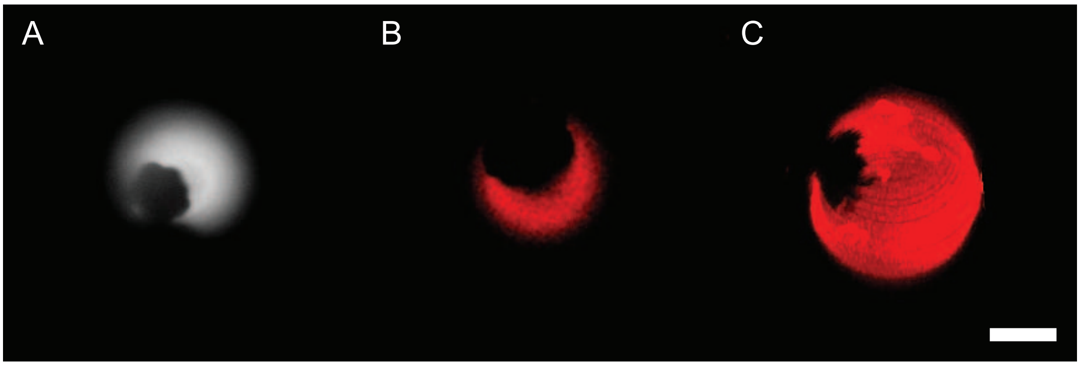

FIGURE 2.9: Comparison between conventional fluorescence microscopy and confocal imaging in visualizing phase separation of GUVs. (A) In epifluorescence the domains are clearly visible, however the contrast is low. (B) Confocal microscopy yields improved contrast, but visualization is dependent of the focal plane. (C) The possibility to reconstruct in 3D the vesicle allows for better quantification of domain area coverage. Scale bar 10 μm.

2.3.2 Laurdan and other environment-sensitive probes

Laurdan (6-Dodecanoyl-2-Dimethylaminonaphthalene) is an organic compound that has been used as a fluorescent dye, particularly in fluorescence microscopy and steady state fluorescence, due to its environment sensitive properties. In particular, Laurdan is very sensitive to membrane phase transition and alterations of membrane fluidity. It was firstly synthesized by Gregorio Weber [84] in 1979 as a probe to study specifically dipolar relaxation on cell and lipid membranes, as it is more sensitive to variation of these characteristics.

Because of its polar sensitive properties Laurdan is used extensively for probing bilayer phase transitions in the presence of membrane altering compound, such as cholesterol [85], proteins [86, 87], peptides [88, 89], and polymers [90]. These studies are performed either with steady state fluorescence, two-photon confocal microscopy or fluorescence lifetime spectroscopy by analysing the emission spectrum of the molecule under different conditions. It has also been used in vitro to investigate local packing of cells' membrane in their native state or in presence of proteins [4, 91].

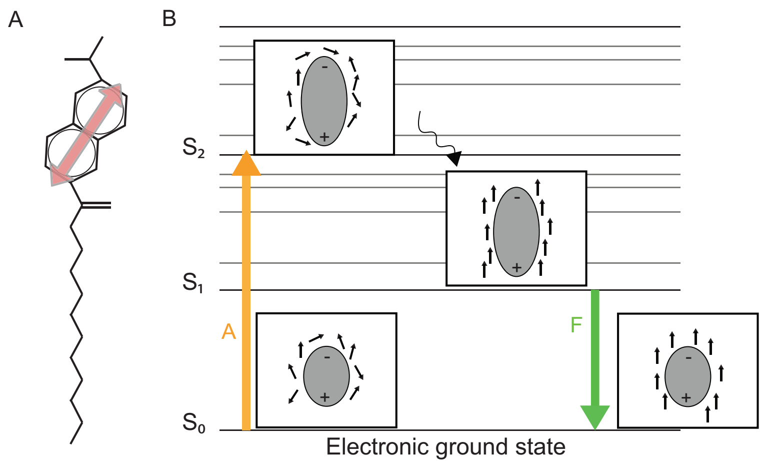

FIGURE 2.10: (A) Chemical structure of Laurdan, with dipole moment highlighted as a red arrow. (B) Jablosnki diagram for a fluorescent probe possessing dipole moment. The reorientation of the dipoles of solvent molecules changes the emission wavelength.

Structure

Laurdan is composed of a chain of lauric (12 carbon) fatty acid (hydrophobic) with a naphthalene molecule linked by an ester bond (hydrophilic) (Fig. 2.10). The fluorescent naphthalene moiety of the Laurdan molecule possesses a dipole moment due to a partial charge separation between the 2 dimethylamino and the 6-carbonyl residues. This dipole moment increases upon excitation and may cause reorientation of the surrounding solvent dipoles. The energy required for solvent reorientation decreases the excited state energy of the probe, which is reflected in a continuous red shift of the probe's emission spectrum [92].

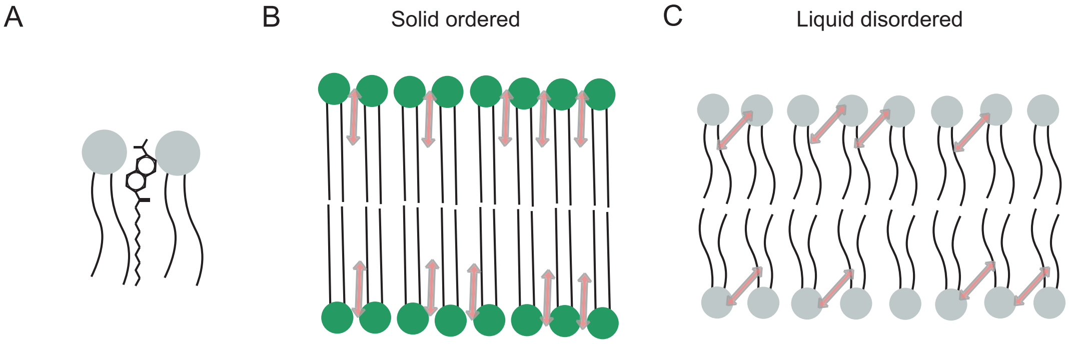

FIGURE 2.11: A) Localization of Laurdan in the bilayer. The naphtalene moiety sits at the water interface, close to the glycerol backbone of phospholipids (B) Distribution of dipole moments of Laurdan in the gel phase. The moments are generally aligned with the acyl chains, yielding low relaxation. (C) Distribution of dipole moments of Laurdan in the liquid crystalline phase. The dipole moment have a wider distribution due to the higher number of water molecules at the interface.

The excitation wavelength is generally centered around 340 – 350 nm, making the molecule most suitable for steady state and two photon, but not for conventional one photon microscopes, due to the high bleaching caused by low quantum yield.

A blue emission is typically associated with a non-polar solvent or environment [93], whereas a red shifted emission is characteristic of polar solvents [94], with maximum emission wavelength of 440 nm and 490 nm, respectively. Due to the lauric tail, Laurdan is easily solubilized within lipid bilayers, with the naphthalene moiety located towards the headgroup – water interface (Fig. 2.11).

When the lipids are in a gel-phase, the emission maximum of Laurdan is centered at 440 nm and when the lipids are in a liquid- crystalline phase the emission maximum is centered at 490 nm. This spectral shift is the result of the dipolar relaxation of Laurdan in the lipidic environment. The origin of this dipolar relaxation has been attributed to a few water molecules present in the bilayer at the level of the glycerol backbone, where the Laurdan naphthalene moiety resides [94].

The shift from blue to red emission can be therefore used to probe phase transition in single and multicomponent systems, as the emission spectra reflect packing structure of the bilayer and local hydration. Conversely, analysis of the excitation spectra and emission anisotropy are as important as the emission, since they provide additional information on the bilayer phase and fluidity.

Emission spectra

The shift of the emission maximum of Laurdan can be quantified using the general polarization (GP), defined as [92, 94]:

$$GP = \frac{I_{440} - I_{490}}{I_{440} + I_{490}} \tag{2.13}$$

where I_{440} and I_{490} are the emission intensities at 440 and 490 nm respectively, albeit other possible wavelength can be chosen [85]. Theoretically, GP can assume any values between 1 and -1, however experimentally typical values for gel phase are $\sim$ 0.5 – 0.6 and $\sim$-0.3 – -0.2 for liquid phase [93, 95–97].

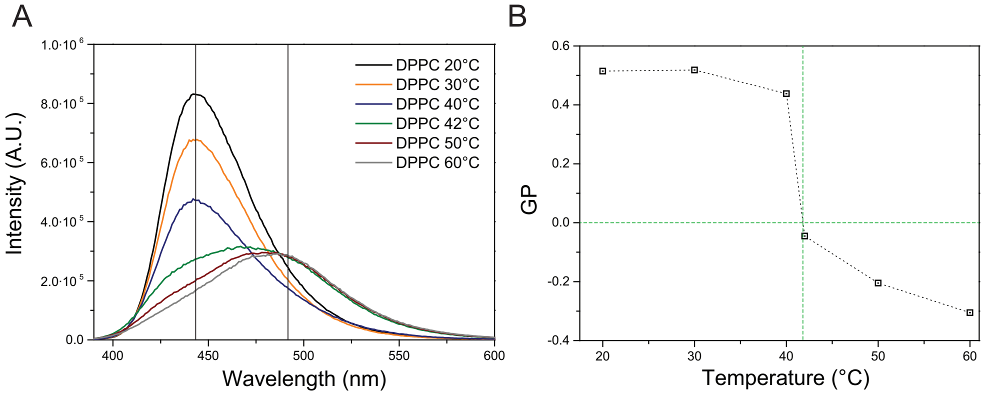

FIGURE 2.12: (A) Typical emission spectra of Laurdan for DPPC bilayer at different temperatures. The information of each spectra can be summarized in a single value using the GP definition, resulting in (B) a GP plot over temperature, which gives information on the lipid packing.

Plotting the GP values over the range of temperatures investigated (Fig 2.12) allows information on the phase behavior of the lipid bilayer, as in the case of the broadening of the GP transition in DPPC vesicles induced by the presence of cholesterol.

Gratton and Parasassi [98] firstly showed the significance in GP analysis of choice of the excitation wavelength. For a single liquid crystalline phase, excitation in the red band of absorption yields lower GP values compared to spectra obtained from λ_{exc} in the blue band (Fig. 2.13). Conversely, in case of S_o-L_α coexisting phases, excitation at ~400 nm results in a higher GP compared to excitation at ~350 nm.

In case of coexisting phase these differences can be explained by the preferential photoselection of one of the two phases under different excitation wavelengths. For a single liquid crystalline phase, Parasassi explained this phenomenon by considering the selection of energetically unfavorable configurations upon excitation in the blue band, which will result in a higher amount of blue emission of Laurdan [98].

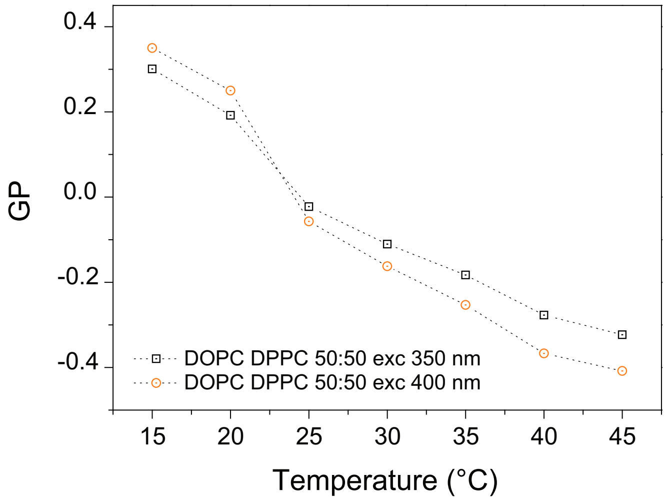

FIGURE 2.13: GP plots for DOPC:DPPC 70:30 obtained by exciting the system at 350 nm (black squares) and 400 nm (orange circles). At low temperature the system display S_o-L_α coexistence and the GP is higher for the 400 nm excitation. At high temperatures the system transitions into a homogenous liquid crystalline phase, and the excitation at 400 nm yields a more negative GP.

Another method used to analyse Laurdan emission spectra is a spectral decomposition, used firstly by Lucio [88] and subsequently used by Bacalum [99]. The principle behind this method is to represent the two emission bands of the dye using a Gaussian model for each, with center of each curve fixed at the maximum of emission for each phase (Fig. 2.14).

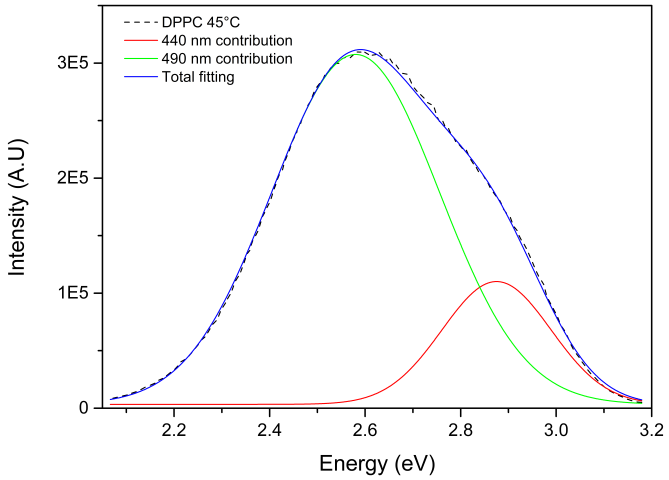

FIGURE 2.14: An example of Gaussian decomposition of Laurdan emission spectra for DPPC bilayer at 45°C. The spectra are plotted in energy rather than wavelength to obtain a better fitting. Black dotted line represents the experimental Laurdan emission spectra and blue line is the resulting fitting. Red and green line represent repsectively the 440 nm and 490 nm contribution obtained via fitting.

Using this approach allows to quantitatively measure the portion of gel and liquid contribution in the overall spectra, and characterize the effects of any molecule on the bilayer in terms of the individual components. Using this method Lucio *e al.* [88] showed that even in pure gel phase exists a fraction of 490 nm emission, that explains the experimental values lower than their theoretically counter part. This presence of liquid-phase signal in a pure gel phase membrane has been explained as being due to the presence of the relaxed excited states that are present in the bilayer at any phase.

Di-4-ANEPPDHQ

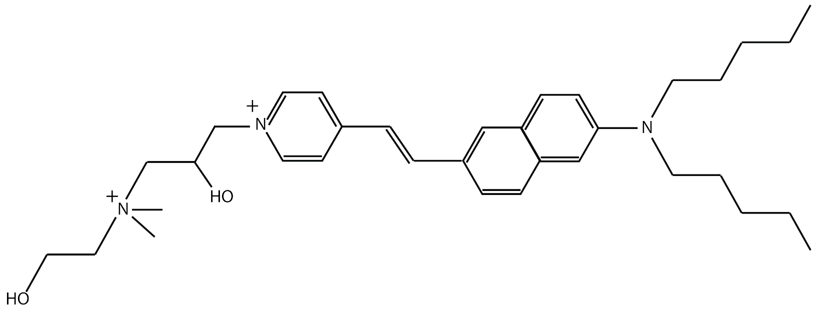

FIGURE 2.15: Chemical structure of Di-4-ANEPPDHQ.

Di-4-ANEPPDHQ (Fig. 2.15), simply referred to as Di-4, is a fluorescent probe that, like Laurdan, displays a shift in emission wavelength depending on the phase of the lipid bilayer. It is a derivative of the Di-4 family of fluorescent probes, which were developed to be sensitive to voltage changes. Di-4, however, was found to be very sensitive to lipid bilayer phase and cholesterol content, therefore has been used recently to study lipid packing in model membranes and cells [100–103].

It has a λ_{exc} in the blue region, which allows for direct imaging using a conventional single-photon confocal microscope. Moreover, it has a high fluorescence quantum efficiency and large stokes shift when bound to the membrane, but very little fluorescence when dissolved in water [104].

Much like Laurdan, Di-4-ANEPPDHQ is influenced by several environmental factors such as acyl chain saturation, charge of the head groups, presence of cholesterol, hydration of the membrane and presence of proteins.

Although both Laurdan and Di-4 are sensitive to membrane packing, their sensitivity has been found to be very different depending on the conditions. Di-4 is less sensitive to temperature phase changes than Laurdan, but it is more receptive to cholesterol content [105]. These differences in the environmental sensitivity have been attributed to the different membrane depth at which Di-4 operates. Both Laurdan and Di-4 share the same mechanism of sensing the reorientation of solvent dipoles. However, Di-4-ANEPPDHQ aligns with the acyl groups deeper in the hydrophobic core.

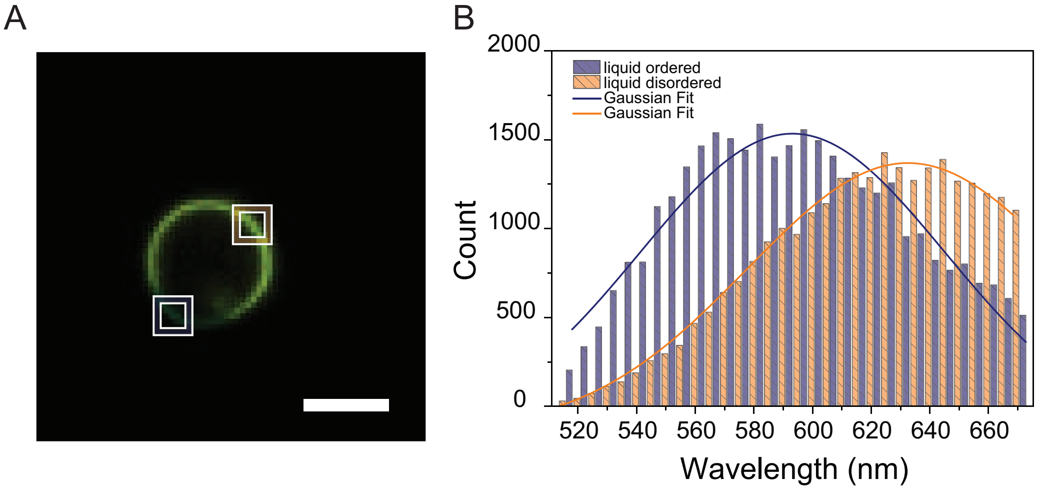

FIGURE 2.16: (A) Example of spectral imaging of DOPC:DPPC:Chol giant vesicles stained with Di-4. It is possible to simultaneously visualize L_d (orange square) and L_o (blue square) phases and to (B) extract the local emission spectra.

Using confocal microscopy it is possible to directly visualize the emission spectra of Di-4 in model membranes and to obtain information on the lipid packing, as shown in Fig 2.16. It is also possible to directly measure the general polarization, which, in case of Di-4, is defined as:

$$GP_{Di-4} = \frac{I_{560} - I_{650}}{I_{560} + I_{650}} \tag{2.14}$$

2.4 Concluding remarks

The phase behavior of the lipid bilayer arises from different properties of the membrane and involves both thermodynamics of the interaction between the molecules, as well as structural changes occuring in the bilayer. In particular, in the case of multicomponent systems the use of complementary techniques is crucial in obtaining a comprehensive picture of the interaction, as changes may occur at different length scales and affect different properties of the membrane.

The techniques presented in this chapter provide an optimal platform to study the phase behavior in model membranes and they have been extensively employed, as they allow to probe different length scales, both from a thermodynamics and structural point of view.

3

Polystyrene in a single component lipid bilayer

The increasing amount of plastic present in ocean waters has become a major issue in recent years, with increasing concerns regarding the potential hazardous effects it may have on living systems. Annual production of plastic has reached almost 300 million tons per year, of which 5 to 13 million tons are estimated to reach the ocean waters by different means [106]. Despite initially being present in large size, external environmental factors like temperature, oxidizing radiation and bacterial degradation can reduce the plastic to micrometric and nanometric fragments [107]. Objects of this scale can easily enter the food chain via digestion and there is increasing evidence of plastic micro objects found in the marine life forms [108–110].

Presence of nanoobjects have not yet being reported, however the lack of evidence can be associated with difficulties in detecting such objects rather than absence of them. Besides plastic degradation, nanometer-size polymer particles are also produced industrially for specific research and technological applications, such as imaging, sensing, and preparation of nanocomposites [111]. The presence of nanosized plastics in research laboratories, industry, and the environment raises questions on their potential toxicity.

Studies have indeed shown that plastic nanoparticles can accumulate in the tissues of living organisms and disrupt their metabolism [112, 113], and that size plays an important role in determining the accumulation of nanoparticles within the organism [113]. Moreover, the surface of plastic particles can adsorb and transport persistent organic pollutants, such as the hydrophobic polycyclic aromatic hydrocarbons, transforming the plastic particles into vehicles of toxic substances into the organism. However, a physicochemical characterization of the interaction between plastic nanoobjects and living organisms is still lacking, especially regarding the mechanisms of potential oxicity.t

The cell membrane is the first barrier encountered by any foreign object entering an organism, and therefore is the primary candidate of investigation in assessing possible toxicity of plastic nano fragments. In particular, the membrane phase behavior plays a crucial role in maintaining cell functionality, and even minute changes in membrane phase properties can result in a potential threat for the organism.

Several coarse-grained molecular simulation studies suggest that polystyrene (PS) may alter the phase behavior and properties of lipid membranes. Rossi *et al.* [114] described that the presence of PS oligomer and polymers changes the beding rigidity of POPC membranes and moreover affects the phase coexistence when cholesterol is present in the bilayer. In a continuation of the study, Bochicchio *et al.* [115] showed that PS stabilized phase coexistance in model bilayers. These results indeed point out to a potential hazard since protein functionality is partially controlled by the membrane organization.

However, experimental study on the effects of polystyrene in cell membrane and model membranes are still lacking. Jung *et al.* [116] reported that incorporation of styrene monomers into DODAB liposomes fluidifies the membrane and reduces the transition temperature of the membrane. Radlinska *et al.* [117] showed that charged polystyrene sulfonated chains of about 2500 monomers (equivalent to a radius of gyration of 10 nm) can penetrate within surfactant bilayers and alter their structural and elastic properties.

In this work we perform a systematic study on the effects of polystyrene oligomers (M_n = 500 Da) on the phase transition of unsaturared lipids. We investigated the changes in transition using small neutron scattering, differential scanning calorimetry, and Laurdan fluorescence spectra to extract information on the structure and the thermodynamics. Moreover, we directly visualized the changes on the membrane at different scale lengths using Cryo-TEM and epifluorescence microscopy.

3.1 Results and discussion

In the following paragraph we will outline the main feature of the interaction between polystyrene and single component lipid bilayer composed of DMPC, DPPC and DSPC. For clarity, we will describe in detail experimental results for only one lipid and summarize the role of chain length in the interplay. Complete experimental results for all lipids investigated can be found in Appendix A.

3.1.1 Estimation of the polymer lateral distibution

To provide for a benchmark for the area coverage of the polystyrene dispersed in the lipid bilayer, we considered first the purely two-dimensional confinement of a polymer in a fluid lipid bilayer.

Let us define σ_{PS} the number of PS oligomers per unit surface. Given the area per lipid A_l and the molar fraction f_{PS}, one has

$$\sigma_{PS} = \frac{2}{A_l} \cdot \frac{f_{PS}}{1 - f_{PS}} \tag{3.1}$$

We now consider the total area occupied by the chain monomers $S_{con} = N \cdot s_0$, estimated by considering the projected area s_0 (Fig. 3.1 A) of single monomer and by summing it over the average chain length (Fig. 3.1 B). For a single styrene monomer we considered a monomer projected area $S_0 = 19.6$ Å^2, and an average chain length $N = 5.5$. The total projected area of a single oligomer is then $S_{con} = 107.9$ Å^2, and complete two dimensional coverage by monomers occurs when $\sigma_{PS} \cdot S_{con} = 1$.

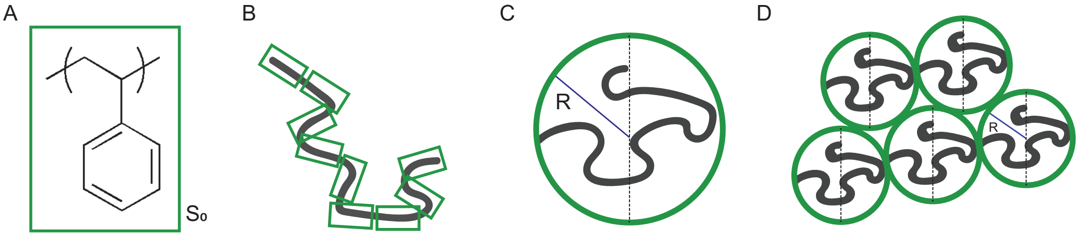

FIGURE 3.1: (A) Projected area S_0 of a single styrene monomer. (B) Projected surface of a polymer chain given as the sum of s_0 over the number of chains. (C) Projected surface of a polymer coil allowing to compute a projected coil area and thus (D) crossover surface density at which coils start to interact.

If the polymer is dissolved in a good solvent in two dimensions, the polymer will assume a coil conformation [118]. The confined polymer area is calculated by considering a two dimensional self avoiding walk (SAW), which gives a total radius R_{coil} [118, 119]:

$$R_{coil} = N^{3/4} \cdot b \tag{3.2}$$

where b is the the polymer segment which was found to be b = 3.1 Å. In this case we obtained R_{PS}^{coil} = 11 Å, which yields a projected area of the polymer of $S_{PS}^{coil} \sim$ 380 Å^2.

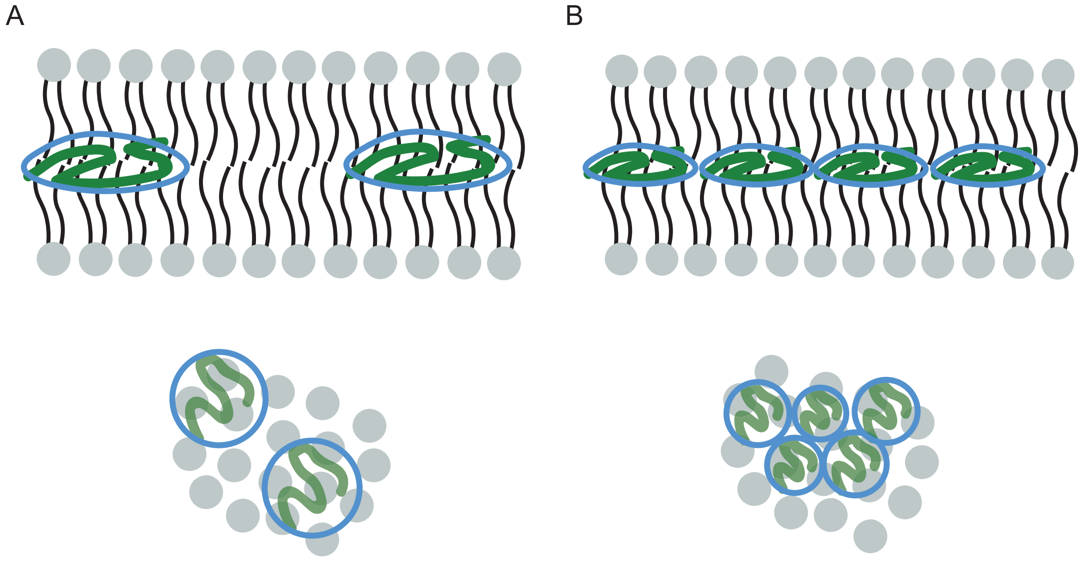

FIGURE 3.2: (A) Schematic of the polymer distribution within the lipid bilayer strictly confined in the membrane midplane below the overlapping surface density. (B) Polymer with coiled conformation confined in the membrane midplane above the overlapping density.

For $\sigma_{PS} \cdot S_{PS}^{coil} \ll 1$ the coils are in a dilute regime (Fig. 3.2 A), and do not interact. For $\sigma_{PS} \cdot S_{PS}^{coil} \gg 1$ the different oligomer coils interact strongly (Fig. 3.2 B). If they stay confined in two dimensions the coil size will be reduced as $R \simeq 1/\sigma_{PS}^{1/2}$. This will however increase the energy of the system providing for a propensity for PS to escape from two dimensional confinement.

By considering the values of area coverage obtained, we observe that already at f_{PS} = 0.1 the area coverage exceeds the overlapping density, and the coils interact, as shown in Table 3.1.

Note also that samples with $f_{PS} = 0.2$ and $f_{PS} = 0.3$ are close to or above the complete monomer coverage $\sigma_{PS} \cdot S_{con} = 1$, further supporting the existence of strong energetic reasons for escape from two-dimensional confinement.

Polystyrene fraction	Number of lipid per PS	Area fraction of polymer coil $\sigma_{PS} \cdot S_{coil}$			Area fraction of projected polymer contour $\sigma_{PS} \cdot S_{con}$		
[% mol]		DMPC	DPPC	DSPC	DMPC	DPPC	DSPC
10	9	1.41	1.34	1.32	0.40	0.38	0.38
20	4	3.17	3.01	2.98	0.90	0.86	0.85
30	2	5.43	5.16	5.10	1.54	1.47	1.45

TABLE 3.1: Calculated polystyrene area coverage for extended and coiled conformations. Dotted line represent crossing point to overlapping chains.

3.1.2 SANS

We investigated the changes of the bilayer structural parameters upon incorporation of polystyrene and change in temperature by acquiring the scattering profile of h-DPPC liposomes with 30% molar fraction of polystyrene at 25°C and 50°C. To maximize the contrast with the hydrocarbon region and minimize incoherent scattering, we used 100% D_2O as a solvent. Figure 3.3 shows scattering profiles for 25°C (Fig. 3.3 A) and 50°C (Fig. 3.3 B) for pure DPPC and DPPC:PS liposomes.

At low temperature (Fig. 3.3 A), in the gel phase, the curve for unloaded h-DPPC displays an inflection point at 0.01 Å^{-1}, followed by a linear decrease of scattering intensity in the intermediate region. The kink observed is consistent with liposomes formed via extrusion method, and the position is associated with formation using a pore size of 50 nm [120], consistent with our preparation method.

Incorporation of polymer results in suppression of the inflection point, indicating a higher polidispersity of the sample induced by inclusion of polystyrene. Moreover, scattering intensity decreases non linearly and more rapidly compared to a lipid-only system.

At 50°C (Fig. 3.3 B) in pure h-DPPC we observe the same kink at 0.01Å^{-1}, showing that crossing from the gel to the fluid phase of DPPC does not significantly affect the polydispersity of the size distribution of the liposomes. The intensity decrease linearly, albeit with smaller slope compared to 25°C, consistent with a reduction of bilayer thickness observed for gel to liquid transition [121]. For the h-DPPC/PS system the inflection is suppressed, albeit less strongly compared to the gel phase. Morevoer, the decrease of intensity is comparable to h-DPPC liposomes, suggesting similar thicknesses between the two membranes.

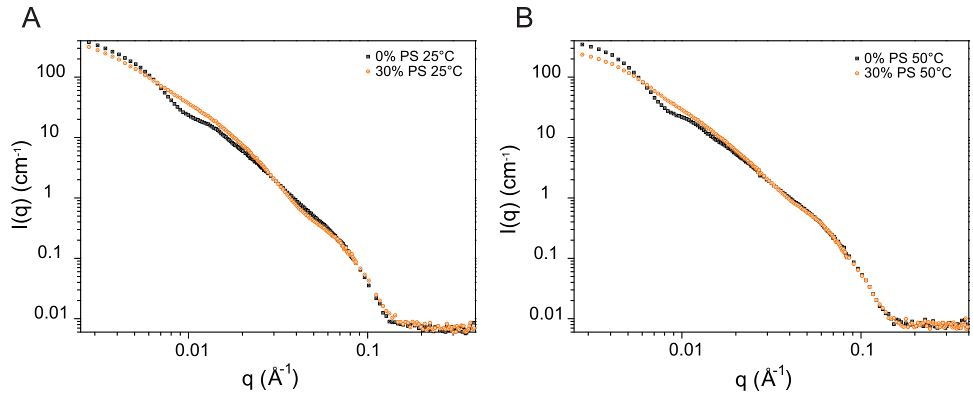

FIGURE 3.3: (A) Raw SANS data for h-DPPC (black) and h-DPPC:PS 70:30 (orange) in D_2O at 25°C. (B) Raw SANS data for h-DPPC (black) and h-DPPC:PS 70:30 (orange) in D_2O at 50°C.

We used two model-free analysis (Fig. A.1 illustrated in Chapter 2 to estimate the structural parameters of the liposomes upon increase of temperature (Table 3.2). To obtain the values for membrane thickness, the data were fitted in the $0.007 < q < 0.12$ interval, since at lower values data shows nonlinear behaviour (Fig. A.1 B).

Pure h-DPPC vescicles show a decrease of the radius of gyration of about 33.5 Å upon increase in temperature. The changes in R_g in liposomes with 30% molar fraction PS are more pronounced with a variation of $\sim$ 57.2 Å.

	25°C		50°C	
	h-DPPC	h-DPPC:PS 70:30	h-DPPC	h-DPPC:PS 70:30
R_g [Å]	407.11 ± 70.21	414.42 ± 74.66	373.61 ± 48.87	357.29 ± 36.32
d [Å]	43.36 ± 3.11	39.62 ± 3.82	39.02 ± 2.98	37.87 ± 3.72

TABLE 3.2: Bilayer structural parameters for h-DPPC and h-DPPC:PS in D_2O obtained from Guinier and Kratky-Porod analysis

The membrane thickness obtained for h-DPPC decreases with increase in temperature. A smaller thickness of the fluid phase compared to the gel phase has been reported by Nagle & Tristam-Nagle [121], from SAXS and volumetry experiments, who observed 45.7 Å at 20°C and 35.1 Å at 50°C. We observe a strong decrease in membrane thickness at low temperature when polystyrene is present. However, in the fluid phase the membrane thickness show comparable values to pure h-DPPC liposomes. Interestingly we observe that already in the gel phase the presence of polymer decreases the d_H to values comparable to h-DPPC in the fluid phase.

Contrast matching

The information obtained using only D_2O as a solvent provide scattering signal as an average of lipid/polystyrene systems, therefore it does not allow to distinguish the scattering due to the lipid bilayer from the scattering of the polymer. In order to estimate the distribution of polystyrene within the membrane, as well as the changes in the lipid bilayer structure, we acquired the scattering signal using a matched contrast for either the bilayer or the polymer (Fig. 3.4). Using a H_2O/D_2O mixture at a contrast matching ratio (Chapter 2) is possible to obtain a scattering lenght density (SLD) for the solvent equal to the SLD of the lipid molecule (Fig. 3.4 B) or of the polystyrene (Fig. 3.4 C).

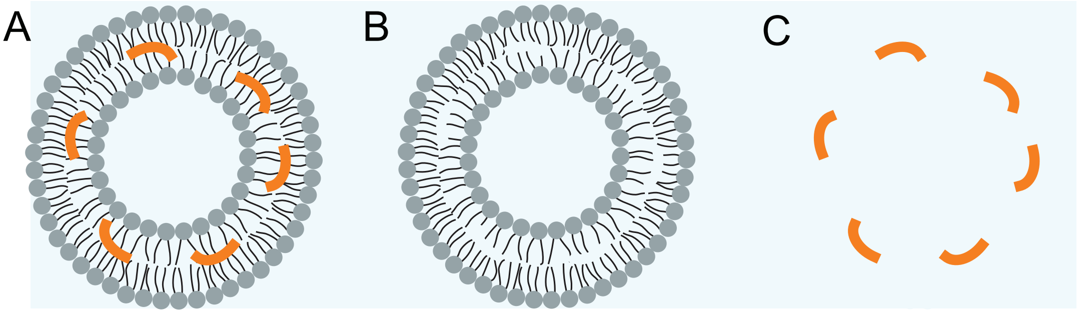

FIGURE 3.4: (A) Bilayer scattering profile for h-DPPC:PS systems in D_2O solvent. (B) Bilayer scattering profile for h-DPPC:PS liposome in polymer matching solvent. (C) Bilayer scattering profile for d62-DPPC:PS liposome in lipid matching solvent.

To obtain more information about the polymer distribution, we performed SANS experiments using d62-DPPC and produced LUVs using a solvent mixture of H_2O/D_2O 92:8 to match the SLD of the lipid molecule. The scattering for pure d62-DPPC and d62-DPPC:PS 70:30 are shown in Figure 3.5.

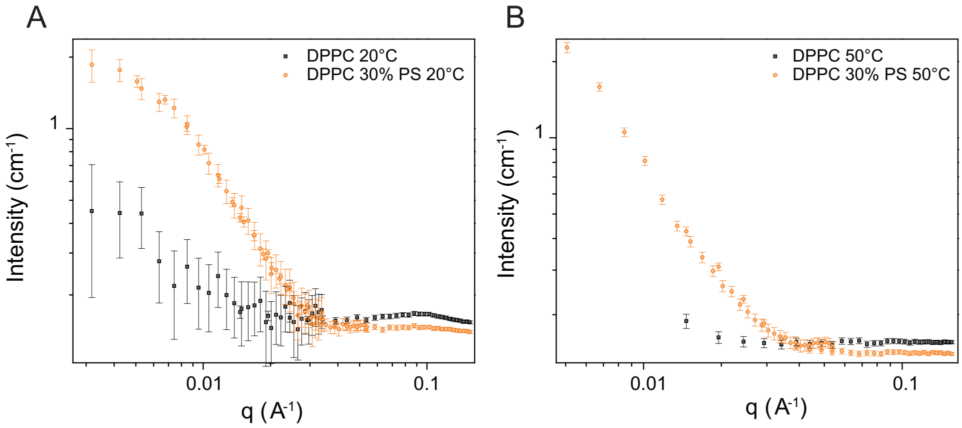

FIGURE 3.5: (A) Raw SANS data for d62-DPPC (black) and d62-DPPC:PS 70:30 (orange) in H_2O/D_2O 92:8 at 20°C. (B) Raw SANS data for d62-DPPC (black) and d62-DPPC:PS 70:30 (orange) in D_2O at 50°C in H_2O/D_2O 92:8. The solvent was chosen to match the deuterated lipid SLD, therefore the signal arises only from the polymer.

For DPPC liposomes at 20°C, we still observe a non-negligible scattering signal (Fig. 3.5 A). This arises from the choice of the SLD of the solvent chosen to match the SLD of DPPC in the fluid phase. For systems containing polystyrene we observe a strong increase of scattering intensity. The plateau located at $\sim$0.007 Å $^{-1}$ indicates a typical size of the scattering sample smaller than the liposome radius. This size could be correlated to aggregates of the polymer in the bilayer which are laterally segregated.

Increase in temperature shows complete loss of signal in the case of polymer-free liposomes, due to the better matching between the SLD of DPPC and the solvent (Fig. 3.5 B). Incorporation of polymer shows once again an increase of scattering intensity comparable to the one measured in the gel phase. Moreover, the scattering curve does not display any inflection point in the low q range. This indicates that the typical size of the polymer distribution increases with temperature, suggesting the loss of lateral segregation.

Guinier analysis of the scattering curves indeed shows that at 20°C the typical size of the polymer is 153.78 ± 12.35 Å^{-1}, much smaller than the liposome radius of 50 nm. At 50°C the lack of a plateau at low q region, due to the different q range probed in the experiments with respect to D_2O solvent, does not allow to perform any estimation on R_g (Fig. A.2).

To further estimate the distribution of the polymer within the membrane we fitted the scattering curves using the Sasview software (www.sasview.org).

For samples at 20 °C we used flat cylinder (disk) model (equations A.1 and A.2 at page 111), following the analysis performed by Dao *et al.* [122]. The model provides a good fitting (χ^2 = 2.6) of the experimental curves (Fig. 3.6 A) with estimated radius of the disk R = 254.1 ± 12.5 Å and a thickness d_{PS} = 43.15 ± 1.25 Å comparable to a typical hydrophobic thicknes of a gel DPPC bilayer [121].

In the case of 50°C, due to the lack of a plateau at low q, we fitted the curves using a polydisperse lamellar model (equations A.3 and A.4 at page 112) with a Log-normal distribution for the bilayer thickness. We obtained a good fitting (χ^2 = 1.54) of the experimental curves (Fig. 3.6 B) with a resulting thicknes of the polymer d_{PS} = 58.54 ± 3.2 Å.

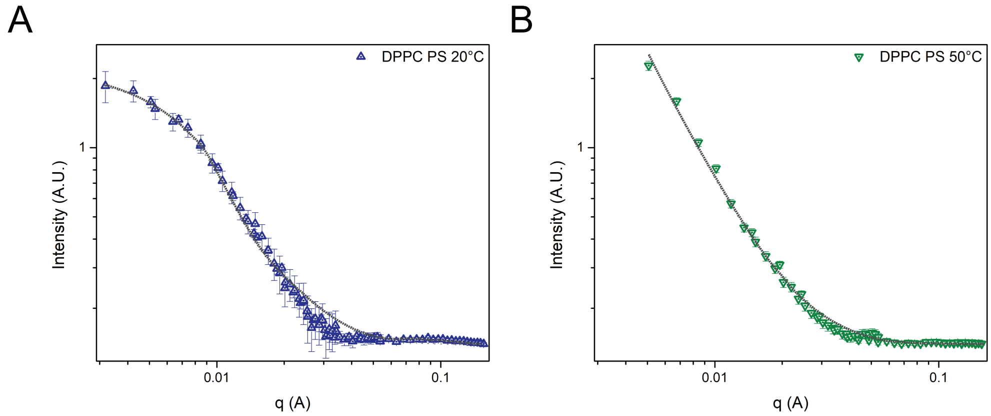

FIGURE 3.6: (A) Disk model fitting (grey) for d62-DPPC:PS 70:30 (blue) in H_2O/D_2O 92:8 at 20°C. (B) Lamellar model fitting (grey) for d62-DPPC:PS 70:30 (gren) in H_2O/D_2O 92:8 at 50°C.

The resulting fitting shows that the distribution of polystyrene within the bilayer is different between S_o and L_α phase. Specifically we observed that in the gel phase the polymer aggregates with a typical size smaller than the liposome, with a thickness smaller than the hydrophobic region thickness of the acyl chains. In the fluid phase the polymer distribution becomes uniform, suggesting the absence of aggregates or segregation. We also measured an increasing thickness of the PS for d62-DPPC:PS liposomes in the fluid phase suggesting an intercalation of the polymer in the acyl chains.

3.1.3 Cryo-TEM

Cryo-TEM allows for visualization of liposomes in their native state, with a resolution in the nanometrice length scale, and was therefore employed to directly observe any changes on the bilayer structure upon incoporation of PS and compare them with SANS scattering results. The choice of DOPC as a model system was motivated by the well established bilayer contrast provided by the lipid in model membranes, which allows for better comparison with polymer-loaded liposomes. Liposomes in gel phase (such as DPPC) observed via Cryo-TEM often present facets and non-spherical morphologies, which makes difficult a thorough analysis of the bilayer profile.

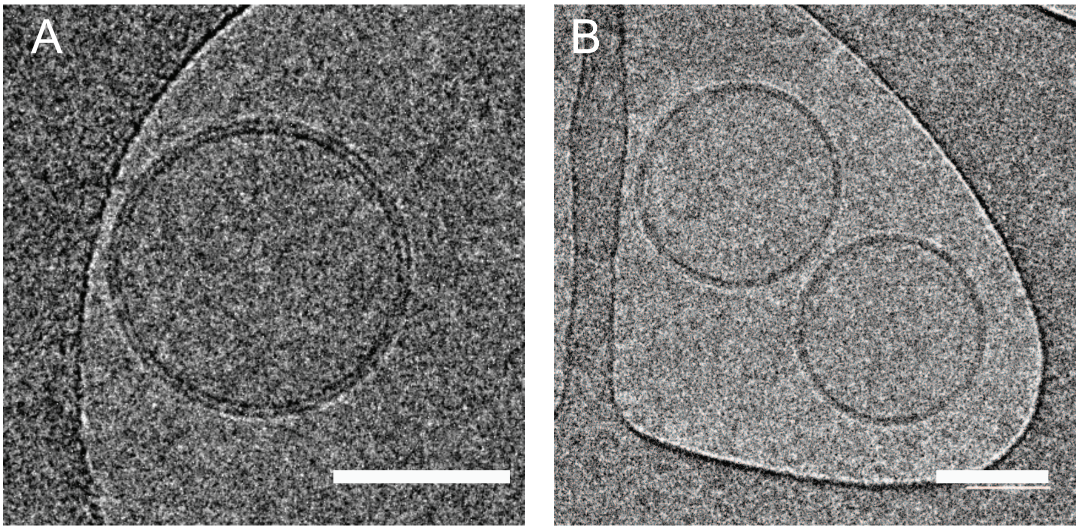

FIGURE 3.7: (A) DOPC liposome acquired via Cryo-TEM. It is possible to see the bilayer as a three stripe region. (B) Cryo-TEM picture of DOPC:PS 40:60 liposomes. The bilayer appears as a uniform gray band. Scale bar 50 nm.

Figure 3.7 shows typical DOPC liposomes and DOPC:PS liposomes prepared with f_{PS} = 0.6 acquired via electron microscopy. For pure DOPC the bilayer is clearly visible as a three stripes region, due to the different electron density between headgroups (black stripes, high density) and the acyl chain region (white stripe, low density). For DOPC:PS liposomes we observe a significant change in the contrast, as the bilayer appears as a rather uniform grey region due to the higher intensity in the acyl chain region (Fig. 3.7 B).

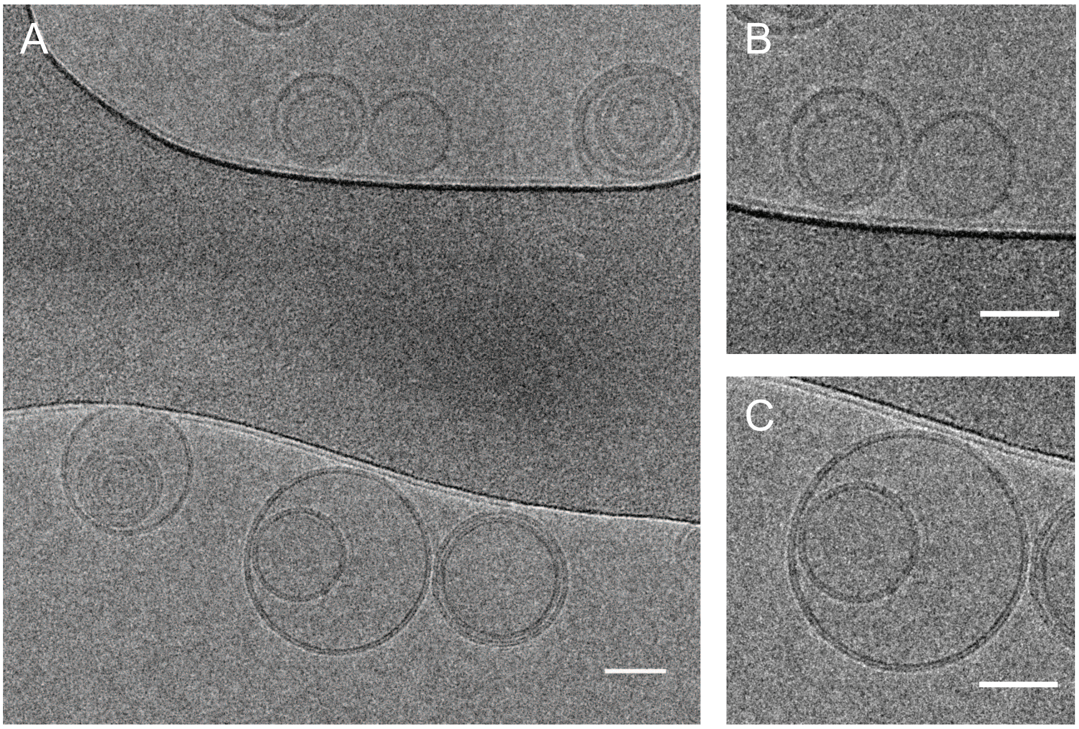

FIGURE 3.8: (A) Cryo-TEM image of a mixed sample of DOPC/DOPC:PS 40:60, showing coexistence of vesicle with well contrasted bilayer and vesicles with blurred contrast. (B) Detail of liposome displaying lower contrast. (C) Detail of liposome displaying high contrast Scale bar 50 nm.

We measured an average thickness of 5.4 ± 0.5 nm for DOPC membranes and 5.2 ± 0.5 nm for DOPC:PS systems. The two values are comparable and therefore incorporation of PS does not produce significant changes in the membrane thickness for the fluid DOPC system.

To verify that the loss of contrast is not due to de-focus of the sample or artifacts, we mixed the DOPC and DOPC:PS liposomes dispersion at 1:1 volume ratio. As shown in figure 3.8, the field of view shares liposome with contrasted bilayer and vesicles with blurred contrast. Since both vesicles are acquired at the same focus, the loss of contrast cannot be explained by any artifact and therefore must be due to the presence of the polymer within the bilayer. The changes in contrast are evident also in the intensity profiles of the two systems (Fig. 3.9). In pure DOPC liposome (Fig. 3.9 A) the three stripes region shows a sharp contrast between the headgroups and the acyl chains. Incorporation of polymer yields a reduction in the intensity of the middle layer (Fig. 3.9 B), which gives a lower contrasted bilayer and suggests that the effects are localized within the hydrophobic region.

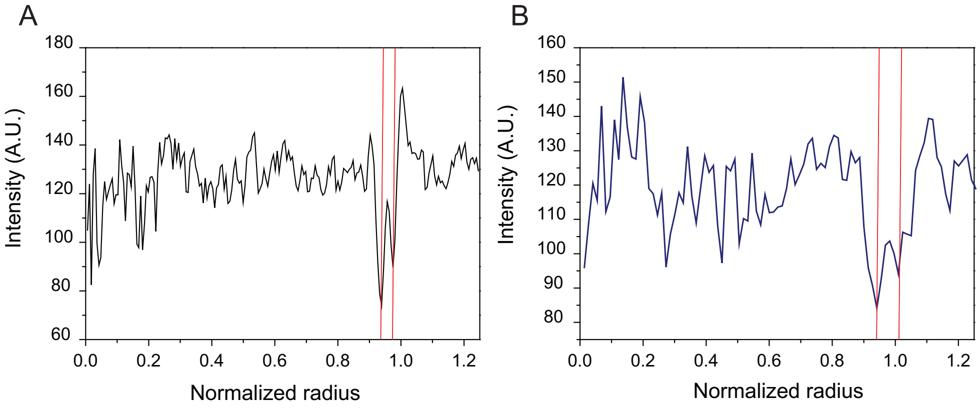

FIGURE 3.9: (A) Intensity profile of the bilayer of DOPC liposomes. We observe a sharp contrast between the two external bands and the middle one. (B) Intensity profile of the bilayer of DOPC:PS liposomes with f_{PS} = 0.6. We observe that the contrast between the two external bands and the middle one is highly reduced.

The differences in contrast can be associated with the presence of polystyrene due to the higher electron density of the benzene ring compared to the hydrocarbon chains, which would result in less intensity in the midplane region of the bilayer. Indeed, Jung *et al.* [123] showed that styrene monomers polymerized with a lipid membrane are observed as dark areas in Cryo-TEM acquisitions. Moreover, we observe that the loss of contrast is uniform over the whole vesicle membrane suggesting a homogeneous distribution of the polymer, in good agreement with our SANS scattering data for DPPC in the fluid phase.

3.1.4 Laurdan emission spectra

The typical emission spectra of Laurdan in DPPC bilayers with different percentages of polystyrene at different temperatures are shown in Fig. 3.10.

In pure DPPC we observe a shift of the emission maximum from 440 nm to 490 nm when temperature changes from 20°C to 60°C (Fig. 3.10 A). At temperatures below T_m the emission spectra is sharp and remains relatively stable and centered at 440 nm. At T_m the spectra display an equal contribution from both emission bands, as expected for a gel-to-liquid melting. For temperatures above transition, Laurdan spectra show a continuos red shift, which indicates a larger number of solvent molecules interacting with the naphtalene moiety of Laurdan.

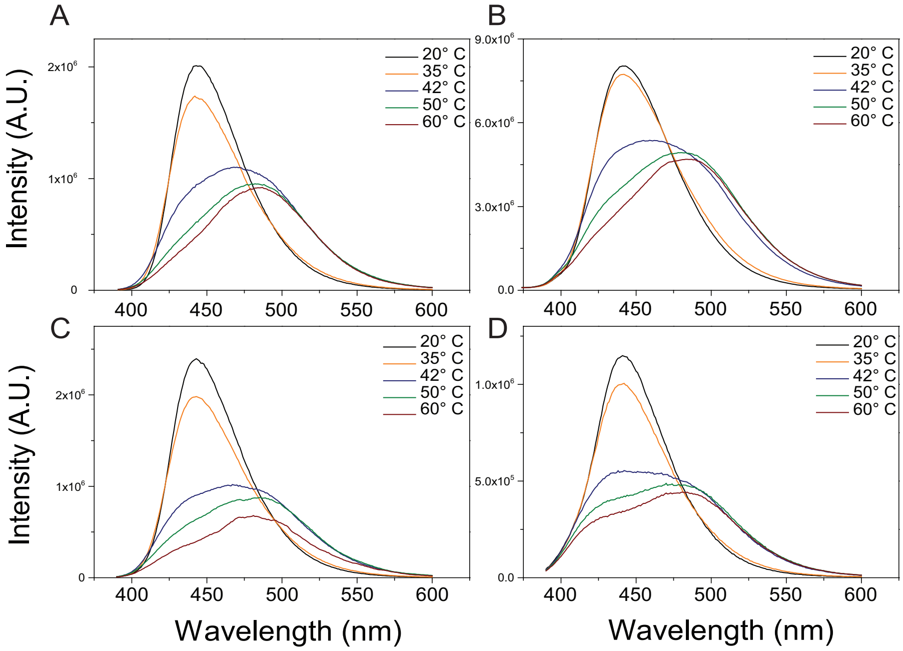

FIGURE 3.10: Comparison of emission curves of Laurdan for pure DPPC (A), DPPC:PS 90:10 (B), DPPC:PS 80:20 (C) and DPPC:PS 70:30 (D) at 20°C (black line), 35°C (orange line), 42°C(blue line), 50°C(green line) and 60°C (red line).

Upon incorporation of polystyrene in the membrane we observe a persistent contribution of the 440 nm band in the liquid phase (Fig. 3.10 B,C,D). The contribution becomes large and more persistent with increasing amount of polymer in the lipid bilayer. Interestingly this additional contribution does not seem to affect the Laurdan spectra for temperatures below T_m. Moreover, the spectra still exhibit a continuous red shift with a lower intensity of the 490 nm contribution with respect to spectra of pure bilayer. Spectra for DMPC and DSPC show a similar trend in their emission spectra (Fig. A.3 and Fig. A.4).

General polarization

To further quantify the spectral changes of Laurdan for bilayers upon interaction with polystyrene, we calculated the general polarization of the emission curves (Fig. 3.11).

For pure DPPC liposomes GP values are independent of temperature in the gel phase, with an almost constant value of 0.50 ± 0.01. With increasing temperature the GP sharply decreases, starting from T_m, to a negative value of -0.33 ± 0.01 at 60°C. Both values obtained for gel and fluid phase are consistent with previously reported GP curves for DPPC [96]. For DMPC (Fig. A.5) and DSPC (Fig. A.6) we observe a similar trend and values for S_o and L_α phases, however the transition becomes less pronounced with smaller chain length. Rather than a sharpness of the phase transition, this behavior can be ascribed to the chain length mismatch between Laurdan hydrophobic region and the acyl chain length [88].

Incorporation of the polymer in the membrane does not significantly modify the GP values in the gel phase, which slightly increase to 0.54 ± 0.01 for 30% molar fraction of polystyrene. In contrast, presence of the polymer strongly shifts the GP to more positive values, up to -0.13 ± 0.01 for the maximal polymer fraction investigated. This behavior is observed for all lipids (Fig. A.5 and Fig. A.6).

The increase of GP in presence of polystyrene is attributed to the persistence of the 440 nm band in the fluid phase, as observed in the emission spectra (Fig. 3.10 D), which is related to a less polar environment surrounding the Laurdan naphtalene moiety.

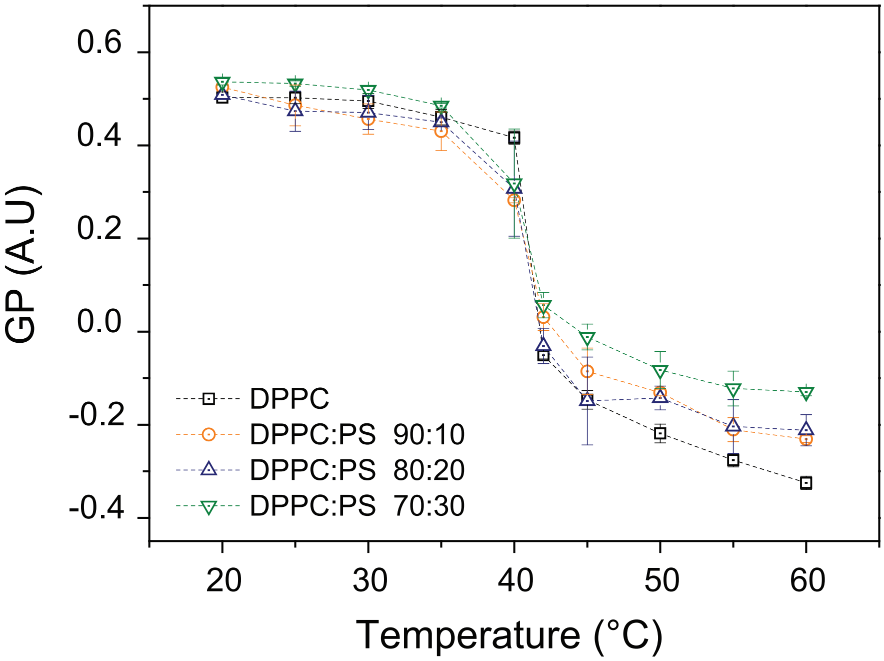

FIGURE 3.11: Variation of general polarization (GP) over temperature for multilamellar liposomes of DPPC formed in water at 0 (black squares), 10% (orange circles), 20% (blue triangles) and 30% (green inverted triangles) molar fraction of polystyrene.

Spectral decomposition

The spectral decomposition performed following the procedure described by Lucio [88] in Chapter 2 is illustrated in Figure 3.12. The relative coverage of the 440 nm contribution was plotted for each temperature to further elucidate the effects of polystyrene in the lipid bilayer. For pure DPPC we observe a relative coverage of ∼0.8 at temperatures below T_m, consistent with values reported [88]. At higher temperatures the contribution sharply decreases and remains stable at ∼0.15 in the liquid phase. The persistence of a 440 nm contribution for temperatures in the liquid phase has been attributed before to the presence of relaxed excited states.

For increasing molar fraction of polymer we observe a higher 440 nm contribution in the spectra, up to ∼0.33 for f_{PS} = 0.3. For DMPC (Fig. A.7) and DSPC (Fig. A.8), we observe similar values of high energy coverage for the gel phase, while in the fluid phase the blue band contribution strongly differs among the lipids. However, the increase of the fraction with incoporation of polystyrene shows similar trends for all three lipids. The blue band contribution remains constant upon increase of temperature following a quasi-linear dependence on the polymer fraction.

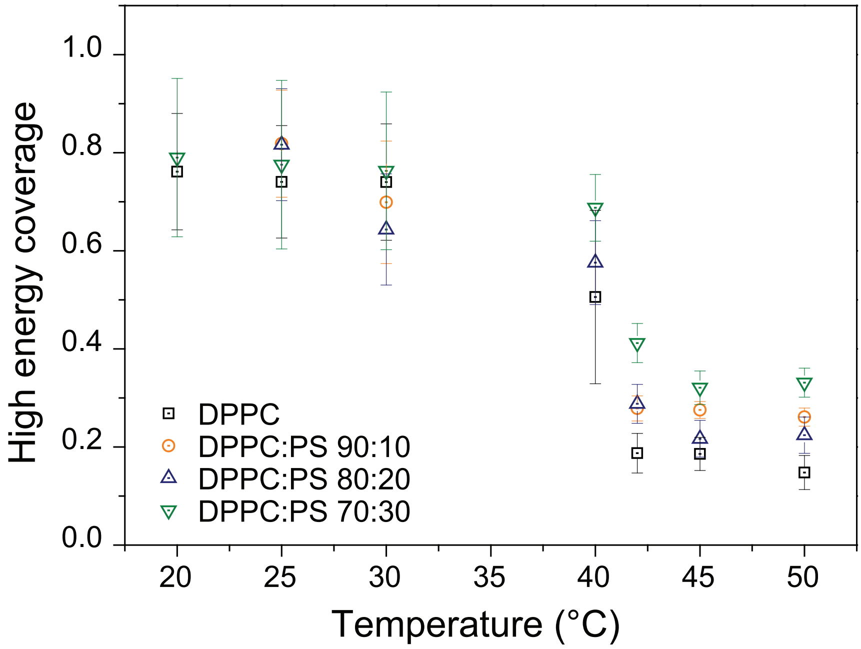

FIGURE 3.12: Area fraction of 440 nm contribution in DPPC liposomes over temperature at 0% (black squares), 10% (orange circles), 20% (blue triangles) and 30% (green inverted triangles) polystyrene molar fraction.

Chain length effect

The effects induced by polystyrene on the lipids are summarized in Figure 3.13. For both the GP variation, calculated as $GP[T_m + 15] - GP[T_m - 15]$, and 440 nm band coverage we observe a linear dependence on the polymer content, with comparable slope for all three lipids. This indicates similar behavior of the polystyrene on the Laurdan environment indipendently of the chain length.

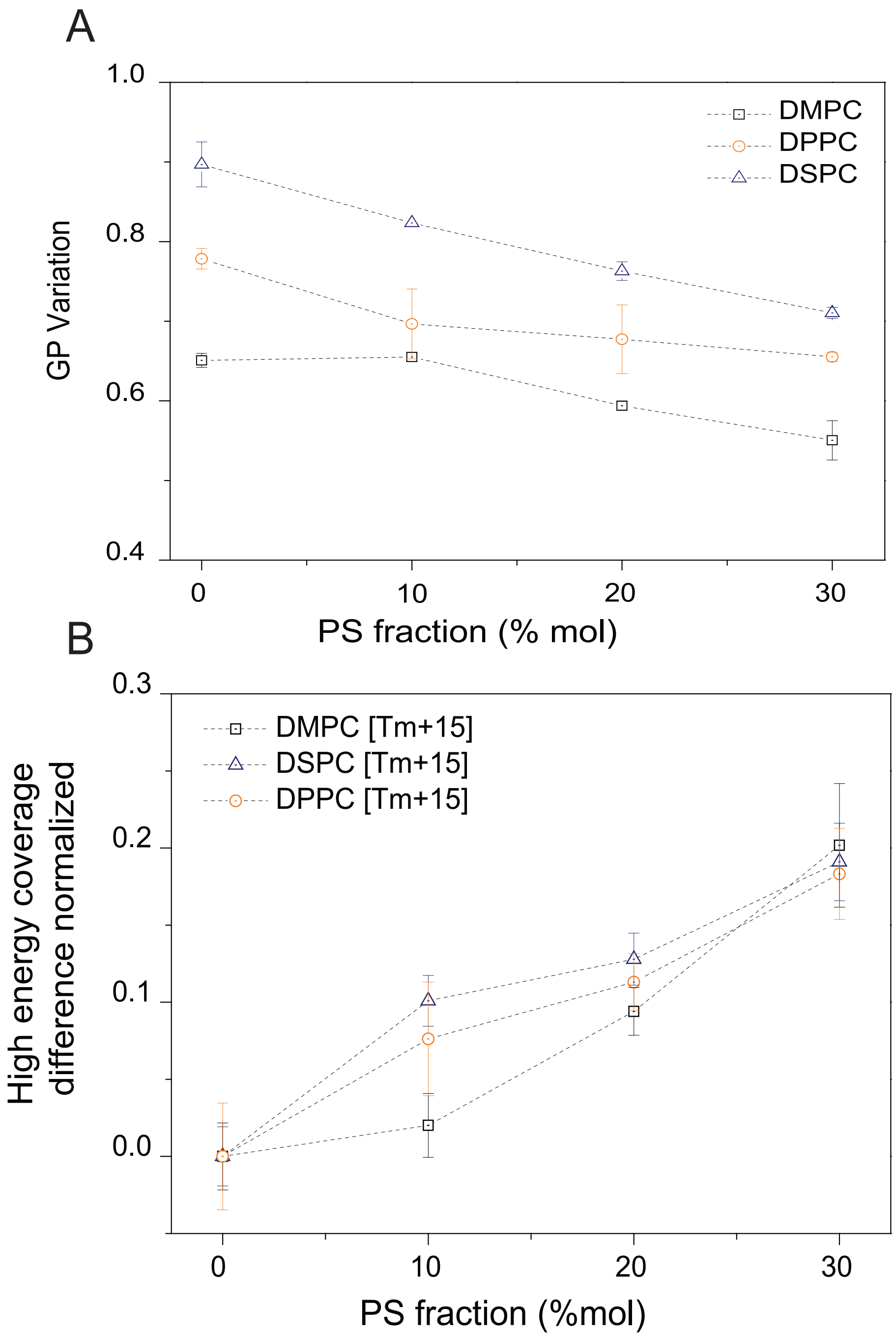

FIGURE 3.13: (A) GP variation at different molar fraction of polystyrene incorporated for DMPC (black squares), DPPC (orange circles) and DSPC (blue triangles). (B) High energy coverage for $T_m + 15$ at increasing molar fraction of polystyrene for DMPC (black squares), DPPC (orange circles) and DSPC (blue triangles).

This suggests that the distribution of the polymer within the bilayer is uniform. The creation of two distinct phases in the membrane due to polystyrene would produce a strongly non linear effect on the Laurdan emission spectra as the ratio between the two phases changes. Moreover, our results in DOPC liposomes observed in Cryo-TEM show an uniform change in the bilayer contrast (Fig. 3.8 B), rather than a laterally segregated effect. The difference in variation of GP, minimal in the gel phase and maximal for the liquid crystalline phase (Fig. A.9), indicate a different partitioning and behavior of the polymer between the S_o and L_α. These results are in good agreement with our neutron scattering curves, which shows an increase of the typical size of the polymer with increasing temperature.

Laurdan sensitivity to chain packing arises from the different number of solvent molecules at the level of the glycerol backbone. The increase in GP therefore suggests that in the liquid phase the bilayer has lower number of molecules due to the presence of polystyrene, hinting a higher packing order of the lipid molecules. However, in the case of a two dimensional confinement of the polymer in the membrane midplane, packing of the lipid would not be significantly affected as the contact between hydrophobic polymer and water molecules is minimal. Conversely, a tighter packing would arise from the presence of oligomers in the acyl chains closer to the glycerol backbone. Indeed, Pham *et al.* [124] reported that incorporation of hydrophobic monoterpenes increases the order parameter of the acyl chains, specifically the carbon groups closer to the interface. Similar results have been also found for benzyl alcohol.

In the case of polystyrene, the lack of a hydroxyl group prevents the polymer from being exposed to the water-acyl chain interface, however the observed shift in GP, indicative of a higher order of the chain closer to the headgroup region, suggest that at least portion of the oligomers is present in the acyl chain rather than only in the midplane. This picture is consistent with neutron scattering results reported by Richter *et al.* [125] in case of styrene monomers interacting with DMPC vesicle, where the distribution of the monomers was found to be a coexistence of molecules highly segregated in the midplane and molecules aligned with the hydrocarbon tails.

3.1.5 DSC

Differential scanning calorimetry thermographs are shown in Fig 3.14. For DPPC bilayers we observe a sharp transition peak centered at 41.8 ± 0.2 °C and a broad pretransition peak at ∼36°C, well in agreement with data from literature [20]. With increasing amount of polystyrene incorporated the transition temperature slightly decreases, to a final value of 40.8 ± 0.4 °C for 30% polymer molar fraction. The peak also significantly decreases in intensity and broadens, suggesting a loss in enthalpy and cooperativity. Calculations of ΔH of the transition yields a value of 38.5 ± 0.6 kJ$\cdot$ mol^{-1} for pure DPPC, consistent with previously reported data [20]. Incorporation of polymer within the bilayer results in a decrease of enthalpy and cooperativity with increase of polystyrene amount, as shown in Table 3.3.

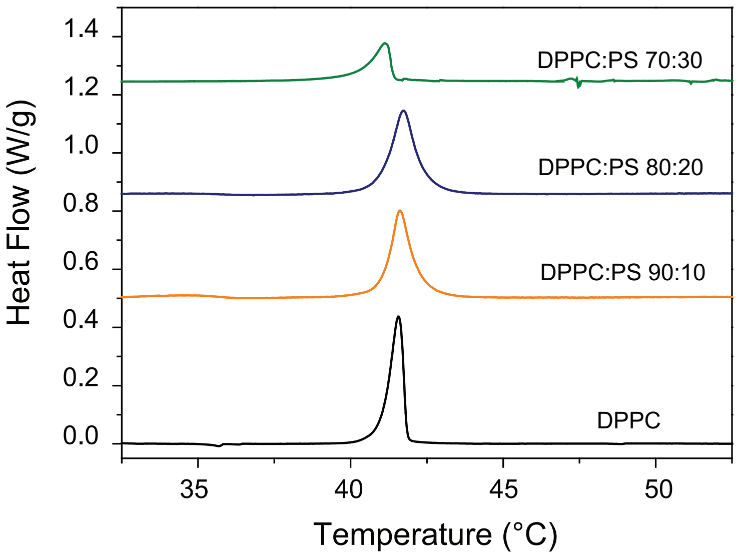

FIGURE 3.14: DSC thermographs of DPPC liposomes containing increasing amount of polystyrene. Each curve represents the second thermographic signal from the full run experiment.

In particular we observe a linear decrease of ΔH and increase of $T_{1/2}$ with respect to polymer content (Table A.1 and A.2), whereas T_m does not vary significantly. Our results differ significantly from the trend reported by Jung for DODAB vesicle contaning $\sim$ 60% molar fraction of styrene monomers [116]. For styrene it was indeed reported that transition temperature would strongly decrease, whereas the enthalpic contribution would be only slightly diminished. However, the trend we observe for polystyrene oligomers is in agreement with the variation of T_m observed for DPPC bilayers containing hydrophobic molecules [126, 127].

Polystyrene fraction [% mol]	ΔH kJ$\cdot$ mol^{-1}	T_m °C	$T_{1/2}$ °C
0	38.5 ± 0.7	41.8 ± 0.2	0.27 ± 0.01
10	30.7 ± 3.8	41.5 ± 0.4	0.29 ± 0.01
20	27.9 ± 1.1	41.2 ± 0.3	0.45 ± 0.01
30	25.1 ± 0.9	40.8 ± 0.4	0.66 ± 0.01

TABLE 3.3: Calculated ΔH, T_m and $T_{1/2}$ for DPPC with increasing molar fractions of polystyrene.

The variation of the thermodynamic parameters is observed for all lipid investigated. Changes of T_m are independent of acyl chain length, as shown in Figure 3.15

B. We observe a strong dependence on the chain length for the variations in the enthalpic contribution, DMPC and DPPC showing smaller variation in ΔH compared to DSPC (Fig. 3.15 B).

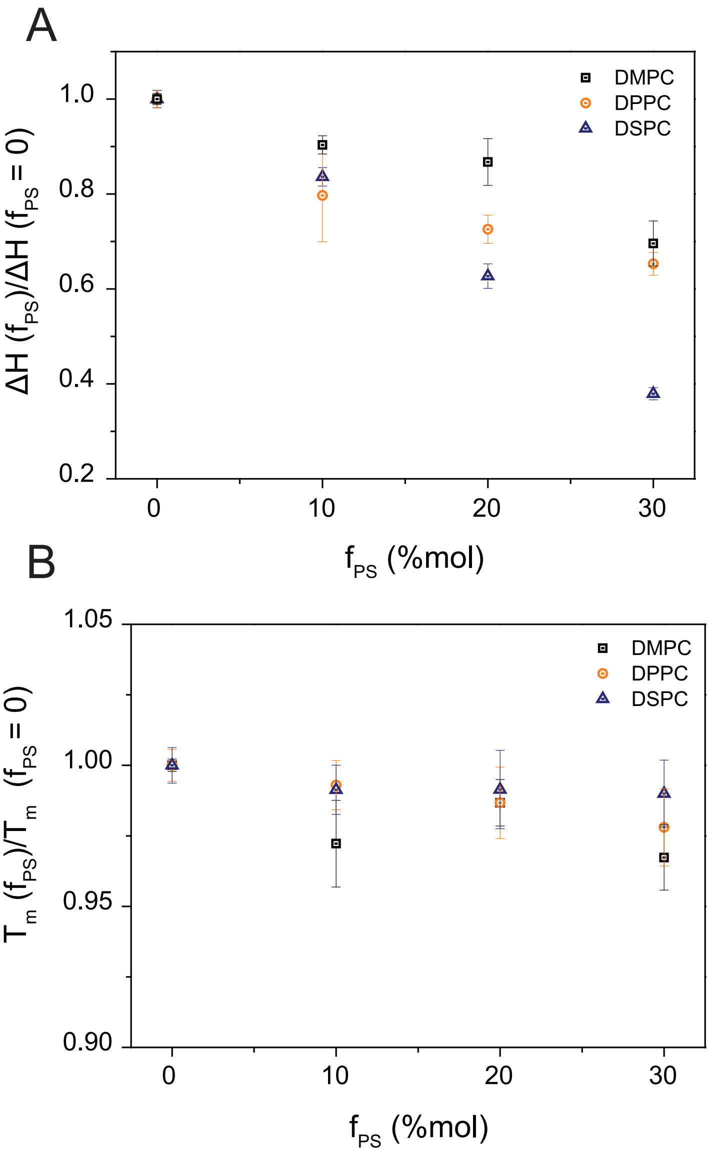

FIGURE 3.15: (A) $\Delta H(f_{PS})/\Delta H(f_{PS}=0)$ calculated from DSC thermographs for DMPC (black squares), DPPC (orange circles) and DSPC (blue triangles). (B) $T_m(f_{PS})/T_m(f_{PS}=0)$ calculated from DSC thermographs for DMPC (black squares), DPPC (orange circles) and DSPC (blue triangles). Each data point is the average of 2 samples over 3 heating/cooling cycles.

We attempted to quantify the differences between different chain lengths using a simple descriptive model [128], for which the enthalpy ΔH for an unsaturated lipid gel-to-liquid transition can be described as:

$$\Delta H = A(n-10) \tag{3.3}$$

where A is the enthalpic contribution of acyl chain pair and n is the acyl chain length. This model, despite minimal, describes well the energy of transition in terms of chain length. We fitted the enthalpies for pure lipid system from our experimental DSC thermographs and obtained a value for A of 6.2 $\pm$ 0.4 kJ$\cdot$ mol^{-1}, in agreement with values found by Matsuki *et al.* [128].

We assume here that the incorporation of polystyrene changes the individual contribution A of a single acyl pair by a factor k. We can then describe the enthalpy of a lipid bilayer containing polystyrene with:

$$\Delta H = A(1 - k \cdot f_{PS})(n - 10) \tag{3.4}$$

where f_{PS} is the molar fraction of polymer within the membrane. The obtained values for the interaction parameter k shows an apporixmately linear dependence on the bilayer thickness (Fig 3.16) of each lipid in the fluid phase [24], indicating that changes in enthalpic contribution correlate well with perturbations propagating through the whole membrane. Other quantities such as area per lipid and chain length correlate poorly with k.

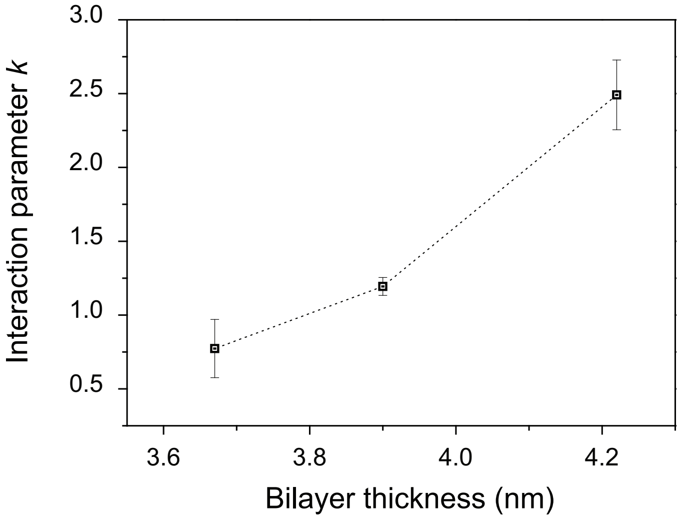

FIGURE 3.16: Variation of interaction parameter k over bilayer thickness.

Although differences on the variation on the chain length cannot yet be fully explained, the overall trend of depression of the melting temperature and broadening of the transition are consistent with some of the trends reported for hydrophobe/lipid bilayer interactions. Wolka *et al.* [129] and Rolland *et al.* [126] reported that incorporation of penetration enhancers reduce the transition temperature of DPPC to 40°C at 10% molar fraction of molecule, as well as a significant increase in the width of the transition peak. Similar results have been found for membrane containing flavonoids, with increasing hydrophobicity of the molecule producing a stronger effect [130, 131]. Borsacchio *et al.* also reported similar behavior for incorporation of pheromones in DOPC bilayers [132].

The majority of strong effects reported show a significant drop in T_m and/or ΔH at relatively small fraction of hydrophobes. Our calorimetric results instead show only strong effects on the enthalpy of the transition, but not for temperature, which is the primary effect to be expected for a bilayer containing hydrophobic contaminants. However, the strong effects reported appear for single molecules of small molecular weight ($<$ 300 Da). Indeed, Abboud *et al.* [133] reported that incorporation of hydrophobes of higher molar mass ($\sim$ 400 Da) results in a smaller depression in the T_m of DPPC liposomes. The size of the molecule has also been reported to play a role in the magnitude of the changes induced by hydrophobic molecules [134, 135].

Our SANS experiments show that polystyrene in the gel phase partially aggregates into larger structures partially confined in the bilayer midplane. This would greatly inhibit the penetration level of the oligomers in the S_o phase thus explaining the small decrease in transition temperature observed. We can therefore partially ascribe the differences in magnitude between our experimental data and the trends reported for other hydrophobes to the higher molecular weight and chain structure of the oligomer we utilized compared to smaller single molecules for which strong effects have been observed.

3.1.6 GUV

Giant unilamellar vesicles (GUVs) of DMPC and DMPC:PS (Fig. 3.17), with f_{PS} = 0.3, at low temperature (20°C) display a homogenous phase characterized by facets and corrugations, a morphology already attributed to giant vesicles in the S_o phase [136, 137]. At 25 °C, close to transition temperature of DMPC ($T_m^{DMPC} \sim$ 24.5 °C) we observe for both systems the appearance of phase separation, characterized by dark domains with no detectable fluorescence due to the partinioning of the fluorescent probe [65, 138]. This is consistent with observation previously reported for membranes close to transition temperature [139]. However, in our observations the phase coexistence persists at higher temperature, albeit with lower area coverage of S_o domains. Above 35°C we do not observe any domains and the membrane appears homogenously in the fluid phase.

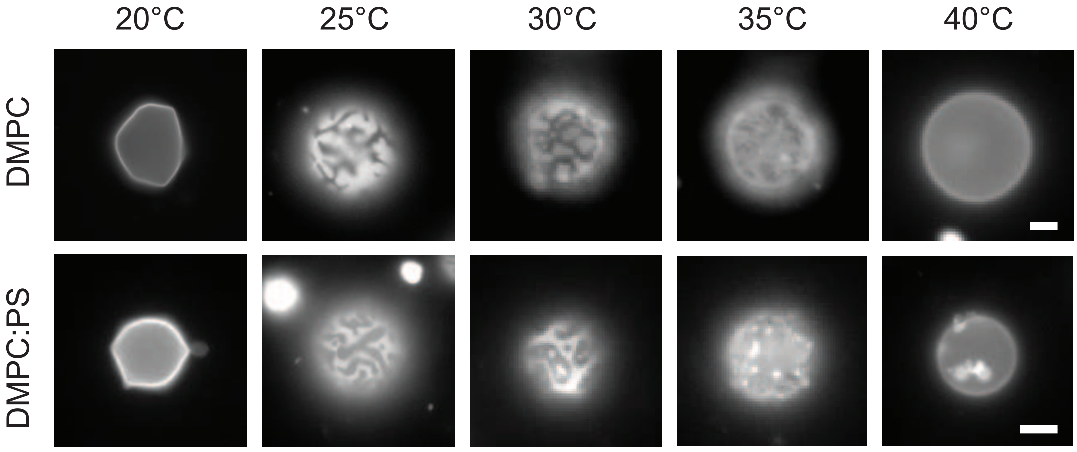

FIGURE 3.17: Epifluorescence microscopy images of GUVs composed of DMPC and DMPC:PS, with f_{PS} = 0.3, at different temperatures.

Although the wide range of temperature displaying S_o-L_α coexistence, which has not been reported before, incorporation of polystyrene does not produce any significant changes in the membrane morphology or phase behavior at any probed temperature.

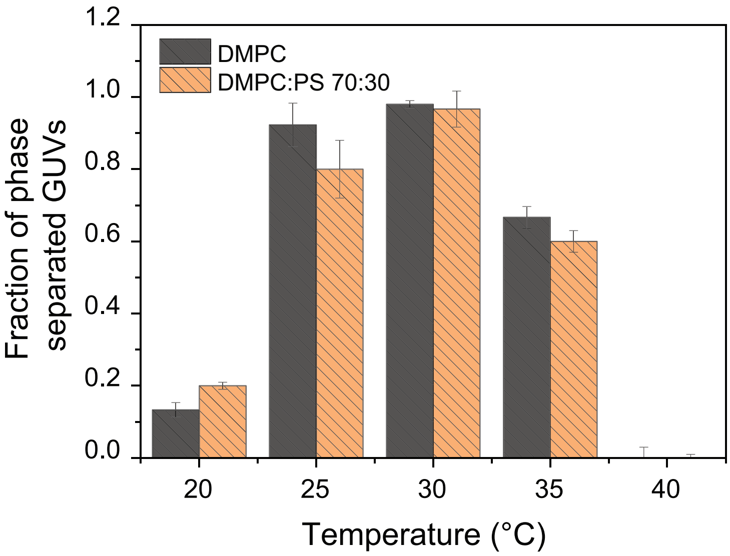

FIGURE 3.18: Summary of 30% molar fraction of polystyrene on the phase behavior of DMPC GUVs. Each data is the average and standard deviation from analysis of 50 GUVs from 2 separate samples.

Analysis of the ratio of phase separation for DMPC and DMPC:PS GUVs indeed shows that the phase coexistence region is not affected by the presence of polymer (Fig. 3.18). A possible explanation for the observed effects is that the typical time of rearrangement of the polymer distribution is much faster than for the lipid domains. Under this assumption, the polymer, upon variation of temperatures, would re-distribute across the membrane without affecting the rearrangement of the coexisting domains, thus not producing any appreciable effect on the macroscopic scale.

3.2 Conclusions

Our results indicate that low molecular weight polystyrene incorporated within the hydrophobic region of a lipid bilayer has a different distribution between the two bilayer phases. For the S_o phase polystyrene is segregated in the membrane midplane, as shown by SANS scattering curves and Laurdan emission spectra. This confinement is due to the poor solubility of the polymer in the tightly packed acyl chain region. As the bilayer melts to the L_α phase, the polymer distribution becomes more uniform, as probed by Cryo-TEM imaging, and intercalates between the acyl chains towards the water interface. The strong variation in GP in the fluid phase, as well the linear dependence of the Laurdan emission and transition enthalpy with polymer content changes strongly supports this scenario.

Incorporation of the polymer was also found to alter the gel-to-liquid main transition and the lipid packing of the membrane in the fluid phase, as indicated by Laurdan emission spectra. These changes can be ascribed to a general hydrophobe/membrane interplay where the the polymer preferentially partitions into the liquid phase, thus depressing the melting temperature of the lipid bilayer. The differences in packing between polymer-free membrane and bilayer containing polystyrene can be accounted for the changes of enthalpic contribution in the gel-liquid transition.

Our results are in good agreement with previously reported data regarding preferential partinioning of polystyrene and polymer distribution in the fluid lipid bilayer, and with the thermodynamic trends observed for other hydrophobic compounds. The alterations of the membrane phase behavior do suggest a possible disruption of cell membranes, calling for studies on more complex and biologically relevant lipid systems. A step in this direction is attempted in the next chapter.

3.3 Materials and methods

Materials

Chloroform solution of DOPC (1,2-dioleoyl-sn-glycero-3-phosphocholine, $C_{44}H_{84}NO_8P$, M_w 786.11), DSPC (1,2-Distearoyl-sn-glycero-3-phosphocholine, $C_{44}H_{88}NO_8P$, M_w 790.15), DPPC (1,2-dipalmitoyl-sn-glycero-3-phosphocholine, $C_{40}H_{80}NO_8P$, $M_w = 734.039$) and DMPC (1,2-dimyristoyl-sn-glycero-3-phosphocholine, $C_{36}H_{72}NO_8P$ $M_w = 677.933$) were purchased from Avanti Polar Lipid (Birmingham, AL). DiI Stain (1,1′-Dioctadecyl-3,3,3′,3′-

Tetramethylindocarbocyanine Perchlorate $C_{59}H_{97}ClN_2O_4$, M_w = 933.8793) was provided by ThermoFisher Scientific (Waltham, MA, USA).Sucrose ($C_{12}H_{22}O_{11}$ M_w = 342.3) and Laurdan (6-Dodecanoyl-N,N-dimethyl-2-naphthylamine) were purchased from Sigma-Aldrich (Saint-Quentin, France). Atactic polystyrene ($(C_8H_8)_n$) M_n = 500) was purchased from Polymer Source Inc. All chemicals had high purity and were used without further purification. The osmolarities of the sucrose solutions were measured with a cryoscopy osmometer Osmomat 030 (Gonotec; Berlin, Germany)

Liposomal preparation

2.5 mg of lipid in chloroform were transferred to a glass vial, and organic solvent was evaporated using an argon stream until completely dried followed by 8h of vacuum pumping. For fluorescence measurements, the lipids were stained with 1% mol Laurdan in chloroform prior to evaporation. The lipid film was then hydrated with aqueous solution (H_2O, D_2O or a H_2O/D_2O mixture) at 70°C to reach desired concentration and gently vortexed. Resulting MLV suspensions were sonicated for 15 min to disperse larger aggregates. Liposomal solutions remained stable over a period of days.

For Cryo-TEM experiments the multilamellar vesicles suspension was also extruded 21 times through a 100 nm diameter pore polycarbonate filter with an Avanti Mini-Extruder. Vesicles prepared in this way generally showed a narrow size distribution as confirmed with Dynamic Light Scattering (DLS).

Liposomes for SANS measurements were instead extruded using an Avanti Mini-Extruder. The sample was first extruded 21 times through 200 nm, subsequently 21 times through 100 nm and finally 21 times through 50 nm diameter pore polycarbonate filters.

Giant unilamellar vesicles preparation

GUVs were prepared by electroformation following the protocol introduced by Angelova [14]. Simply, 5 μl of 2 mg/mL solution of DMPC and polystyrene at the desired molar ration in chloroform. stained with 1% mol of diI, were spread on each cathode of a custom made electroformation stage. The stage was kept under vacuum for at least 1 hour to ensure complete evaporation of solvent and subsequently the lipid film was hydrated using the necessary solution (water or sucrose at different concentrations) at 55°C.

We applied a sinusoidal electric field of 1 V peak-peak intensity at 10 kHz for 1 hour while keeping the sample heated above the transition temperature. The resulting GUV suspension was kept at 20°C water bath to ensure complete stabilization of the sample. Vesicles were used on the same day of preparation.

Fluorimeter

3 mL of liposomal suspension stained with Laurdan of total concentration 3 mg/mL was placed in a quartz silica cuvette with 1 mm path length. Acquisition of Laurdan

emission spectra was performed with a Jobin Horiba FluoroMax equipped with a Peltier unit to control temperature. Excitation wavelength was set at 350 nm with a bandpass of 1 nm and emission was also recorded with slit of 1 nm. The solution was equilibrated at given temperature for 10 min before each acquisition. For each sample (n=3) we performed two cycles of heating and cooling.

General polarization (GP) was calculated using the standard expression provided by Parasassi [140]:

$$GP = \frac{I_{440} - I_{490}}{I_{440} + I_{490}} \tag{3.5}$$

where I_{440} and I_{490} are the intensity recorded at 440 nm and 490 nm respectively.

Differential Scanning Calorimetry

The calorimetry measurements were performed with high sensitivity differential scanning calorimeter (μDSC Setaram). The measuring cell was filled with the sonicated sample (MLVs at different concentrations of sucrose), while the reference cell was filled with the same sucrose solution. The temperature of the cells was changed with a constant rate (heating rate: 0.5 K·min^{-1}, cooling rate: 0.3 K·min^{-1}). The system was equilibrated $\sim$ 20 min before each heating or cooling ramp. The analysis of DSC data was performed using OriginPro 9.0 (Northampton, Ma, USA). For each sample (n=2) we performed three cycles of heating and cooling

Optical Microscopy

Imaging of GUVs labelled with DiI was performed using a confocal laser scanning microscope Nikon Eclipse TE2000-E equipped with a Nikon camera. The objective was a Nikon 60x water immersion, NA 1.2 (Nikon). GUVs samples prepared at different sugar concentrations were initially swelled by diluting the external medium with ~5% volume of pure water. The samples were kept at 5°C for at least 2 hours after preparation to ensure complete transition to gel (also called S_o) phase. Prior to experimental observation, GUVs were kept at 20°C for at least 1 hour to stabilize the temperature. 100 μL of a GUV solution were placed in a custom-made heating stage through which we could control the temperature of the sample. For each temperature, we stabilized the sample for at least 1 hour before acquiring images.

Cryo-transmission electron microscopy (Cryo-TEM)

A laboratory-built humidity-controlled vitrification system was used to prepare the samples for Cryo-TEM. Humidity was kept close to 80% for all experiments and the temperature was set at 22°C. 5 μL of the sample was placed onto a grid covered by the lacey carbon film (Ted Pella), which was rendered hydrophilic via glow discharge (Elmo, Cordouan Technologies). Excess sample was removed by blotting with filter paper and the sample grid was vitrified by rapid plunging into liquid ethane (-180°C). The grids were kept in liquid nitrogen before being transferred into a Gatan 626 Cryo-holder. Cryo-TEM imaging was performed on an FEI Tecnai G2 TEM (200 kV) under low dose conditions with an Eagle slow scan CCD camera.

Small Angle Neutron Scattering (SANS)

The samples were mounted in a 2 mm thick quartz cuvettes (Hellma). The small angle Neutron Scattering data were collected on the beam line D11 at the Institut Laue-Langevin (ILL) in Grenoble, France. The h-DPPC and h-DPPC/h-PS samples were prepared in D_2O, while d_{62}DPPC (both deuterated chains) and d_{62}-DPPC:PS samples in H_2O/D_2O to match the scattering length density of the lipids or of the polymer. The neutron wavelength resolution was $2 \cdot \Delta\lambda/\lambda = 0.1$. All scattering data were corrected for background, and incoherent scattering from 1 mm thick D_2O or H_2O solutions were used to correct for the deviation in uniformity of the detector response. The final data were converted to absolute scale. All experiments were first performed at low temperature (25 °C) and then at 50°C.

4

Changes in multi-component lipid bilayers upon incorporation of polystyrene

The phase behaviour of cell membranes is modulated by the lipid composition and cholesterol content of its lipid bilayer [65, 141]. It has been reported that the functionality of many membrane proteins highly depends on the lipid-protein interactions, and factors such as hydrophobic mismatch, membrane fluidity, lipid head group and cholesterol content can affect the protein conformation and activity [9, 142]. Moreover, proteins have been shown to preferentially partition into a specific phase of the membrane. This interplay is crucial for cell viability, pointing to potential hazardous effects of plastic nanoparticles incorporating in the cell membrane, a concern that has become over the years an important focus of research. As briefly mentioned in Chapter 3, the effects of polystyrene on the phase behaviour of lipid membranes have been investigated, using coarse grained molecular dynamics simulations. Rossi *et al.* [114] showed that incorporation of 10 % in mass of polystyrene polymers (chain length = 100) disrupts the phase behaviour of DLiPC:DPPC:Chol lipid bilayers. In particular they demonstrated that the polymer preferentially partitions in the liquid crystalline phase and uniformly distributes within it. Moreover, upon interaction with PS, the L_d-L_o coexistence was stabilized upon increase in temperature, whereas in a polymer free bilayer the temperature change would induce a transition to a homogenous liquid disordered phase. The stabilizing effect of polystyrene was further confirmed by Bochicchio *et al.* [115] via coarse grained simulations.

Despite several simulation studies performed on the subject, experimental studies on the polystyrene interaction with membranes displaying liquid-liquid coexistence are lacking. Moreover, to date no studies, theoretical or experimental, are present on the interaction with membrane possessing liquid-solid phase coexistence.

In this work we expand our investigation of the interaction of polystyrene with lipid model membranes probed in Chapter 3, employing the same experimental techniques. We incorporate small molar fractions (< 20%) of short chained PS within membranes composed of DOPC:DPPC and DOPC:DPPC:Chol of different molar ratios, and extrapolate changes in their phase behaviour using Laurdan and Di-4 spectroscopy and confocal microscopy.

4.1 Results and discussion

4.1.1 Binary mixtures

Laurdan emission spectra

Fig. 4.1 shows typical Laurdan emission spectra for DOPC:DPPC liposomes at different DPPC molar fraction containing no polymer or 10 mol % of polystyrene. We observe that for liposomes composed of 0.4 molar fraction of DPPC (Fig. 4.1 A) the spectrum at low temperature is broad with emission maximum at 440 nm. The broad peak can be associated with phase coexistence due to the presence of both liquid and gel phase in the membrane. With increasing temperature we observe a continuous red shift of the spectra, reaching a stable broad peak centered at 490 nm at 40°C, associated with fluid phase. Incorporation of polymer yields a sharper peak for low temperature (Fig. 4.1 B). Increasing temperature still displays the red shift, however we observe a shoulder centered at 440 nm which persists even in the fluid phase.

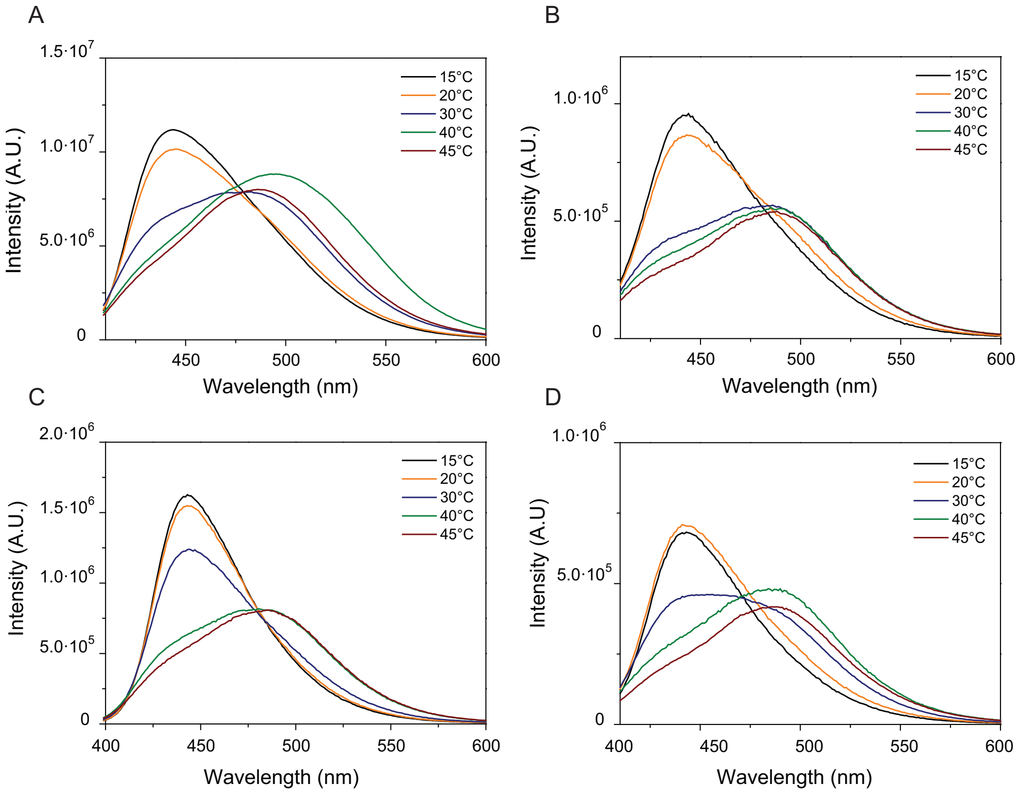

FIGURE 4.1: (A) Comparison of emission curves of Laurdan for DOPC:DPPC 60:40 MLVs at 15°C (black), 20°C (orange), 30°C (blue), 40°C (green), and 45°C (red). (B) Comparison of emission curves of Laurdan for DOPC:DPPC:PS 54:36:10 MLVs at 15°C (black), 20°C (orange), 30°C (blue), 40°C (green), and 45°C (red). (C) Comparison of emission curves of Laurdan for DOPC:DPPC 40:60 MLVs at 15°C (black), 20°C (orange), 30°C (blue), 40°C (green), and 45°C (red). (D) Comparison of emission curves of Laurdan for DOPC:DPPC:PS 36:54:10 MLVs at 15°C (black), 20°C (orange), 30°C (blue), 40°C (green), and 45°C (red).

For liposomes containing 0.6 molar fraction of DPPC the spectra appears sharper, indicating indeed higher fraction of gel phase.. Above 30°C, the spectra show the characteristic red shift in emission maxima, indicating the melting to an homogenous fluid phase. The presence of the polymer does not affect significantly the emission spectra, with the notable difference in the emission at 30°, where we observe an equal contribution between the 440 and 490 nm bands. This changes indicate a drop in miscibility temperature between S_o and L_α phases.

GP

Calculation of general polarization yield GP curves illustrated in Fig. 4.2 . For pure DOPC:DPPC liposomes we observe a broad transition, starting from a value of 0.27 ± 0.01 and 0.45 ± 0.01 at 15°C to -0.25 ± 0.02 and -0.21 ± 0.01 at 45°C for DPPC molar fraction of 0.4 and 0.6, respectively. The values at low temperature are much lower than the GP of pure DPPC bilayer [96], indicating a gel/liquid phase coexistence. The transition temperature T_m, obtained for the value at which GP = 0, is approximately 29.0 ± 1.1 °C for X_{DPPC} = 0.4 and 36.0 ± 0.5 °C for X_{DPPC} = 0.6, consistently with values of miscibility obtained from theoretical and experimental phase diagrams [143, 144]. The values of GP and curve broadness are in agreement with a membrane displaying L_d/S_o coexistence at low temperature and a homogenous liquid disordered phase above T_m.

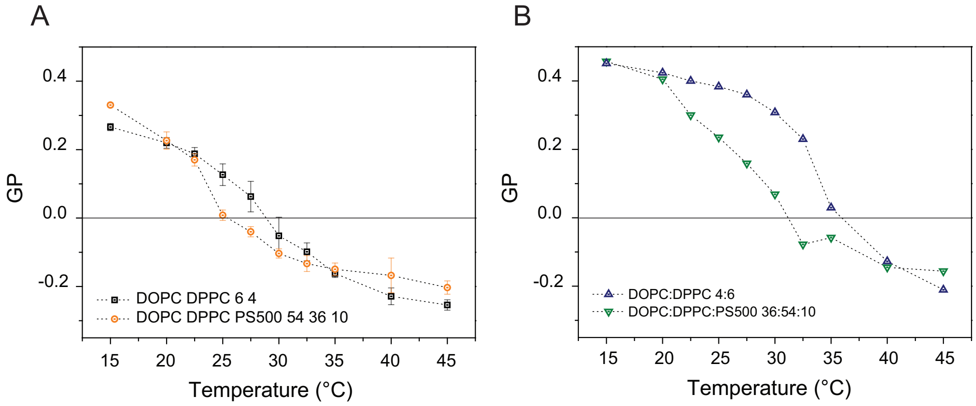

FIGURE 4.2: (A) Variation of General Polarization over temperature for multilamellar liposomes of DOPC:DPPC 60:40 (black squares) and DOPC:DPPC:PS 54:36:10 (orange circles). (B) Variation of general polarization over temperature for multilamellar liposomes of DOPC:DPPC 40:60 (blue triangles) and DOPC:DPPC:PS 36:54:10 (green inverted triangles).

In the case of systems with the same lipid ratio and additional incorporation of polystyrene, we observe significant changes in the Laurdan GP values. For 0.4 DPPC molar fraction the initial value is highly increased to 0.33 ± 0.01 at 15°C, as well as the value in the liquid crystalline phase displays higher GP, with value of 0.22 ± 0.02 at 45°C. Moreover, the transition temperature decreases to 25.6 ± 0.5 °C and the curve becomes sharper. Increasing fraction of DPPC in the membrane seems to slightly reduce this effects, as for X_{DPPC} = 0.6 the initial values of GP are comparable, while at 45°C we observe a slight increase to -0.16 ± 0.02.

The increase of GP both at low and high temperature in the presence of polystyrene suggests that the polymer strongly partitions in the L_d phase, as was indicated by the results of Chapter 3. The decrease of miscibility temperature cannot be solely explained by the contribution of PS to the GP, as a constant increase of GP would produce a higher miscibility temperature. therefore variation of T_{misc} are due to polystyrene and its ability to reduce the T_m of DPPC.

Excitation wavelength dependence

Further information on the phase coexistence of the bilayer can be obtained by probing Laurdan emission spectra at different λ_{exc}. Fig 4.3 shows the GP values for

DOPC:DPPC at different DPPC content with and without polystyrene obtained using different excitation wavelength.

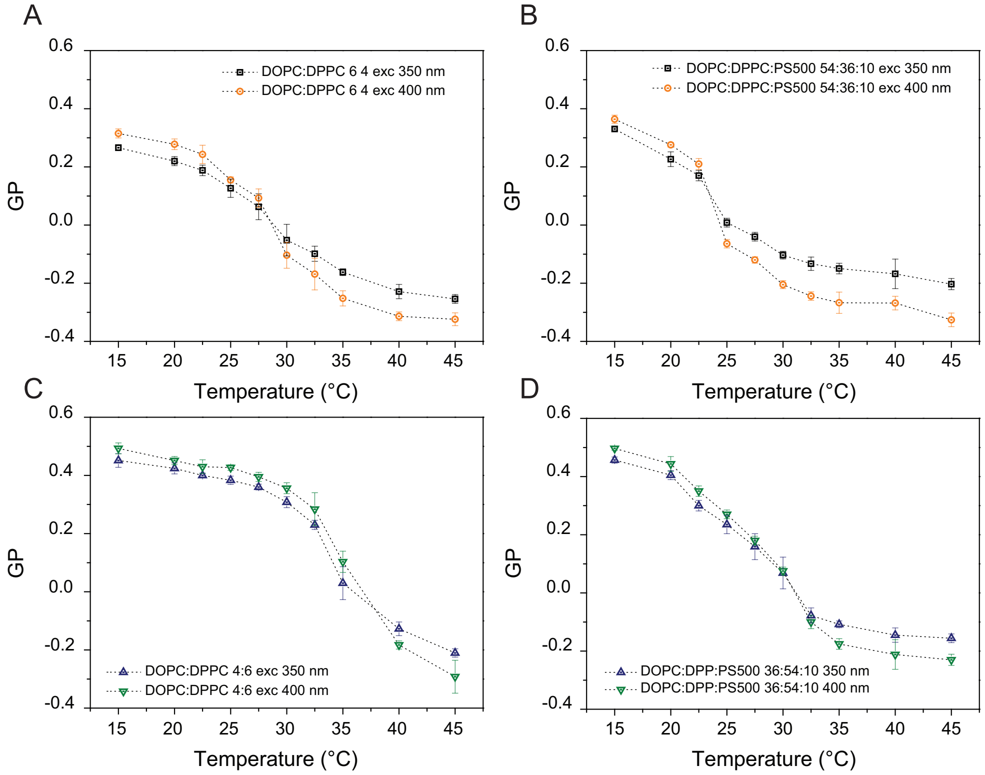

FIGURE 4.3: (A) Variation of general polarization over temperature for multilamellar liposomes of DOPC:DPPC 60:40 excited at 350 nm (black squares) and 400 nm (orange circles). (B) Variation of general polarization over temperature for multilamellar liposomes of DOPC:DPPC:PS 54:36:10 excited at 350 nm (black squares) and 400 nm (orange circles).(C) Variation of general polarization over temperature for multilamellar liposomes of DOPC:DPPC 40:60 excited at 350 nm (blue triangles) and 400 nm (green inverted triangles). (D) Variation of general polarization over temperature for multilamellar liposomes of DOPC:DPPC:PS 36:54:10 excited at 350 nm (blue triangles) and 400 nm (green inverted triangles).

For all composition we observe that the excitation at 400 nm results in a higher GP values compared to 350 nm for temperatures below melting. This has been previously reported to be a clear indication of phase coexistence between two states with different packing order [98]. Conversely, in the fluid phase, exciting in the red band would produce more negative GP values, which we observe for all systems above T_{misc}.

Incorporation of polystyrene therefore does not disrupt the phase coexistence, however the variation of GP in presence of polymer is smaller compared to DOPC:DPPC system. This variation suggests a lower amount of gel phase coexisting in the membrane, possibly as a result of the drop in T_{misc} observed.

Domains coverage in GUVS

Giant unilamellar vesicles formed of DOPC:DPPC display characteristic gel domains of irregular or hexagonal morphology (Fig. 4.4 A B), consistent with previous reported studies. For each vesicle we calculated the area fraction of S_o domains in the pure lipid case and upon incorporation of polystyrene, using the arc lenght approximation described in Appendix B.

For vesicle composed only of DOPC:DPPC we observed a total area coverage of 0.17 ± 0.03 and 0.47 ± 0.03 for DPPC content of 0.4 and 0.6, respectively. These values are in good agreement with gel fraction reported by Chen [143] and by others.

Addition of 10 mol% of polystyrene while maintaing the same DOPC:DPPC ratio shows intact domain morphology (Fig 4.4 C D). Vesicles containing PS still exhibit S_o/L_α coexistence, however the solid domain fraction is greatly reduced. Analysis of the domain coverage yielded a fraction for the solid phase of 0.077 ± 0.021 and 0.28 ± 0.06 for 60:40 and 40:60 mixtures, respectively.

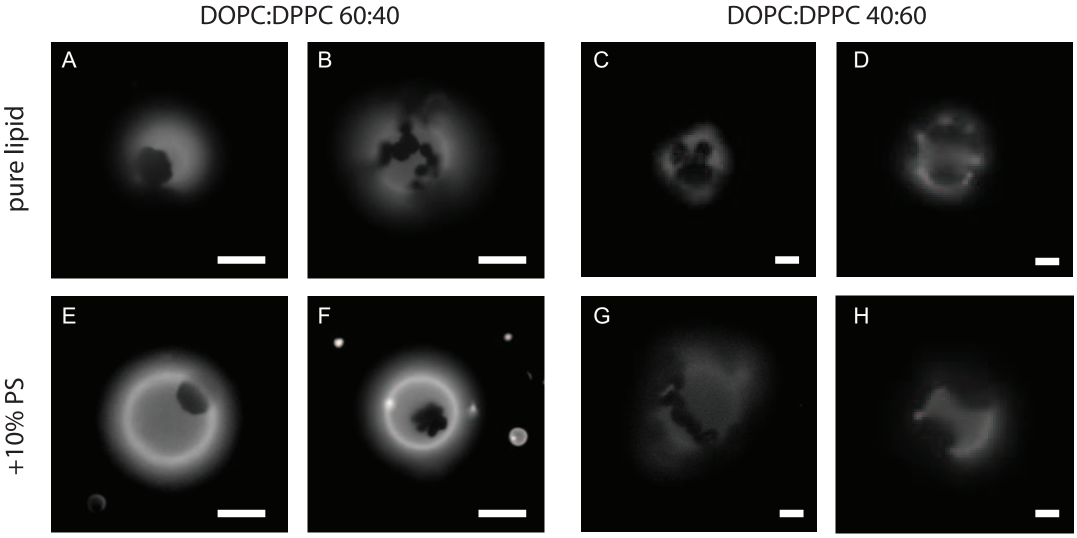

FIGURE 4.4: (A)(B) Typical DOPC:DPPC 60:40 GUVs stained with DiI. (C)(D) Typical DOPC:DPPC:PS 54:36:10 GUVs stained with DiI. (E)(F) Typical DOPC:DPPC 40:60 GUVs stained with DiI. (G)(H) Typical DOPC:DPPC:PS 36:54:10 GUVs stained with DiI. The bright area represents presence of fluorophore, which partitions in the L_α phase. Dark spots are S_o domains. Scale bar 5μm.

A reduction of gel phase domains in GUVs has been reported before by Ostroumova *et al.* [145] for DOPC:DMPC GUVs interacting with flavonoids, and the effect was found to be stronger for more hydrophobic molecules. The reduction of S_o area coverage, indicative of a depression of the melting point of the gel phase, has been commonly observed for small hydrophobic molecules incorporated within the lipid bilayer, and it has been ascribed to a preferential partitioning of the hydrophobe towards the L_α phase [146].

DOPC:DPPC phase diagram

We compared the melting temperature obtained from the Laurdan emission spectra for DOPC:DPPC liposomes with previously reported phase diagram for the binary mixture. Our result for polymer-free membranes are in good agreemnt with values of the liquidus line obtained by Chen [143] using GUVs.

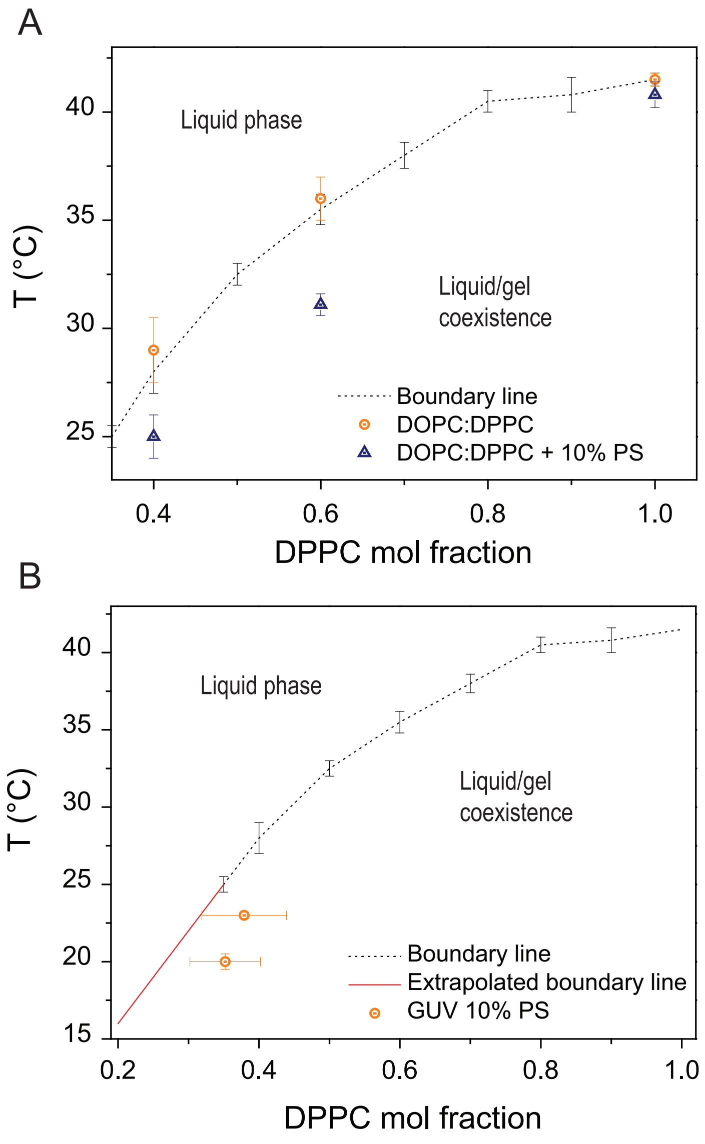

FIGURE 4.5: (A) Comparison between liquidus line points obtained via analysis of Laurdan emission spectra for DOPC:DPPC (orange) and DOPC:DPPC:PS (blue) and liquidus line reported by Chen [143]. (B) Obtained liquidus line points for DOPC:DPPC:PS obtained by area coverage of S_o domains in GUVs (orange) and liquidus line reported by Chen [143].

To compare our observations on the gel phase area coverage in GUVs, we employed the lever rule using the phase diagram proposed by Chen. The liquidus line up to T = 20°C was extrapolated from the experimental data of Chen in the range [0.2 - 0.7] of X_{DPPC}. Assuming a constant solidus line X_b = 0.95 for the considered DPPC molar fraction interval, it is possible to estimate the area fraction of gel phase using the relation:

$$f_g(T) = \frac{X_a(T) - X}{X_b(T) - X_a(T)} \tag{4.1}$$

where X is the DPPC molar fraction of the sample, and $X_a(T)$ and $X_b(T)$ are the DPPC molar fraction corresponding to a temperature T in the liquidus and solidus lines, respectively. Values of area fraction at different molar fractions of DPPC are summarized in Table 4.1, and are consistent with values previosuly reported [143].

DPPC molar fraction	Experimental S_o fraction	Theoretical fraction for gel phase of pure DPPC	Theoretical fraction for gel phase of 0.95 DPPC	S_o fraction with 10% polystyrene
0.4	0.17 ± 0.03	0.18 ± 0.01	0.20 ± 0.01	0.08 ± 0.02
0.6	0.47 ± 0.03	0.42 ± 0.01	0.47 ± 0.01	0.28 ± 0.06

TABLE 4.1: Summary of S_o area coverage for DOPC:DPPC GUVs at different composition. Each value represents average and standard deviation of two separate samples of 40 vesicles each.

The values of solid area fraction obtained with GUVs allow to estimate the tie line for 20°C in presence of 10% polysterene. By considering a constant X_b = 0.95, we obtained values for X_a^{PS} of 0.35 ± 0.05 for 20°C and 0.38 ± 0.06 for 23°C.

We compared our experimental results with a thermodynamics model for binary phase diagrams developed by Wolff *et al.* [144]. Simply, for a binary lipid mixture in a mean-field Ising model the gel-to-liquid transition can be written as:

$$\begin{aligned} \mathcal{G}^l(T,\phi_1,\phi_2,m) = &-m[h_1(T)\phi_1 + h_2(T)\phi_2] - 2Jm^2 \\ &+ (\frac{1+m}{2})ln(\frac{1+m}{2}) + (\frac{1-m}{2})ln(\frac{1-m}{2}) \end{aligned} \tag{4.2}$$

with

$$\begin{aligned} h_1(T) &= \frac{\Delta H_1}{2RT_1^2}(T - T_1) \\ h_2(T) &= \frac{\Delta H_2}{2RT_2^2}(T - T_2) \end{aligned} \tag{4.3}$$

where ϕ_1 and ϕ_2 are the area fractions of the two lipid species, J is the energy associated with the interaction between two neighboring lipids, m is a scalar order parameter restricted to interval [-1, 1], R is the gas constant, ΔH_1 and ΔH_2 are the lipid characteristic gel-to-liquid enthalpies and T_1 and T_2 their respective transition temperatures.

For DOPC:DPPC bilayers we calculated the phase diagram using values of $\Delta H^{DPPC} = 38.5$ kJ·mol^{-1} and $T_m^{DPPC} = 41.8$°C for DPPC, obtained from our DSC experiments, and $\Delta H^{DOPC} = 7.7$ kJ·mol^{-1} and $T_m^{DOPC} = -21.3$°C obtained from literature. For the cooperativity of the interaction between neighboring lipids we chose a value of J = 0.31. The theoretical model is in good agreement with our experimental data from Laurdan emission spectra and with the DOPC:DPPC phase diagram reported by Chen [143] (Fig. 4.6).

For systems containing polystyrene, we kept all model parameters constant, except for the different enthalpy and transition temperature obtained from calorimetry experiments, namely $\Delta H^{PS} = 30.7$ kJ·mol^{-1} and $T_m^{PS} = 41.5$°C, to calculate the new boundary line. The cooperativity was kept at the same value based on the measurement of $T_{1/2}$ from DSC experiments. The boundary line in presence of polystyrene indeed shows good agreement with our experimental observation. This indicates that the changes induced by the polymer in DPPC bilayers is the main driving force behind depression of the liquidus line towards lower temperature.

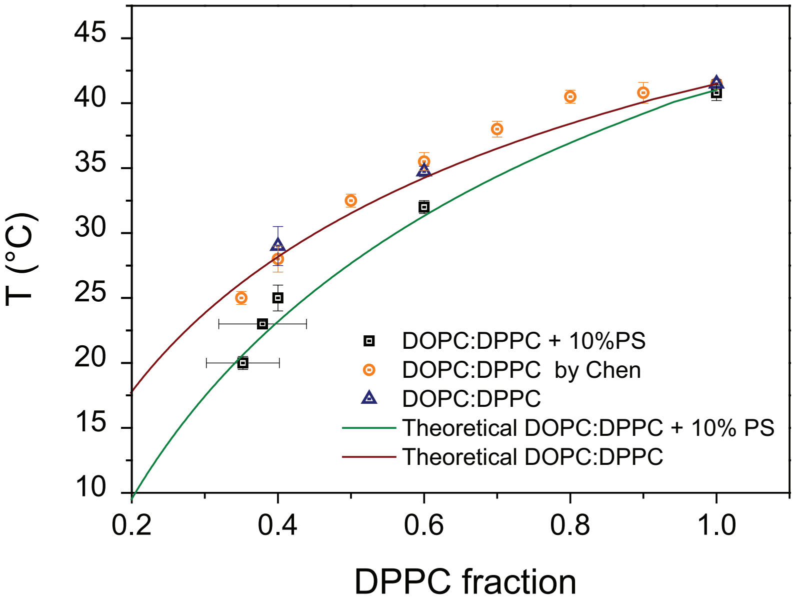

FIGURE 4.6: Comparison between experimental data point for the liquidus line obtained by Chen (orange, ref. [143]), experimental data point for DOPC:DPPC (blue triangles) and DOPC:DPPC:PS (black squares) obtained from Laurdan emission spectra, and theoretical predictions of liquid lines for DOPC:DPPC (red) and DOPC:DPPC + 10%PS (green).

4.1.2 Systems containing cholesterol

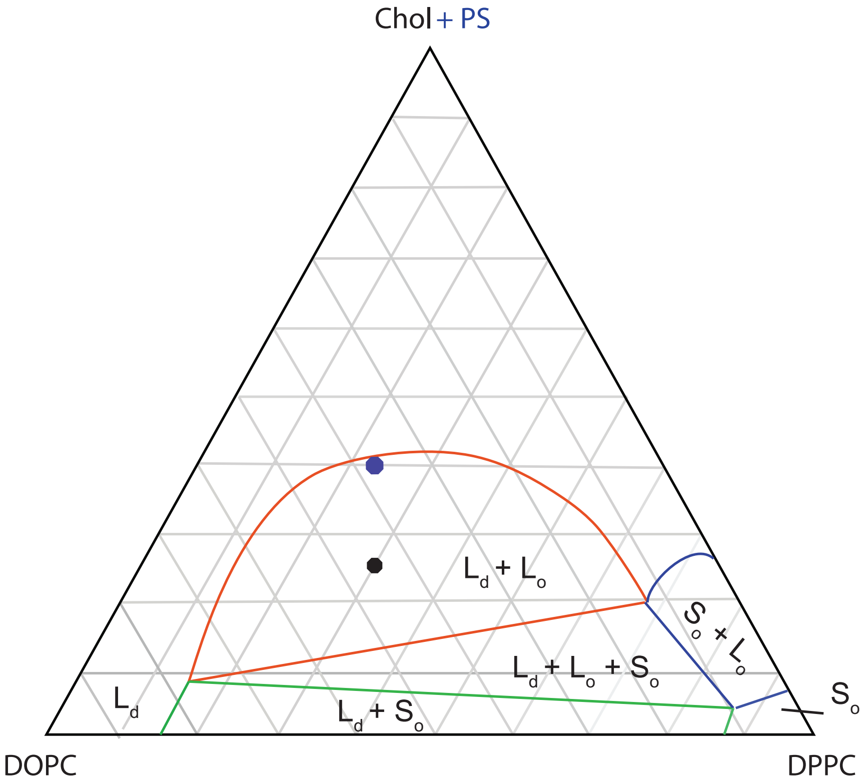

FIGURE 4.7: Position in the DOPC:DPPC:Chol phase diagram of the composition of GUVs with only cholesterol (black) and with both cholesterol and polystyrene (blue).

To investigate the variation of the phase behavior induced by polystyrene in membranes containing cholesterol, we performed confocal spectral imaging of GUV composed of DOPC:DPPC:Chol and DOPC:DPPC:Chol:PS stained with Di-4 (Fig. 4.9). Due to the different packing of the bilayer, L_o domains appear as blue and L_d domain are green. All GUVs observed display clear liquid/liquid phase coexistence with circular domains characteristic of L_o phase. The presence of visible domains indicates that cholesterol and polystyrene act differently on the phase behavior, as for the chosen lipid composition the liquid-liquid coexistence would approach the critical point and the phase separation would be inhibited (Fig. 4.7).

We calculated the number of domains in GUVs 1 hour and 36 hours after preparation to evaluate the coarsening and coalescence of domains, which are related to the mobility of the lipids in their respective phase. Domain coarsening is expected to be relatively fast, in the order of minutes, as probed by many studies on supported bilayers and GUVs. However, beyond the diffusion limit, L_o domains can still coalesce, albeit at a smaller rate.

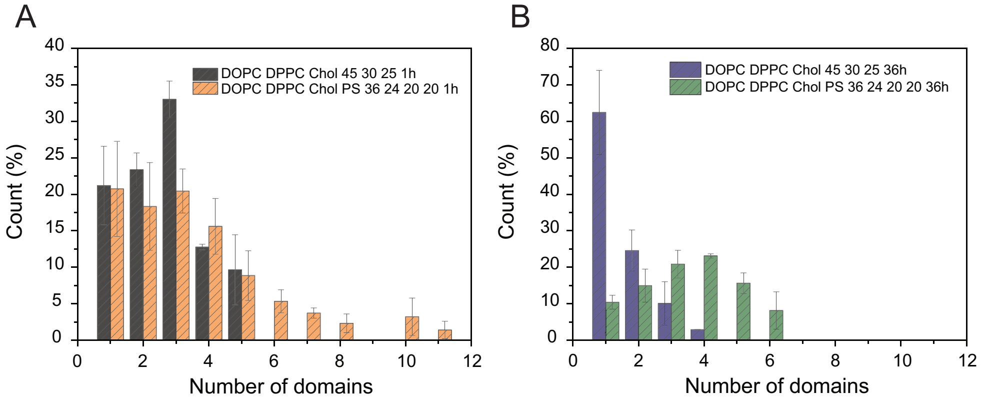

FIGURE 4.8: (A) Statistical distribution of number of domains in GUVs composed of DOPC:DPPC:Chol 45:30:25 (black) and DOPC:DPPC:Chol:PS 36:24:20:20 (orange) after 1 hour of stabilization. (B) Statistical distribution of number of domains in GUVs composed of DOPC:DPPC:Chol 45:30:25 (blue) and DOPC:DPPC:Chol:PS 36:24:20:20 (green) after 36 hour of stabilization.

In the case of DOPC:DPPC:Chol, we observe that the number of L_o domains steadily decreases over a large period of time, favoring a complete phase separated membrane. Due to the time scale, this effect is associated with coalescence rather than growth or coarsening.

Incorporation of polystyrene significantly changes the domains behavior, as observed in Figure 4.9 B. Already after 1 hour we observe a significant increase in the average number of of domains, with prevalently smaller domains (Fig. 4.9 B). After 36 hours of stabilization the coalescence is greatly inhibited, with an average number of domains larger than the average obtained for DOPC:DPPC:Chol (Table 4.2.

Stabilization time [hours]	DOPC:DPPC:Chol 45:30:25	DOPC:DPPC:Chol:PS 36:24:20:20
1	2.66 ± 0.43	3.96 ± 1.36
36	1.53 ± 0.40	3.65 ± 1.14

TABLE 4.2: Summary of average number of domains for ternary GUVs composed of DOPC:DPPC:Chol and DOPC:DPPC:Chol:PS. Each value represents average and standard deviation of two separate samples of 70 vesicles each.

The presence of a larger number of domains might indicate that PS prevents large scale domains from merging together. Therefore polystyrene appears to inhibit the coalescence of L_o domains. These results are in good agreement with simulations performed by Rossi [114] and Bochicchio [115], which reported that polystyrene can stabilize the phase coexistence of liquid/liquid membranes.

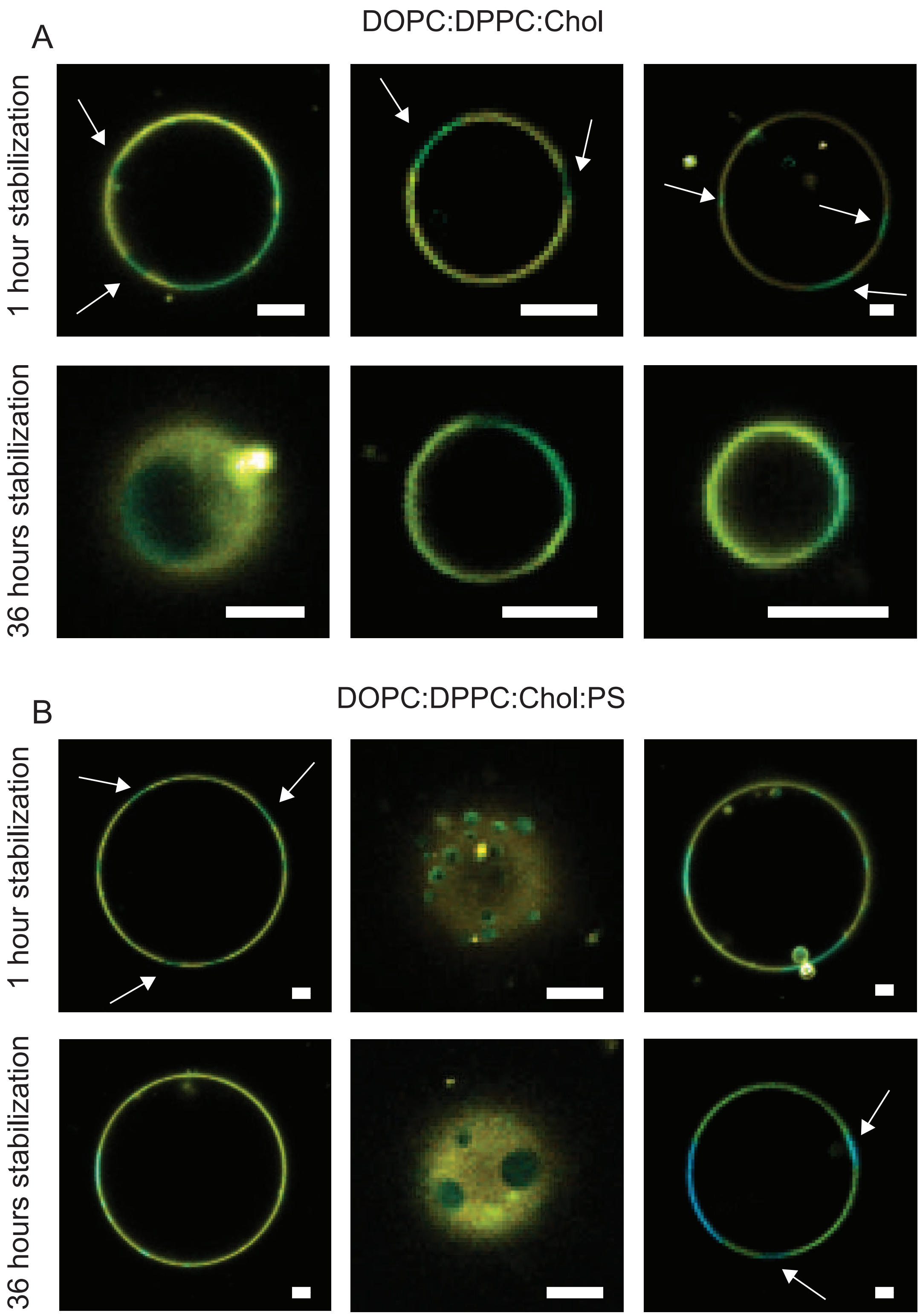
A
DOPC:DPPC:Chol
1 hour stabilization
36 hours stabilization
B
DOPC:DPPC:Chol:PS
1 hour stabilization
36 hours stabilization

FIGURE 4.9: (A) Typical GUVs composed of DOPC:DPPC:Chol 45:30:25 after 1 hour and 36 hour of stabilization. (B) GUVs composed of DOPC:DPPC:Chol:PS 36:24:20:20 after 1 hour and 36 hour of stabilization. Green represents the liquid disordered phase while blue represent the liquid ordered domain. White arrow indicate L_o domains. Scale bar 20 μm.

To further investigate the effects of the polymer, we analyzed the local emission spectra of Di-4 in the L_d and L_o phases. For systems containing only cholesterol we observe two distinctive emission maxima, centered at 587 ± 4 nm and 629 ± 2 nm, associated respectively with DPPC:Chol and DOPC phase. The values we obtained are in good agreement with previously reported Di-4 spectra for DPPC:Chol and DOPC systems [147].

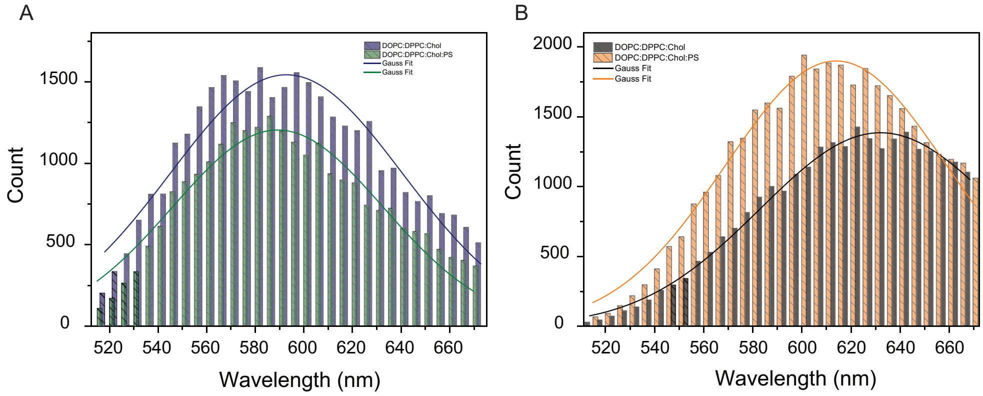

FIGURE 4.10: (A) Typical emission spectra of Di-4 for the liquid ordered phase for GUVs composed of DOPC:DPPC:Chol 45:30:25 (blue) and DOPC:DPPC:Chol:PS 36:24:20:20 (green). (B) Typical emission spectra of Di-4 for the liquid disordered phase for GUVs composed of DOPC:DPPC:Chol 45:30:25 (blue) and DOPC:DPPC:Chol:PS 36:24:20:20 (green). Lines represent gaussian fitting of the distribution.

In the case of systems containing both cholesterol and polystyrene, the characteristic emission for the L_o phase is unaffected, centered at 589 ± 5 nm (Fig. 4.10 A). However the L_d phase shows a shift in emission maximum to smaller wavelength, at 619 ± 2 nm (Fig. 4.10 B). This variation indicates that the polymer preferentially partitions into the liquid phase, as suggested by our results in single and binary systems, as well by Rossi *et al.* using molecular dynamics simulation [114]. In particular, such a shift in the emission maxima has been reported by Szegin *et al.* [147] for DOPC membrane containing cholesterol and is associated with a higher order of the bilayer. The emission shift we observe in presence of polystyrene might be therefore associated with a higher ordered liquid phase, as observed in the case of single lipid membranes in Chapter 3.

	Emission maximum L_o phase [nm]	Emission maximum L_d phase [nm]
DOPC:DPPC:Chol 45:30:25	587 ± 5	624 ± 2
DOPC:DPPC:Chol:PS 36:24:20:20	589 ± 5	619 ± 3

TABLE 4.3: Emission maxima of Di-4 in ternary lipid membrane and ternary lipid membranes containing cholesterol. Each value represents average and standard deviation of two separate samples of 70 vesicles each.

In particular we can observe that at least part of the polymer chains are aligned with the lipid acyl chains. Di-4 dipole moment resides, when incoporated in a lipid bilayer, at the level of the acyl chains, and therefore is more sensitive to presence of molecules in the hydrophobic regions compared as to Laurdan. Indeed it was shown that compared to Laurdan, Di-4 is highly insensitive to temperature changes [105], but more susceptible to cholesterol content. Therefore variations in the emission spectra indicate presence of molecules in the acyl chain region, consistently with the results we obtained in single component membranes (Chapter 3).

4.2 Conclusions

We observed that polystyrene significantly alters the phase behavior of multicomponent lipid bilayers with a different effect depending on the presence of cholesterol.

In the case of binary system the presence of polymer shifts the S_o and L_α miscibility towards lower temperatures, due to the similar order between the two phases induced by polystyrene. This behavior is similar to the reported phase behavior alteration of hydrophobic molecules incorporated in the hydrophobic region of the lipid bilayer which, by preferentially partitioning in the fluid phase, broadens the main phase transition and reduces the melting temperature. Our results are in good agreement with inhibition of membrane phase coexistence previously reported. However in our case, insertion of PS does not change the transition temperature of single component lipid membranes.

Moreover we observed that polystyrene partitions preferentially in the liquid disordered phase with less cholesterol, consistently with molecular simulations and experimental studies on hydrophobic molecules incorporated in membrane containing cholesterol. The presence of the polymer in membranes displaying liquid ordered domains stabilizes the lateral phase segregation and prevents the coalescence of domains.

Our results provide good agreement with previously reported studies and indicate that even a small amount of polystyrene might be potentially dangerous for biological membranes, specifically due to its antagonist behavior with cholesterol.

4.3 Materials and methods

Materials

Chloroform solution of DOPC (1,2-dioleoyl-sn-glycero-3-phosphocholine, $C_{44}H_{84}NO_8P$, M_w 786.11), DPPC (1,2-dipalmitoyl-sn-glycero-3-phosphocholine, $C_{40}H_{80}NO_8P$, M_w = 734.039) and cholesterol ((3S,8S,9S,10R,13R,14S,17R)-10,13-dimethyl-17-[(2R)-6-methylheptan-2-yl]-2,3,4,7,8,9,11,12,14,15,16,17-dodecahydro-1H-cyclopenta[a]phenanthren-3-ol, $C_{27}H_{46}O$, M_w 386.65) in powder were purchased from Avanti Polar Lipid (Birmingham, AL). DiI Stain (1,1′-Dioctadecyl-3,3,3′,3′-Tetramethylindocarbocyanine Perchlorate $C_{59}H_{97}ClN_2O_4$, M_w = 933.8793) and Di-ANEPPDHQ were provided by ThermoFisher Scientific (Waltham, MA, USA). Sucrose ($C_{12}H_{22}O_{11}$ M_w = 342.3) and Laurdan (6-Dodecanoyl-N,N-dimethyl-2-naphthylamine) were purchased from Sigma-Aldrich (Saint-Quentin, France). Atactic polystyrene ($(C_8H_8)_n$) M_n = 500) was purchased from Polymer Source Inc. All chemicals had high purity and were used without further purification. The osmolarities of the sucrose and glucose solutions were measured with a cryoscopy osmometer Osmomat 030 (Gonotec; Berlin, Germany)

Liposomal preparation

2.5 mg of lipid in chloroform were transferred to a glass vial, and organic solvent was evaporated using an argon stream until completely dried followed by 8h of vacuum pumping. For fluorescence measurements, the lipids were stained with 1% mol Laurdan in chloroform prior to evaporation. The lipid film was then hydrated with aqueous solution (buffer or sucrose solution) at 70°C to reach desired concentration and gently vortexed. Resulting MLV suspensions were sonicated for 15 min to disperse larger aggregates. Liposomal solutions remained stable over a period of days.

Giant unilamellar vesicles preparation

GUVs composed of DOPC:DPPC and DOPC:DPPC:Chol, both in absence of presence of polystyrene, were prepared by electroformation following the protocol introduced by Angelova [14]. Simply, 5 μl of 2 mg/mL solution of DOPC:DPPC or DOPC:DPPC:PS at the desired molar ratio, stained with 1% mol of diI, in chloroform were spread on each cathode of a custom made electroformation stage. The stage was kept under vacuum for at least 1 hour to ensure complete evaporation of solvent and subsequently the lipid film was hydrated using the necessary solution (sucrose at different concentrations) at 55°C.

We applied a sinusoidal electric field of 1 V peak-peak intensity at 10 kHz for 1 hour while keeping the sample heated above the transition temperature. The resulting GUV suspension was kept at 20°C water bath to ensure complete stabilization of the sample. Vesicles were used on the same day of preparation.

For GUVs stained with Di-ANEPPDHQ, a solution of the fluorescent probe in water was added to the GUV suspension to reach a 1% molar ratio with respect to lipids and incubated above melting temperature for 30 min in absence of illumination.

Fluorimeter

3 mL of liposomal suspension stained with Laurdan of total concentration 3 mg/mL was placed in a quartz silica cuvette with 1 mm path length. Acquisition of Laurdan emission spectra was performed with a Jobin Horiba FluoroMax equipped with a Peltier unit to control temperature. Excitation wavelength was set at 350 or 400 nm nm with a bandpass of 1 nm and emission was also recorded with slit of 1 nm. The solution was equilibrated at given temperature for 10 min before each acquisition. For each sample (n=2) we performed two cycles of heating and cooling.

General polarization (GP) was calculated using the standard expression provided by Parasassi [140]:

$$GP = \frac{I_{440} - I_{490}}{I_{440} + I_{490}} \tag{4.4}$$

where I_{440} and I_{490} are the intensity recorded at 440 nm and 490 nm respectively.

Optical Microscopy

Imaging of GUVs labelled with DiI was performed using a confocal laser scanning microscope Nikon Eclipse TE2000-E equipped with a Nikon camera. The objective was a Nikon 60x water immersion, NA 1.2 (Nikon) using an excitation line of 543 nm with a mercury lamp. For GUVs labelled with Di-ANEPPDHQ the conventional three-band filter was substituted with a 20/80 R/T filter to perform spectral imaging, using a 488 excitation line Ar laser.

GUVs samples were initially swelled by diluting the external medium with a slighly ipoosmotic glucose solution (<10 mosm/Kg) to also facilitate the fall of the vesicles on the glass surface.

DOPC:DPPC samples were kept at ambient temperature °C for at least 2 hours after preparation to ensure complete stabilization of domains. 100 μL of a GUV solution were placed on a borosilicate glass slide and sealed with a silicon spacer and an additional glass slide to prevent any leakage or solvent evaporation.

For each lipid composition of binary mixtures we acquired images from two (n = 2) separate samples of 40 vesicles each, and for mixtures containing cholesterol two separate samples (n = 2) of 70 vesicles each.

5

DPPC bilayers in solution of high sucrose content

Disaccharides and sugars in general play a key role in preserving the structure and the functionality of biological membranes during period of environmental stress [148]. Many reports have shown that membranous structures are particularly stabilized by small sugars [149, 150].

Besides their significant role in cellular regulation, carbohydrates have also a broad range of applications in biophysics and industrial research, particularly in the field of biopreservation and cryopreservation. Their interactions with membranes have therefore been the focus of many studies.

Some sugars such as sucrose and trehalose are very efficient cryprotectors [149, 151, 152]. They have shown to readily reduce the liquid-gel transition temperature T_m in highly dehydrated lipid bilayers, and to increase survivability of membrane undergoing freeze/thawing processes. While this mechanism was initially associated with the ability of disaccharides to insert between adjacent lipid head groups during dehydration and hydrogen bond to them, an alternative model has been proposed that explains the observed effects in terms of the sugars' changes on the hydration repulsion [153].

Moreover, it has been proven that sugars play a role in the properties of hydrated bilayers. Dobereiner *et al.* [154] obtained a strong influence of glucose on the spontaneous curvature of liposomes. Genova *et al.* [155] showed by fluctuation analysis that high concentration of sucrose reduces the bending modulus of SOPC giant vesicles up to 25%, whereas Vitkova [156] found 60% reduction using micropipette aspiration. Nagle [157] showed as well by X-ray scattering that the bending rigidity of DOPC bilayers is reduced, although it should be noted that recently the opposed effect has been reported [158].

Characteristic chain melting temperatures T_m of phospholipid dispersions was found to increase as the activity of water decreases in the presence of increased solutes[159, 160]. Strauss *et al.* [160] found that addition of more than 10% sucrose to hydrated multilamellar vesicles of DPPC elevated the melting temperature; they suggested a hydrogen bonded sucrose network as the cause. Crowe and Crowe [161] found that several mono- and disaccharides raise T_m and broaden the main transition of DPPC (MLV). However, addition of sugars to unilamellar vesicles created multiple thermodynamic populations. High concentrations of trehalose, sucrose, and fructose created a low-temperature shoulder on the DPPC endotherm, indicating a second population with a lower T_m than that of pure hydrated DPPC.

Despite the many effects of sugars on dry, semi-dry and hydrated bilayers, relatively few studies have been conducted in order the understand the main effect of disaccharide on the lipid bilayer phase transition, and the mechanisms of interaction are yet to be understood. While there is some agreement that high concentration of sugar increases the transition temperature of the bilayer melting, the effect on the enthalpic contribution are quite discording, reporting in certain cases no effect on the enthalpy of the transition, and in other studies a significant decrease of the energy.

In this work we expose well hydrated bilayers of DPPC to high concentrations of sucrose and investigate the effects on the membrane phase behavior for increasing concentrations of sucrose using a combination of differential scanning calorimetry and Laurdan emission spectra to obtain structural and thermodynamical information. We also utilize giant unilamellar vesicles to visualize changes in phase behavior and kinetics of transition. Based on our experimental observation we propose a thermodynamical model for the lipid bilayer – sugar interaction to explain our results and the ones reported by previous studies.

5.1 Results and discussion

5.1.1 Laurdan emission spectra

Figure 5.1 illustrates emission spectra of Laurdan for DPPC MLVs at different concentration of sucrose at 20°C (Fig. 5.1 A) and 60°C (Fig. 5.1 B). During the phospholipid main transition the spectra show a continuous shift to longer wavelengths (Fig. C.1).

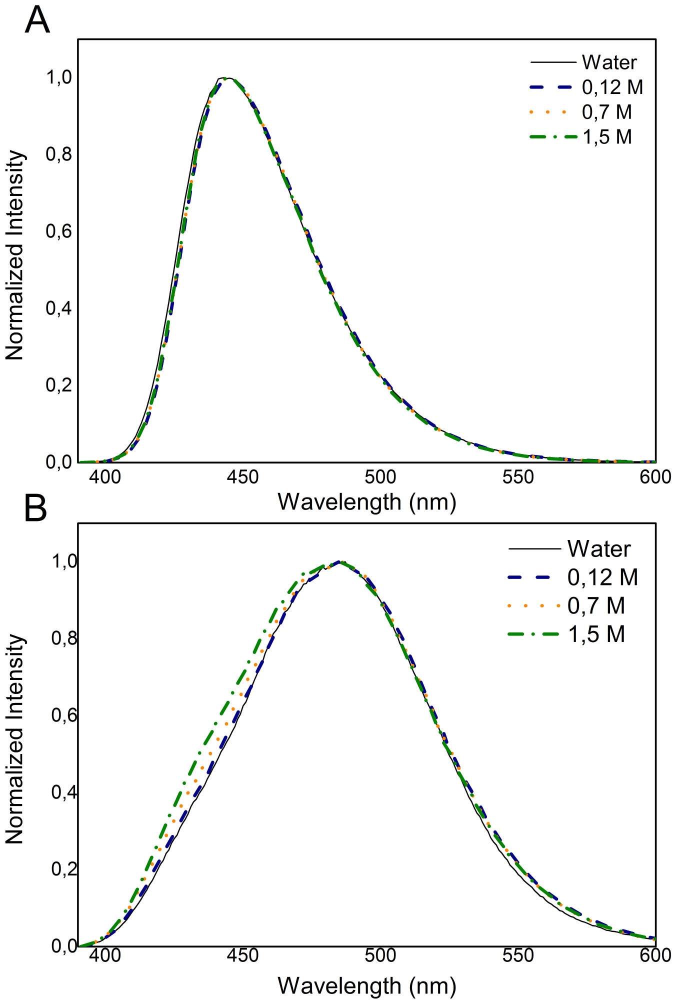

FIGURE 5.1: (A) Laurdan emission spectra for DPPC at different concentration of sucrose at 20°C. (B) Laurdan emission spectra for DPPC at different concentration of sucrose at 60°C

.

At 20°C, the maximum intensity is centered at 440 nm, corresponding to the signal associated with the gel phase. The spectra at any concentration of sucrose are identical to those observed for the DPPC system in water (Fig. 5.1), indicating that the presence of sugar does not significantly modify the structure or order of the bilayer.

As temperature was increased above the transition temperature of DPPC, we observe a red emission shift with maximum at 490 nm, with a decrease of total intensity and a broader emission spectra (Fig 5.1 B). Such a decrease of intensity has been reported before [97]. Increasing concentration of sucrose results in persistence of a 440 nm shoulder in the emission spectra. This additional contribution is found to be dependent on the sucrose concentration and remains at any temperature above T_m. Laurdan emission centered at 490 nm is attributed to a more relaxed Laurdan excited state, which would be favoured by a more hydrated environment [95, 162].

Conversely, contribution at 440 nm reflects a stiffer and/or less hydrated system surrounding the Laurdan naphthalene moiety.

To further quantify the spectral changes, we calculated the GP from each emission spectra using 440 nm and 490 nm as maximum emission for each phase. Fig. 5.2 displays the temperature dependence of Laurdan GP values for DPPC MLVs in water and at different concentration of sucrose.

The values for DPPC in water are comparable to values reported by Bagatolli *et al.* [96], as the GP decreases from 0.51 ± 0.02 for temperature below T_m to -0.33 ± 0.01 for the liquid disordered phase. The extracted value for T_m is 41.5 ± 0.3 °C, which is in good agreement with our DSC measurement of 41.3°C and with previously reported values. The GP transition from gel phase to liquid crystalline phase is sharp for any concentration of sucrose, although a higher transition temperature has been estimated for larger concentrations of sugar. The values of GP at temperatures below T_m are almost independent of sucrose content, although for temperatures near the transition (35 °C and 40 °C) a slight increase of GP with increasing amount of sugar can be observed.

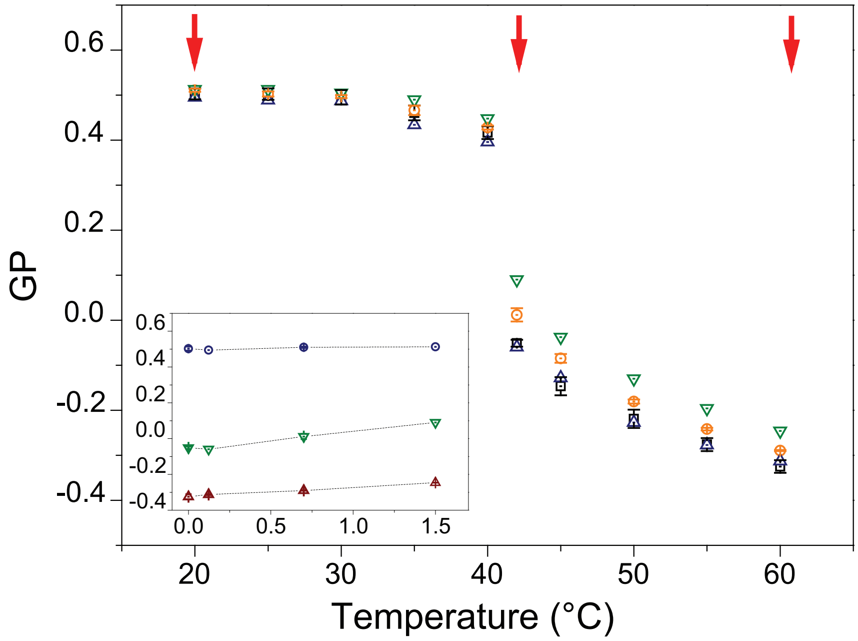

FIGURE 5.2: Variation of General Polarization over temperature for multilamellar liposomes of DPPC formed in water and at different sucrose concentration. It is possible to observe a rise in GP values proportional to sucrose concentration. Inset: Dependance of GP on sucrose concentration for 20°C (blue), 42°C (green) and 60°C (red)

In the liquid phase, above T_m, the GP curve shows a significant increase of GP values with higher sucrose concentration, with GP of 0.09 ± 0.01 and -0.22 ± 0.02 for T_m and 60°, respectively, at 1.5 M sucrose. Interestingly, the maximum variation can be observed for T_m, and at higher temperatures the difference with respect to GP values of DPPC in pure water gradually decreases (Fig. 5.2 inset). The variation owed to the presence of sucrose appears to follow a linear dependence with sugar concentration in bulk for any analysed temperature

Laurdan is insoluble in water, therefore any information from the emission spectra and GP arises entirely from the probe in the membrane. In lipid bilayers the fluorescent moiety of Laurdan is located at the level of the glycerol backbone and the emission shift upon changes in temperature is due to a dipolar relaxation process [162]. For MLVs formed in water, the red shift and decrease in GP generally associated with phase transition are caused by a change in lipid packing, as the more disordered membrane allows deeper penetration of polar solvent molecule in the interfacial region.

Variations of emission spectra and GP as the one showed in this study have been reported before in the case of high ionic strength or in the presence of cations in the solvent for DMPG liposomes [88, 163]. In these studies the effect was due to changes in lipid packing upon electrostatic attraction caused by ionic charges. Despite sucrose being highly polar, our results clearly show that when it is present in high concentration, the Laurdan emission spectra is similar to that of an apolar environment [97]. Conversely, increased GP values in presence of sugar are linked to a lower mobility of water or a lesser number of water molecules around the Laurdan naphthalene moiety.

Two possible mechanisms can be invoked to explain such an effect: i) A tighter lipid packing of the membrane, as observed for example in liquid ordered (L_o) phases in presence of cholesterol, ii) A depletion of water molecules at the lipid headgroup region which reduces the emission shift of Laurdan.

Simulations and previous experimental studies showed that the adsorption of sugar to the membrane leads to a lower number of water molecules around the lipid headgroup [152]. These results are consistent with our GP data that show a progressive reduction of water molecules surrounding the Laurdan napthalene moiety resulting in a higher GP values.

5.1.2 Differential scanning calorimetry

To better understand the changes in the bilayer structure due to the presence of sucrose, we performed differential scanning calorimetry on DPPC multilamellar vesicles (MLSVs) hydrated with water, 0.39 M, 0.7 M and 1.5 M sucrose (Fig 5.3). The energy associated with the transition from gel to liquid crystalline phase gives information on the local packing of the membrane upon melting. Fig 5.3 A shows DSC curves of the liposomal systems in pure water and at each sucrose concentration.

The DSC profiles display a striking asymmetry under all conditions, with a sharp variation of intensity at higher temperatures and a smoother curve at low temperatures. This feature has been reported before and it is usually associated with instrumental imprecision, therefore is not characteristic of the transition itself [164].

The intensity of the peaks decreases with increasing amount of sugar, and the centre of the peaks shifts to slightly higher temperature when MLVs are in high sucrose concentration. Overall the curves remain sharp, indicating that the transition is still highly cooperative. Broadening of peaks is usually associated with disruption of the lipid packing and cooperativity [165], as it has been reported by Mannock [166] for cholesterol. In our experimental observations, such large broadening is not present, suggesting that the packing and the phase of the lipid bilayer remains the same at all sucrose content.

To quantitatively measure the variation on the transition, we extracted the enthalpy (ΔH), transition temperature (T_m) and half intensity temperature interval ($T_{1/2}$) of the peaks. The results are summarized in Table 5.1.

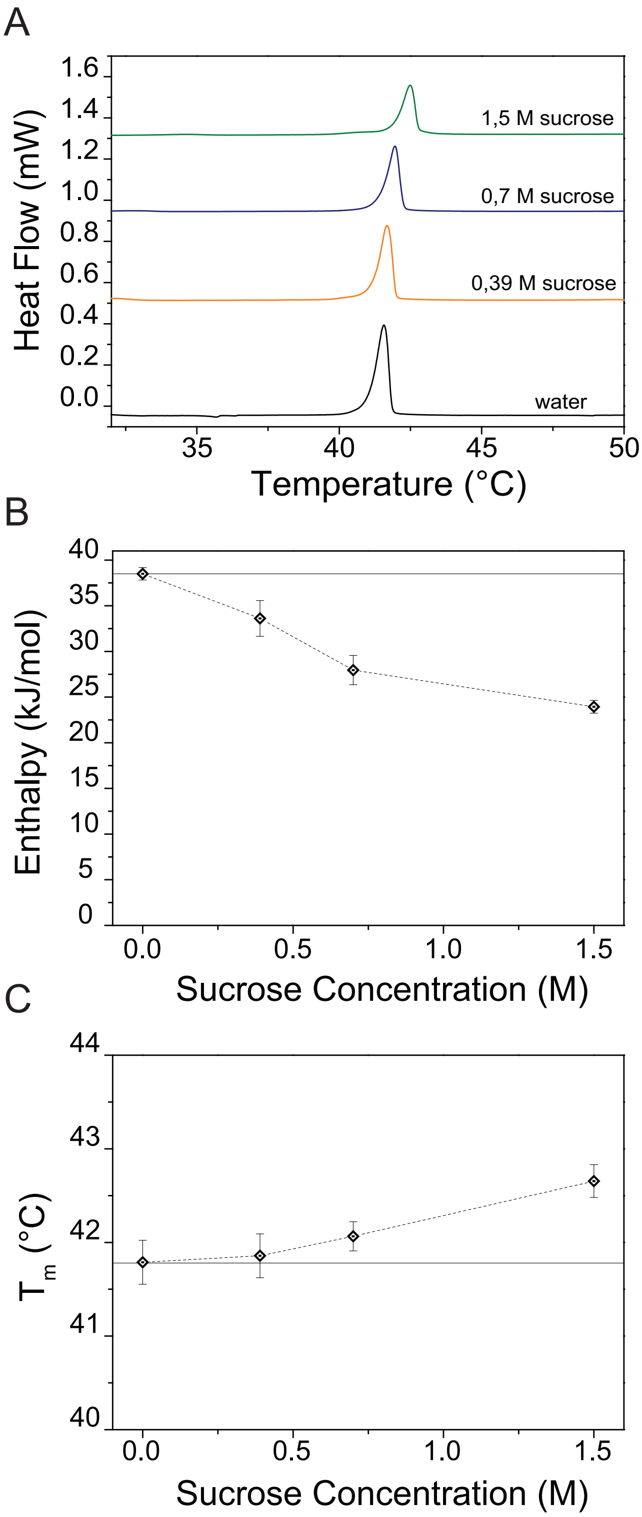

FIGURE 5.3: (A) DSC calorimetric signal (B) Variation of T_m over sucrose concentration (C) Decrease of enthalpy at different sucrose concentration. In both B) and C) straight line represent initial value in pure water.

For system formed in pure water we obtained an enthalpic contribution of 38.5 kJ $\cdot$ mol^{-1} and T_m of 41.8 °C, well in agreement with previously reported values. In presence of sucrose we observe a significant drop of enthalpy, with a final value

23.9 kJ · mol^{-1} at 1.5 M sucrose. Such an effect of sucrose on the DPPC enthalpy has been observed before by Chowdry and Chen [167, 168]. Our values are in good agreement with a variation of 10.9 kJ · mol^{-1} for 1 M sucrose observed by Chowdry. Chen, however, reported a drop of 11.6 kJ · mol^{-1} at already 0.2 M sucrose, which we do not observe. Surprisingly, our results show a nonlinear trend for enthalpy change with respect to sucrose concentration (Fig 5.3 B). The enthalpy reaches a steady state at 1.5 M, suggesting a saturation of the sucrose effect on the membrane transition. This saturation could be linked to a maximum adsorption of sucrose at the surface, as it was observed with ESEEM measurements by Konov [169], which observed a Langmuir adsorption of sucrose for DPPC bilayers.

The transition temperature for DPPC with sucrose is slightly increased, with final value of 42.7°C for 1.5 M of sucrose. These changes in T_m, albeit small, are in good agreement with an increase of 0.6°C at 1 M reported by Chowdhry, measured via calorimetry [167]. Stumpel [170] also observed a shift of $\sim$ 1°C in T_m of DMPC MLVs in presence of 40% sucrose. Similar effects have been reported on DMPC vesicles [171]. Other studies instead reported little or no changes in T_m, contrary to our results.

Sucrose concentration [M]	T_m [°C]	$T_{1/2}$ [°C]	ΔH [kJ · mol^{-1}]
0	41.8 ± 0.2	0.40 ± 0.01	38.5 ± 0.7
0.39	41.9 ± 0.2	0.44 ± 0.01	33.6 ± 1.9
0.7	42.1 ± 0.1	0.48 ± 0.01	27.9 ± 1.6
1.5	42.7 ± 0.2	0.55 ± 0.02	23.9 ± 0.7

TABLE 5.1: Summary of DSC results for DPPC liposomes in sucrose solution

Many studies report variations of T_m of lipid bilayer upon interaction with macromolecules located either at the surface or in the hydrophobic region of the membrane.

An increase of the transition temperature is generally linked to a tighter packing of the lipids, which can arise from many reasons. In this study, we argue that the observed shift of T_m to higher temperature is due to a dehydration of the lipid bilayer. Sugar molecules, by accumulating on the membrane surface, substitute water molecules from the outer most hydration layer and increase the transition temperature. Our observation of Laurdan emission spectra indicates a decrease of the number of water molecules at membrane interface.

Gabrielle-Delmont [172] reported for DPPC vesicles an enthalpy drop and T_m comparable to the value obtained in this study in the case of 20% water content. However, under our experimental conditions water content has been calculated to be $\sim$60% for 1.5 M sucrose. Moreover the DSC curve does not diplay a high temperature contribution reported for lipid bilayers under low hydration conditions. Therefore simple dehydration or substitution of water molecules by sucrose is not enough to explain our experimental data.

Finally, we observe a slight increase of $T_{1/2}$, consistently with values reported by Chen [168].

5.1.3 Giant unilamellar vesicles

We observed giant unilamellar vesicles of DMPC to probe the micrometric phase behaviour at temperatures below and above T_m. Typical vesicle morphology for each sucrose concentration at different temperatures are summarized in Figure 5.4 together with statistics of phase separation in Figure 5.5.

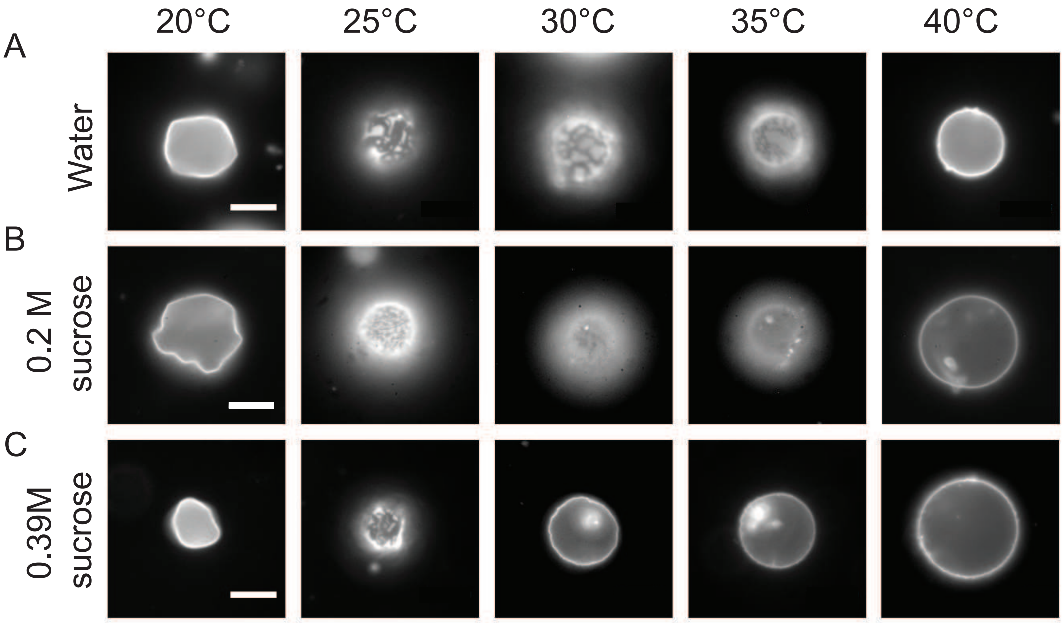

FIGURE 5.4: Summary of sucrose effects on GUVs formed with DMPC. (A) Typical GUV phase behavior for DMPC in water, (B) in 0.2 M and (C) in 0.39 M sucrose in the temperature interval [20°C - 40°C]. Scale bar 10 μm.

In DMPC vesicles we observe a homogeneous phase at 20°C. The corrugations of the membrane and steep angle defects have been previously reported for DMPC vesicles and are characteristic of a S_o gel phase [136, 137]. Increasing the temperature to 25°C results in phase separation displayed by fluorescent probe partitioning. DiI has been shown to readily partition into the liquid disordered phase [65, 138], therefore black domains observed are gel phase domains in liquid phase. Domains are still observed for both 30°C and 35°C, however they gradually decrease in size with increasing temperature. The partitioning of DiI also decreases as the contrast between domains becomes less sharp. At 40°C the membrane is in a liquid phase and displays homogenous fluorescence.

Vesicles formed in 0.2 M sucrose (Fig. 5.4 B) display a similar behavior to GUVs formed in water, however gel domains readily disappear at a lower temperature. Moreover the partitioning of DiI gradually diminishes already at 30°C, and at 35°C contrast between domains and fluid phase is very low. For 0.39 M sucrose (Fig 5.4 C) we observe instead a narrower window of coexistence as domains that are visible only at 25°C, whereas at 30°C or higher a single homogeneous fluid phase is present. Below the transition temperature we observe a homogenous S_o phase, characterized by steep angles and rough surface.

Under all sucrose concentration the area coverage of the S_o domains for each temperature is the same and gradually decreases as the temperature rises above T_m. Although we observe different typology of domains, namely stripes, hexagonal and random, they can be attributed to different states of tension of the individual vesicle and they can all be associated with S_o domains. A statistical analysis performed on each sample shows the temperature window of phase coexistence for each concentration of sucrose.

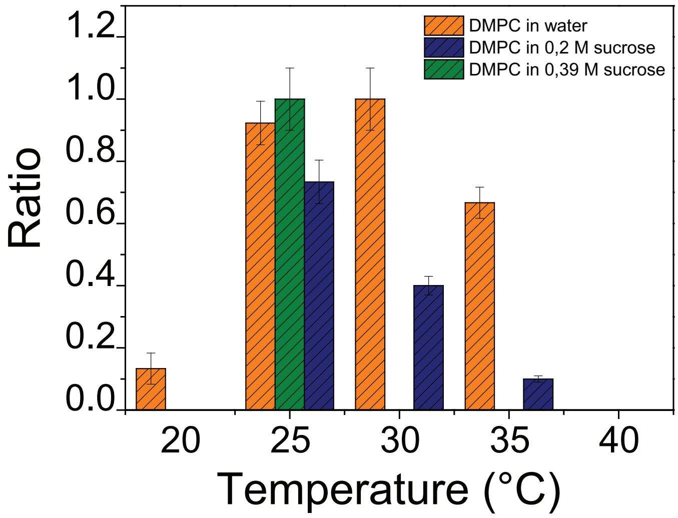

FIGURE 5.5: Statistics of DMPC GUVs phase separation at different sucrose concentrations. Each bar represents average and standard deviation of two different samples of 60 vesicles each.

Our observation for pure DMPC GUVs reveals a large temperature interval of phase coexistence, which has not been reported before in giant vesicles experiments. Although phase coexistence is expected to appear around T_m[139], the persistence of gel domains at higher temperatures may indicate metastability produced by the low rate of heating employed in the experimental setup.

The disappearance of phase coexistence for temperatures above T_m can be interpreted as a lowering of the energy involved with gel-liquid contact. The size of gel domains in the liquid phase is mainly driven by the minimization of the energy involved with hydrophobic mismatch (such as a S_o/L_d coexistence) [173]. Several studies have proposed that sucrose can alter the head-head distance in lipid bilayers under low hydration conditions [149, 174]. Sucrose can therefore act as a reliever of hydrophobic mismatch allowing thus for smaller domains existence, by covering the portion of chains exposed by the mismatch. Therefore, it is possible that the presence of sugar can enhance the dissolution of domains or reduce the time scale of meta-stable states.

5.1.4 Thermodynamics model

Based on our experimental observations we attempt to derive a thermodynamics description of the interaction between sucrose and the DPPC lipid bilayer. In discussing the interaction between dry bilayers and sugars, a frequent model is the water replacement hypothesis (WRH), which postulates direct hydrogen bonding between sugars and phospholipids [149]. By creating H-bonds with lipid headgroups, sugars keep lipids separated in the liquid phase upon dehydration. In some case the hypothesis considers the sugars to be able to penetrate in the interfacial region of the membrane, and therefore keeping the lipids apart. Although our data do support the removal of water molecules from the membrane, the WRH model cannot explain both increase in T_m and decrease of enthalpy.

Another proposed model is the hydration forces explanation (HFE) [175, 176], which assumes no direct interaction between sugars and lipids. Sugars' non-specific volumetric and osmotic effects are the cause of changes in the bilayer phase transition. This model has been able to quantitively predict changes in the transition temperature [153, 177], however the variations of enthalpy reported here and in previous studies have not been accounted for.

A full thermodynamics model that would fully explain the observed phenomena must include: i) an increase of transition temperature, ii) a significant drop in enthalpy and iii) a decrease of the cooperativity of the transition.

We propose a model in which the adsorption of sucrose at the membrane surface locally dehydrates the lipid bilayer, resulting in the formation of clusters with an intrinsic different transition temperature. As phase transition occurs only a portion of lipid participates, resulting in a lower enthalpic contribution and a higher effective melting temperature, coupled with broader peak.

To physically describe this model, we use a formalism previously used by Heimbourg [178] and others [179, 180] to succesfully describe the gel-to-liquid transition. This description is akin to an Ising spin model, where however the spin represents the phase of the lipid, and a full derivation of the model can be found in Appendix C. Following this formalism, the Gibbs free energy for a bilayer can written as

$$\Delta G = n_l(\Delta h - T\Delta S) - J n_{gl} \tag{5.1}$$

where n_l is the number of lipids in the liquid phase, Δh is the invidual lipid enthalpic contribution to transition, ΔS is the enthropic contribution, J is the cooperativity energy and n_{gl} the number of gel-liquid lipid pairs in contact with each other.

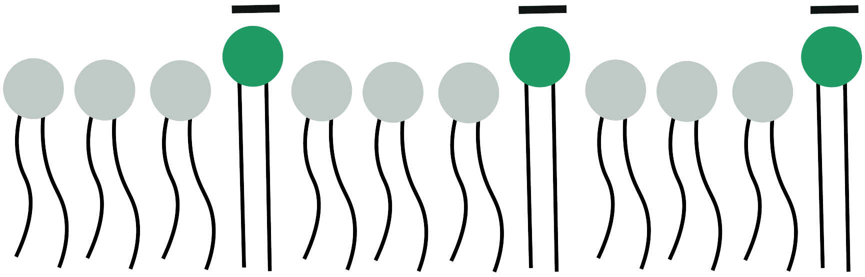

FIGURE 5.6: Schematic representation of interaction of sucrose with the lipid bilayer. The sugar bounds to a lipid, creating two populations with different transition themodynamics. Free lipids (grey) melt as expected while bound lipids (green) are dehydrated and therefore undergo a transition at different temperature.

We assume that sucrose, by adsorbing to the membrane, can change the number of water molecules surrounding a lipid and that this process is not necessarily homogenous. Effectively this will affect the Gibbs free energy and T_m of a lipid so that we have a new $\Delta G'$ for lipid interacting with sucrose:

$$\Delta G' = n_l'(\Delta h - T\Delta S)' - J' n_{gl}' \tag{5.2}$$

and the total energy of the system can be then described by

$$\begin{aligned}\Delta G^{tot} =& n_l(\Delta h - T\Delta S) + n_l'(\Delta h - T\Delta S)' - \\ &- J' n_{gl}' - J n_{gl} - J'' n_{gl}''\end{aligned} \tag{5.3}$$

where Jn_{gl} represents the free lipid-free lipid contact, $J'n'_{gl}$ the free lipid-bound lipid contact and $J''n''_{gl}$ the bound-bound contact. The number of lipids in the gel or liquid state will depend thus on the site coverage of sucrose σ and the probability p for a lipid to be in a specific state. We have then

$$\begin{aligned} n_l &= N \cdot (1-\sigma) \cdot p_l \\ n_g &= N \cdot (1-\sigma) \cdot (1-p_l) \end{aligned} \tag{5.4}$$

for free lipids and

$$\begin{aligned} n'_l &= N \cdot (1-\sigma) \cdot p'_l \\ n'_g &= N \cdot (1-\sigma) \cdot (1-p'_l) \end{aligned} \tag{5.5}$$

for bound lipids. To estimate the cooperativity term we use a mean field approach

$$\begin{aligned} n_{gl} &= (1-\sigma)^2 \cdot \frac{\eta N}{2} \cdot 2p_l(1-p_l) \\ n'_{gl} &= 2\sigma(1-\sigma) \cdot \frac{\eta N}{2} \cdot [p_l(1-p'_l) + p'_l(1-p_l)] \\ n''_{gl} &= \sigma^2 \cdot \frac{\eta N}{2} \cdot 2p'_l(1-p'_l) \end{aligned} \tag{5.6}$$

Based on this we can write the total enthalpy as

$$\Delta H = \Delta h p_l + \Delta h' p'_l + J_{tot} \tag{5.7}$$

where J$_{tot}$ is the sum of all enthalpic cooperativity terms. We should point out that in this study we choose to consider the cooperativity term as an enthalpic term. This choice is arbitrary as the formalism has a degree of freedom in choosing the ratio of enthalpic and enthropic contribution for J_{tot}. We performed numerical simulation using our model with the following parameter: $T_m = 314.95\text{K}$, $T'_m = 319.95\text{K}$, $\tilde{J} = 1.94$; $\tilde{J}' = \tilde{J}'' = 0.97$, $\mathcal{N}_A \Delta h = \mathcal{N}_A \Delta h' = 56\ \text{kJ} \cdot \text{mol}^{-1}$.

By comparing the values of ΔH obtained from DSC and theoretical predictions, we obtained the dependence of the area coverage on the sucrose concentration (Fig. 5.7 A) and extracted the conversion value between σ and concentration using a linear fitting.

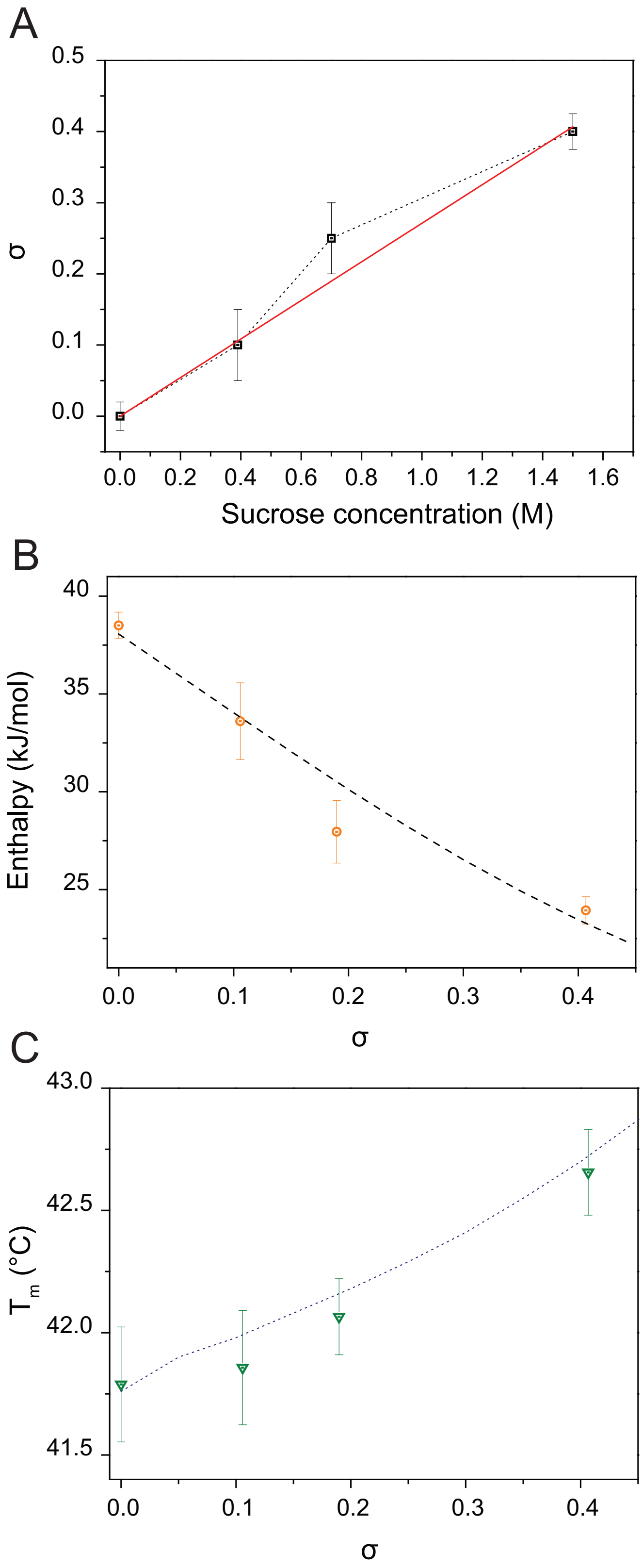

FIGURE 5.7: (A) Dependence of sucrose coverage σ on the sucrose concentration (black squares) and linear fitting (red line). (B) Experimental values of ΔH for the DPPC gel-to-liquid transition at different concentration of sucrose (orange circles), alongside with the theoretical predictions from the thermodynamics model (black dotted line).(B) Experimental values of T_m for the DPPC gel-to-liquid transition at different concentration of sucrose (green), alongside with the theoretical predictions from the thermodynamics model (blue dotted line).

The experimental values for enthalpic contribution (Fig. 5.7 B) and transition temperature (Fig. 5.7 C) are in good agreement with the theoretical predictions obtained via numerical simulations. The thermodynamics model therefore proves valid for low sucrose coverages.

5.2 Conclusions

In this study we have shown that sucrose can alter the gel-liquid phase transition of DPPC lipid bilayers, increasing its T_m and lowering the enthalpy of the transition. These results confirm and expand the observations reported in previous studies concerning the effects of sugars in well hydrated lipid bilayers, with possible implications in the field of byopreservation. We grouped the observed effects from different techniques as a result of a local dehydration of lipids due to high concentration of sucrose near the membrane, with a formation of small lipid clusters that would melt at a different temperature than T_m. This interaction is successfully described by a simple thermodynamic model that takes into account the two populations that undergo phase transition at different temperatures, and provides excellent agreement with our experimental data.

5.3 Materials and methods

Materials

Chloroform solution of DPPC (1,2-dipalmitoyl-sn-glycero-3-phosphocholine, $C_{40}H_{80}NO_8P$, $M_w = 734.039$) and DMPC (1,2-dimyristoyl-sn-glycero-3-phosphocholine, $M_w = 677.933$) were purchased from Avanti Polar Lipid (Birmingham, AL). DiI Stain (1,1′-Dioctadecyl-3,3,3′,3′-Tetramethylindocarbocyanine Perchlorate $C_{59}H_{97}ClN_2O_4$, $M_w = 933.8793$) was provided by ThermoFisher Scientific (Waltham, MA, USA). Sucrose ($C_{12}H_{22}O_{11}$ $M_w = 342.3$) and Laurdan (6-Dodecanoyl-N,N-dimethyl-2-naphthylamine) were purchased from Sigma-Aldrich (Saint-Quentin, France). All chemicals had high purity and were used without further purification. The osmolarities of the sucrose solutions were measured with a cryoscopy osmometer Osmomat 030 (Gonotec; Berlin, Germany)

Liposomal preparation

2.5 mg of DPPC in chloroform were transferred to a glass vial, and organic solvent was evaporated using an argon stream until completely dried followed by 8h of vacuum pumping. For fluorescence measurements, the lipids were stained with 1% mol Laurdan in chloroform prior to evaporation. The lipid film was then hydrated with aqueous solution (buffer or sucrose solution) at 70°C to reach desired concentration and gently vortexed. Resulting MLV suspensions were sonicated for 15 min to disperse larger aggregates. Liposomal solutions remained stable over a period of days.

Giant unilamellar vesicles preparation

GUVs were prepared by electroformation following the protocol introduced by Angelova [14]. Simply, 5 μl of 2 mg/mL solution of DMPC stained with 1% mol of diI in chloroform were spread on each cathode of a custom made electroformation stage. The stage was kept under vacuum for at least 1 hour to ensure complete evaporation of solvent and subsequently the lipid film was hydrated using the necessary solution (water or sucrose at different concentrations) at 55°C.

We applied a sinusoidal electric field of 1 V peak-peak intensity at 10 kHz for 1 hour while keeping the sample heated above the transition temperature. The resulting GUV suspension was kept at 20°C water bath to ensure complete stabilization of the sample. Vesicles were used on the same day of preparation.

Fluorimeter

3 mL of liposomal suspension stained with Laurdan of total concentration 3 mg/mL was placed in a quartz silica cuvette with 1 mm path length. Acquisition of Laurdan emission spectra was performed with a Jobin Horiba FluoroMax equipped with a Peltier unit to control temperature. Excitation wavelength was set at 350 nm with a bandpass of 1 nm and emission was also recorded with slit of 1 nm. The solution was equilibrated at given temperature for 10 min before each acquisition. For each sample (n=3) we performed two cycles of heating and cooling.

General polarization (GP) was calculated using the standard expression provided by Parasassi [140]:

$$GP = \frac{I_{440} - I_{490}}{I_{440} + I_{490}} \tag{5.8}$$

where I_{440} and I_{490} are the intensity recorded at 440 nm and 490 nm respectively.

Differential Scanning Calorimetry

The calorimetry measurements were performed with high sensitivity differential scanning calorimeter (μDSC Setaram). The measuring cell was filled with the sonicated sample (MLVs at different concentrations of sucrose), while the reference cell was filled with the same sucrose solution. The temperature of the cells was changed with a constant rate (heating rate: 0.5 K·min^{-1}, cooling rate: 0.3 K·min^{-1}). The system was equilibrated $\sim$ 20 min before each heating or cooling ramp. The analysis of DSC data was performed using OriginPro 9.0 (Northampton, Ma, USA). For each sucrose concentration, three consecutives heating/cooling cycles were performed in two separate samples.

Optical Microscopy

Imaging of GUVs labelled with DiI was performed using a confocal laser scanning microscope Nikon Eclipse TE2000-E equipped with a Nikon camera. The objective was a Nikon 60x water immersion, NA 1.2 (Nikon). GUVs samples prepared at different sugar concentrations were initially swelled by diluting the external medium with $\sim$5% volume of pure water. The samples were kept at 5°C for at least 2 hours after preparation to ensure complete transition to gel (also called S_o) phase. Prior to experimental observation, GUVs were kept at 20°C for at least 1 hour to stabilize the temperature. 100 μL of a GUV solution were placed in a custom-made heating stage through which we could control the temperature of the sample. For each temperature, we stabilized the sample for at least 1 hour before acquiring images.

6

Interaction of cholesterol grafted polymer with lipid membranes

Traditional cancer therapeutics are designed to interact with proteins and nucleic acids to treat the tumoral cells. However, in recent years, development of scientific tools concerning lipids and lipid metabolism opened new aspects of tumor cells understanding, indicating possible differences in lipid composition and membrane function of tumor cells compared to healthy cells [181]. The development of lipidomics therefore has postulated that modulation of, or interaction with, lipids could change lipid composition, membrane properties or alter the properties in tumoral cells to interfere specifically with cancer cell membranes [182]. Indeed, proteins like integrins, adherins and receptors, involved in tumor progression and invasion, are located in lipid rafts [183, 184] and their abundance in tumor cells are linked with a higher invasive potential and a decreased fluidity of membranes [185].

The functionality of proteins interacting with the membrane is often modulated by the host bilayer [186, 187]. The regulation induced by membrane lipids may occur through chemical interaction between proteins and individual lipid molecules, and to non-specific interaction due to the collective physical properties of the lipid bilayer [188, 189]. In particular, membrane parameters such as thickness, fluidity, charge, and curvature have been found to regulate the folding, activity and stability of membrane proteins [142].

Cholesterol, a lipid present in all eukaryotic cells, has been found to significantly affect the activity of membrane proteins and ion channels, due to its relevant properties in affecting both the hydrophobic mismatch and fluidity in lipid model membranes [190].

Recently, a newly developed cholesterol grafted polymer has been synthetized as an effort to develop a delivery agent that could alter the membrane fluidity and cholesterol content in a triggerable manner (Chen, data not published).

This cholesterol-grafted PLP, coined PPCHOL, belongs to the family of PLP derivatives first developed by Chen [191]. They are CPP-mimicking, lysine based polymers derived from hydrophobic modification of poly(L-lysine isophthalamide) with amino acids, and display different conformation under varying pH conditions. They have been succesfully reported to enable efficient cytoplasmic delivery of small-molecule model drugs and bioactive macromolecules in vitro and in vivo [192, 193].

In this work we investigate the effects of the cholesterol-grafted polymer on the phase behavior of giant unilamellare vesicles displaying gel-liquid phase coexistence using confocal spectra imaging of DI-4-ANEPPDHQ emission spectra.

6.1 Results and discussion

6.1.1 Polymer conformation at different pH conditions

To characterize the changes of the polymer conformation at varying pH, we performed DLS measurements of 250 μg/mL PPCHOL (Fig. 6.1) solution in PBS at progressively acidic pH.

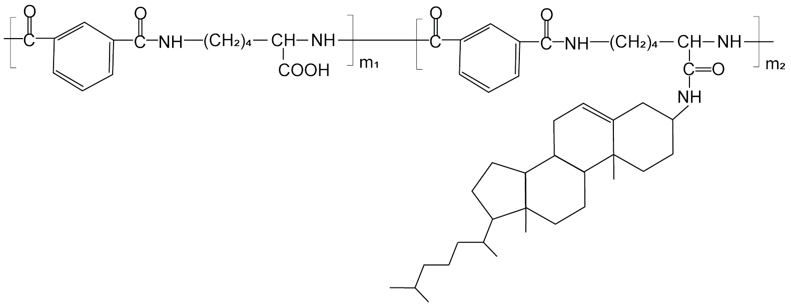

FIGURE 6.1: Chemical structure of PPCHOL.

We observe an average diameter of 35.2 ± 2.9 nm at pH 7.3, with increasing acidification resulting in decrease of polymer size up to 8.73 ± 2.9 nm at pH 5.9. The size values of the diameters at neutral pH are significantly lower than the values of $\sim$ 100 nm for phenylalanine-grafted polymers (Wang, data not published). This difference suggests that already at neutral pH the polymer is already in a globular or condensed conformation, with a higher hydrophobicity than the amino acids grafted counterparts. The reduction of diamater upon acidification however indicates that the polymer possesses a partial pH-sensitivity.

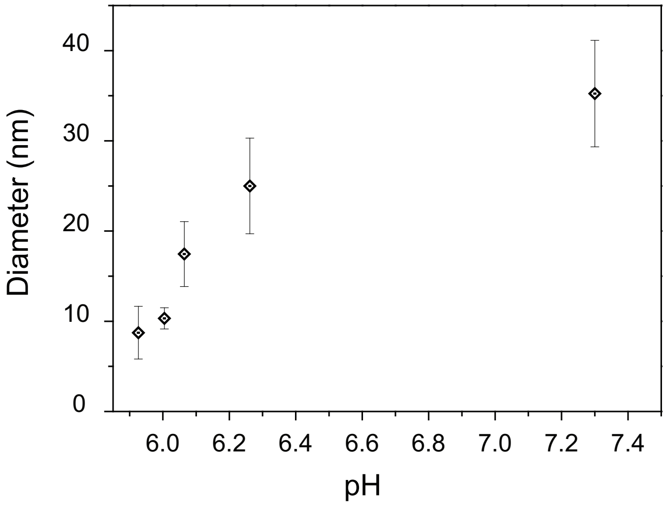

FIGURE 6.2: Average diameter of 250μg/mL solution of PPCHOL15 in PBS at different pH.

The grafting of cholesterol on the PLP backbone therefore inhibits the pH sensitive feature of the polymer, which remains in a globular or less extended conformation even at neutral pH. This is caused by the low grafting percentage (15%) of the lipid to the poly(L-lysine isophthalamide) backbone. The pH-mediated conformational change observed in amino acid grafted polymers is regulated by the balance between the hydrophobic moieties and the charged carboxyl groups, with the hydrophobic backbone with carboxyl groups undergoing random-coil to globular conformational transitions [191].

6.1.2 GUVs formed in PPCHOL solution

We compared the phase of GUVs for DOPC:DPPC 6:4 formed in PBS (Fig. 6.3 A) and DOPC:DPPC 6:4 formed in 0.5 mg/mL polymer solution in PBS (Fig. 6.3 B) by analyzing the emission spectra of Di-4 incorporated in the lipid bilayer.

Vesicles formed in polymer-free buffer display clear phase coexistence between S_o and L_α domains. Gel domains appear as dark spot due to the preferential partinioning of the fluorescent probe in the fluid phase [147]. Analysis of the emission spectra shows a single emission maximum located at 648.3 ± 8.3 nm, a value consistent with Di-4 spectra reported for pure DOPC membranes [147].

Formation of vesicles in 500 μg/mL of polymer results in significant changes in the membrane phase behaviour. The bilayer displays homogenous fluorescence intensity with no visible domains (Fig. 6.3 B). The lack of domains indicates an increase of miscibility between the two lipids induced by the presence of the polymer. Moreover, Di-4 emission spectra are significantly different and display two separate contributions.

The presence of the two peaks suggest the existence of two distinct populations at sub-resolution level. Moreover, the higher wavelength maximum for vesicle formed in polymer solution are shifted with respect to polymer-free GUVs to lower wavelengths (Fig. 6.4).

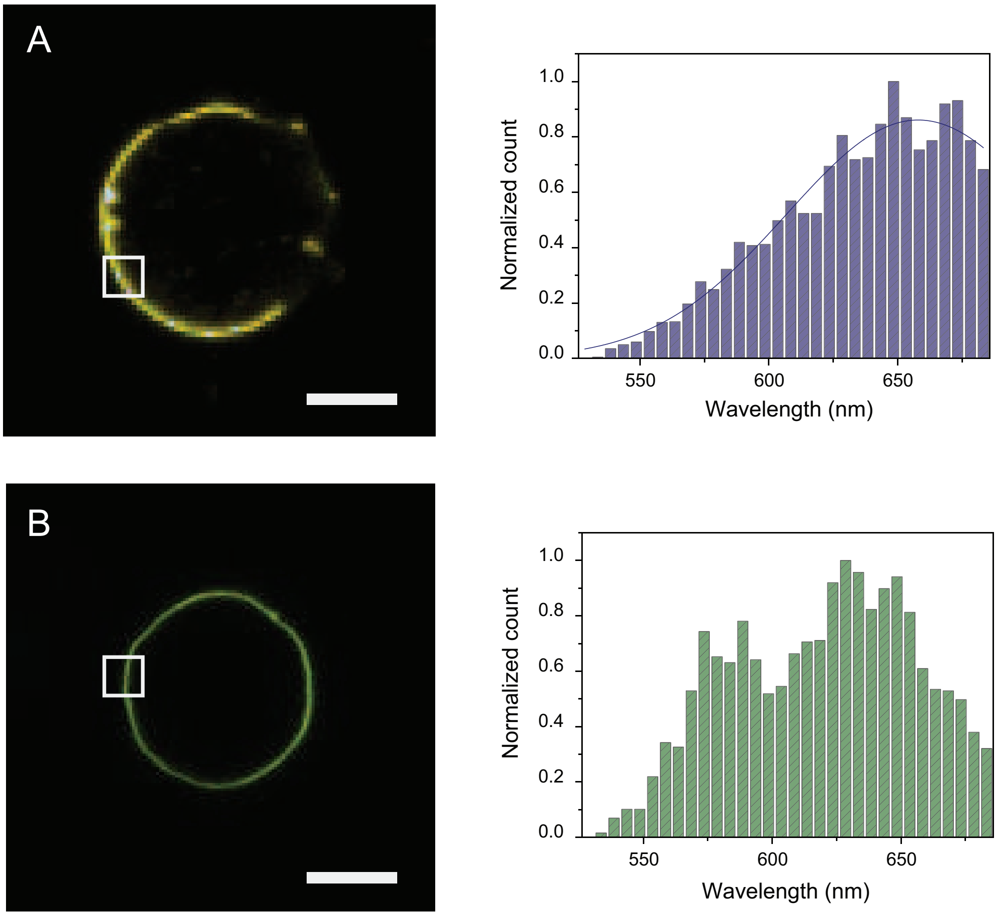

FIGURE 6.3: (A) Typical GUVs composed of DOPC:DPPC 6:4 formed in PBS at pH 7.4 and relative local Di-4 emission spectra. (B) Typical GUVs composed of DOPC:DPPC 6:4 formed in 500 μg/mL PPCHOL solution in PBS at pH 7.4 and relative local Di-4 emission spectra. Scale bar 10 μm.

To confirm whether the resulting emission spectra is due to two separate populations or a single uniform signal, we performed a fitting on the emission spectra using a single contribution and a two contribution Gaussian model. Fitting with a single curve (Fig. 6.5 A) shows good agreement (χ^2 = 0.016) with experimental data, yielding an emission maximum of 625.6 ± 2.7 nm, close to values reported for DOPC:DPPC:Chol bilayers [147].

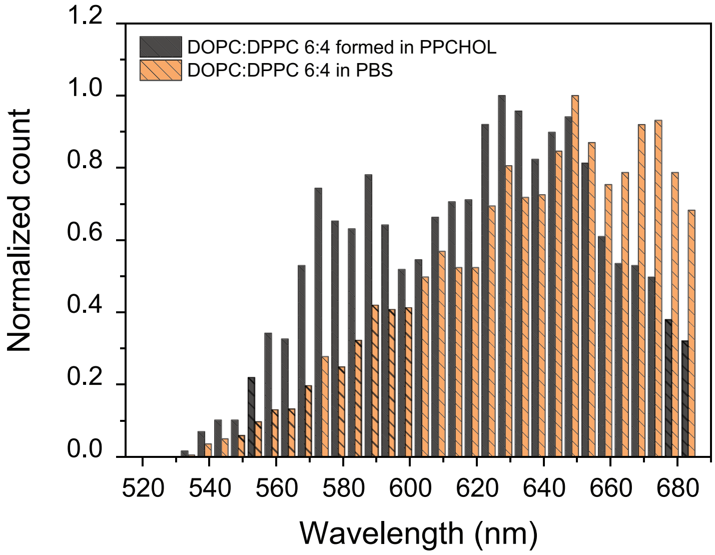

FIGURE 6.4: Average emission spectra of Di-4 for GUV composed of DOPC:DPPC 6:4 formed in PBS at pH 7.4 (orange) and DOPC:DPPC 6:4 formed in 500 μg/mL solution of PPCHOL in PBS at pH 7.4.

Using a two-component model also provides very good fitting (χ^2 = 0.005) with respective emission maxima located at 576.6 ± 1.6 nm and 636.6 ± 1.7 nm. Sgnificantly, these values are consistent with Di-4 reported for DPPC:Chol and DOPC:Chol, respectively [147]. Although it is not possible to univocally indicate whether the resulting emission spectra is due to a single phase or a coexistence of two distinct populations, the value obtained for the characteristic wavelengths indicate the presence of cholesterol within the membrane.

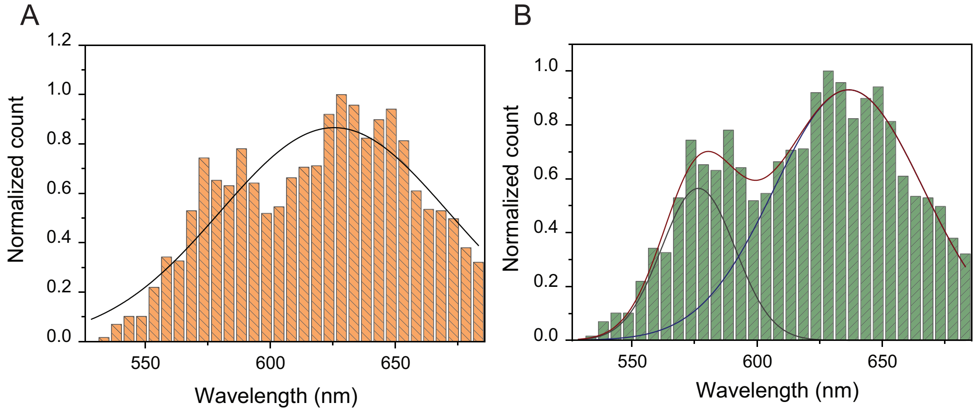

FIGURE 6.5: (A) Single gaussian fitting (black line) of Di-4 emission spectra for GUVs formed in 500 μg/mL PPCHOL solution (orange). (B) Double gaussian fitting (red line) of Di-4 emission spectra for GUVs formed in 500 μg/mL PPCHOL solution (green), showing the two individual fitting contributions

We argue that the presence of the polymer and of cholesterol in the membrane reduce the hydrophobic mismatch between DOPC and DPPC, thus increasing the miscibility between the two lipids.

6.2 Conclusions

Our results show that the presence of the cholesterol-grafted polymer significantly disrupts the phase behavior of DOPC:DPPC membranes, inducing a mixing between the two lipids either by intercalation of cholesterol or polymer chains. The emission spectra obtained show that although mixing occurs at optical scale, two separate populations exists, close to the L_o and L_d observed for ternary lipid membranes containing cholesterol.

Albeit preliminary, our data suggest that grafting of membrane altering molecules on the backbone of polymers is a viable approach in developing therapeutic strategies for varying the properties of cell membranes.

6.3 Materials and methods

Materials

Chloroform solution of DOPC (1,2-dioleoyl-sn-glycero-3-phosphocholine, $C_{44}H_{84}NO_8P$, M_w 786.11) and DPPC (1,2-dipalmitoyl-sn-glycero-3-phosphocholine, $C_{40}H_{80}NO_8P$, $M_w = 734.039$) were purchased from Avanti Polar Lipid (Birmingham, AL). PBS and Di-ANEPPDHQ were provided by ThermoFisher Scientific (Waltham, MA, USA). All chemicals had high purity and were used without further purification. PPCHOL was synthesized and provided by Alex Chen, University of Cambridge, as a part of a joint collaboration within the ITN SNAL consortium. The osmolarities of the PBS solutions were measured with a cryoscopy osmometer Osmomat 030 (Gonotec; Berlin, Germany)

Giant unilamellar vesicles preparation

GUVs composed of DOPC:DPPC were prepared by gel assisted formation following the protocol introduced by Weinberger [194]. Simply, 5 μl of 2 mg/mL solution of DOPC:DPPC at the desired molar ratio in chloroform were spread a PVA coated borosilicate glass. The formation glass was kept under vacuum for at least 1 hour to ensure complete evaporation of solvent and subsequently the lipid film was hydrated using the necessary solution (PBS or PPCHOL in PBS) at 55°C. Solution of Di-ANEPPDHW in PBS was added to the GUV suspension to reach a 1% molar ratio with respect to lipids and incubated above melting temperature for 30 min in absence of illumination.

Optical Microscopy

Imaging of GUVs was performed using a confocal laser scanning microscope Nikon Eclipse TE2000-E equipped with a Nikon camera. The objective was a Nikon 60x water immersion, NA 1.2 (Nikon) using an excitation line of 543 nm with a mercury lamp. The conventional three-band filter was substituted with a 20/80 R/T filter to perform spectral imaging, using a 488 excitation line Ar laser. DOPC:DPPC samples were kept at ambient temperature °C for at least 2 hours after preparation to ensure complete stabilization of domains. 100 μL of a GUV solution were placed on a borosilicate glass slide and sealed with a silicon spacer and an additional glass slide to prevent any leakage or solvent evaporation. For each lipid:PS composition we acquired images of two (n = 2) separate samples of 40 vesicles each.

7

Conclusions and future outlook

The plasma membrane is the primary barrier between the cell interior and the external environment; it regulates its functionality and it is a part of the cell signalling processes. Lipids are the primary membrane components, responsible for the structural integrity and mechanical properties. Active processes in the cell regulate lipid composition in the membrane, so to maintain membrane fluidity. Lipids coexist and display different structures depending on the type of lipid and external factors like temperature, an important property known as phase behaviour. Biological systems are inherently complex, therefore any small variation on the membrane phase behaviour can potentially perturb cell functionality.

In this work we succesfully investigated the effects of simple hydrophilic and hydrophobic molecules on the phase behaviour of lipid model membranes. Using a combination of steady-state fluorescence, differential scanning calorimetry (DSC), and fluorescence microscopy, we extracted structural information of the membrane, as well as on the thermodynamics of phase transition, upon interaction with different molecules. The use of environment-sensitive fluorescent probes to extract relevant information at the nanometer and micrometer length scales is also a key aspect of this work. Moreover, by using state-of-the art Cryo-TEM and neutron scattering we obtained a comprehensive picture of the interaction at the nanoscale level.

The main project of this thesis focuses on changes in the lipid bilayer phase behavior upon incorporation of polystyrene oligomers, motivated by an increasing concern regarding the presence of plastic waste in oceans, and their consequent degradation into possibly hazardous nanoparticles.

We performed a systematic study on the main phase transition of single component lipid bilayers composed of either DMPC, DPPC and DSPC. The incorporation of the polymer showed a clear decrease in enthalpic contribution, as observed by DSC, coupled with a small variation in melting temperature. The analysis of Laurdan emission spectra showed an increase of the bilayer order with increasing molar ratio of polymer. The information on the bilayer was complemented with SANS measurements and Cryo-TEM imaging, which demonstrated that polystyrene is more segregated in the S_o phase, and upon phase transition distributes homogenously in the lipid bilayer. The uniform distribution of the polymer within the membrane produces a tighter packing of the lipids due to the intercalation of the polymer in the acyl chains.

We further studied the potential hazard of small polystyrene chains on the cell membrane by investigating the effects of polystyrene on multicomponent lipid membranes. We demonstrated that for binary lipid systems, polystyrene induced a depression of the liquidus line between the S_o/L_α phase coexistence region and the fluid phase, as shown by Laurdan fluorescence spectroscopy and analysis on GUVs. The shift in temperature of the phase diagram induced by the polymer was successfully described using a thermodynamics model, which showed that the reduction of enthalpic contribution can be ascribed as the main driving force. Moreover, it was demonstrated that polystyrene induces different alterations in membranes containing cholesterol. Direct visualization of Di-4 emission spectra in GUVs composed of DOPC:DPPC:Chol showed a preferential partitioning of the polymer in the L_α phase, with a stabilizing effect on the L_d/L_o coexistence. Our results indeed show that polystyrene disrupts the phase coexistence of multicomponent membrane, thus reinforcing the suggestion that nanometric polymers are hazardous for membrane viability and provides indications for future studies on the effects of plastic nanomolecules on lipid membranes.

The second project of this work is devoted to the study of changes induced by high concentration of sucrose on the phase transition of DPPC model membranes, motivated by the crucial role sugars play in the biopreservation and cryopreservation field. Our experimental observations suggest that sucrose can induce a dehydration of the bilayer, as recorded by Laurdan emission spectra. The removal of water molecules, coupled with the formation of lipid-sucrose clusters, reduces the overall enthalpy of the transition and increases the transition temperature, as measured by DSC. We successfully described the interaction using a thermodynamic model and performed numerical simulations that are in good agreement with our experimental data. Our results provide a novel interpretation on the sucrose/lipid interplay and is relevant in understanding interactions with other hydrophilic molecules.

Last, together with our ITN SNAL collaborators at the University of Cambridge, we started the characterization of the interaction between model lipid membranes and a cholesterol grafted polymer as a potential membrane altering agent. The molecule synthetized by our collaborators (named PPCHOL) has a cholesterol grafted to its pH-sensitive backbone, and due to this feature, it is believed to change the fluidity of the membrane upon adsorption at physiological pH, therefore it is a potential carrier for novel lipidomic therapeutic strategies. Our preliminary results show that the grafting of cholesterol inhibits the pH sensitivity of the polymer and decreases its solubility, as measured by DLS. In physiological conditions, however, formation of DOPC:DPPC giant unilamellar vesicles containing the polymer show a drastic increase of the miscibility between the two components. Moreover, the DI-ANEPPDHQ emission spectra, probed locally via confocal spectral imaging, show a unique signal which has never been reported before, that we interpreted as the coexistence of small clusters of L_o and L_d phases. This exciting result does prove that the polymer may act as a membrane altering system, and calls for further investigation of the interaction.

In conclusion, this Ph.D. thesis presents a comprehensive study of the effects of hydrophobic/hydrophilic molecules on the phase behaviour of lipid membrane. We demonstrated that the combination of environment sensitive fluorescent probes, calorimetry and confocal imaging is a powerful set of tools to characterize variations in phase behavior, thus providing a clearer picture of the interactions taking place.

A

Supplementary material for: Polystyrene in a single component lipid bilayer

A.1 Supplementary figures

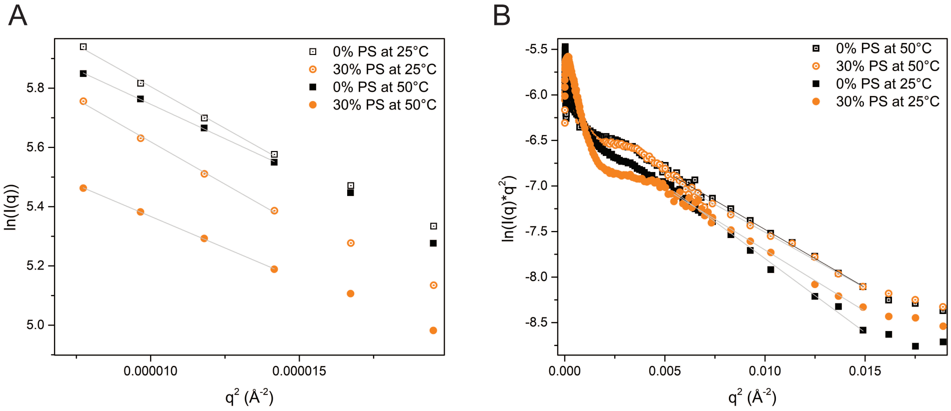

Figure A.1: (A) Guinier plot for h-DPPC (black squares) and h-DPPC:PS (orange circles) at 25°C (empty symbols) and 50°C (filled symbols) in D_2O solvent. (B) Kratky-Porod plot for h-DPPC (black squares) and h-DPPC:PS (orange circles) at 25°C (empty symbols) and 50°C (filled symbols) in D_2O solvent.

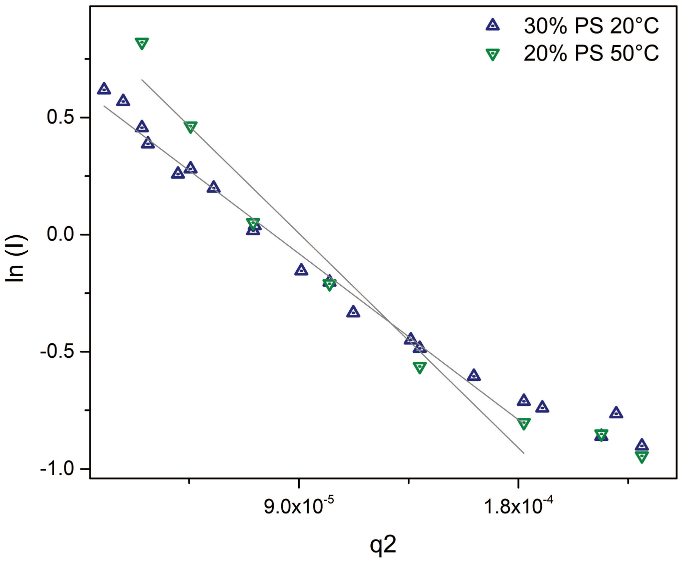

FIGURE A.2: (A) Guinier plot for d62-DPPC:PS at 20°C (blue triangle) and 50°C (green inverted triangles) in H_2O/D_2O 92:8 solvent.

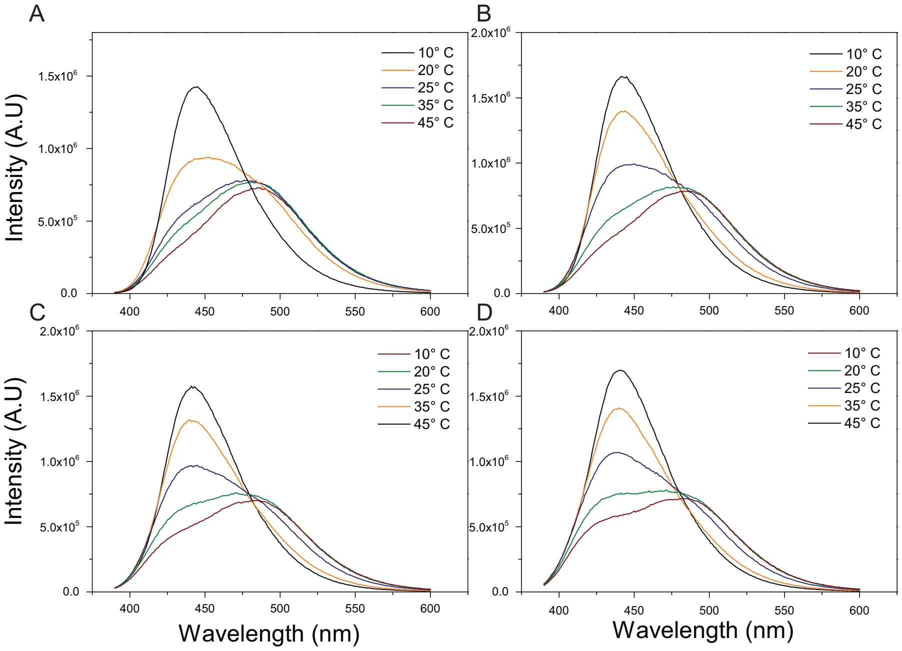

FIGURE A.3: Comparison of emission curves of Laurdan for pure DMPC (A), DMPC:PS 90:10 (B), DMPC:PS 80:20 (C) and DMPC:PS 70:30 (D) at 10°C (black line), 20°C (orange line), 25°C(blue line) 40°C(green line) and 50°C (red line).

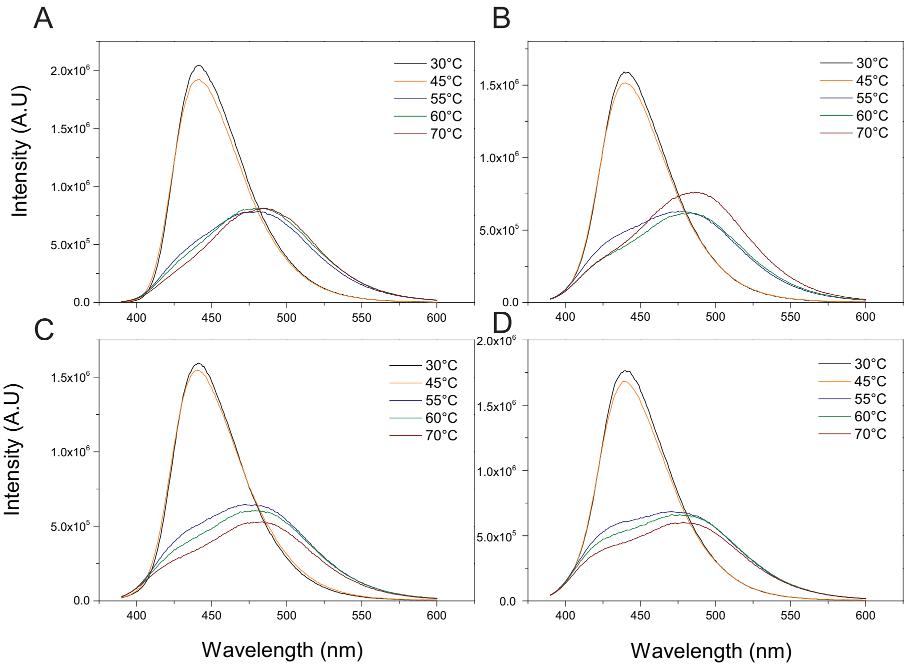

FIGURE A.4: Comparison of emission curves of Laurdan for pure DSPC (A), DSPC:PS 90:10 (B), DSPC:PS 80:20 (C) and DSPC:PS 70:30 (D) at 30°C (black line), 45°C (orange line), 55°C(blue line), 60°C(green line) and 70°C (red line).

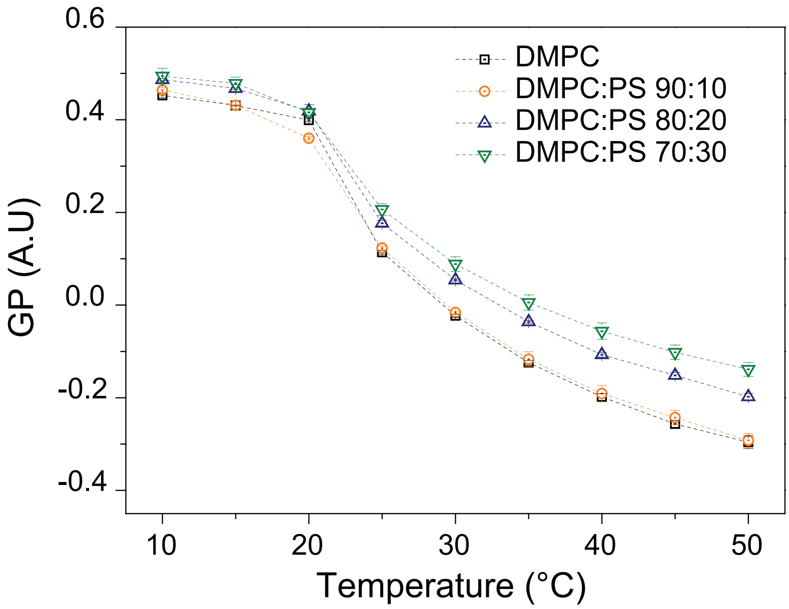

FIGURE A.5: Variation of General Polarization over temperature for multilamellar liposomes of DMPC formed in water at 0 (black squares), 10% (orange circles), 20% (blue triangles) and 30% (green inverted triangles) molar fraction of polystyrene.

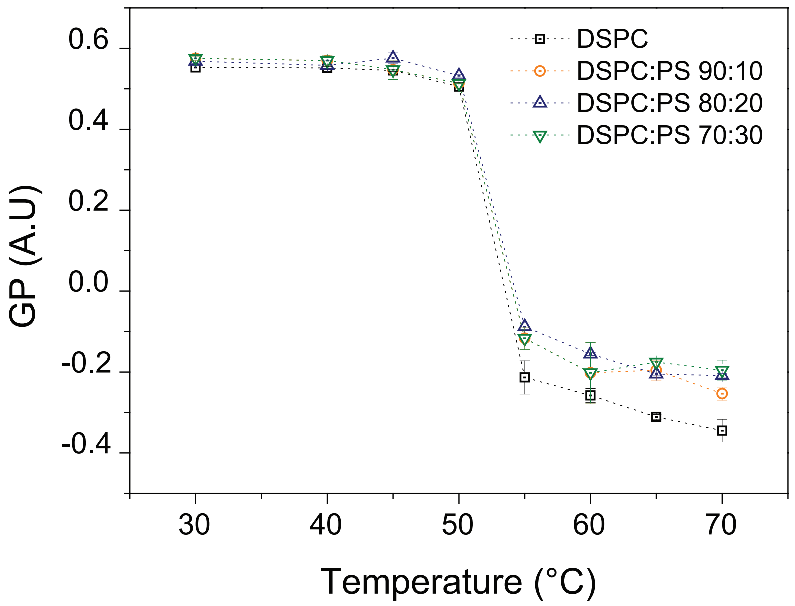

FIGURE A.6: Variation of General Polarization over temperature for multilamellar liposomes of DSPC formed in water at 0 (black squares), 10% (orange circles), 20% (blue triangles) and 30% (green inverted triangles) molar fraction of polystyrene.

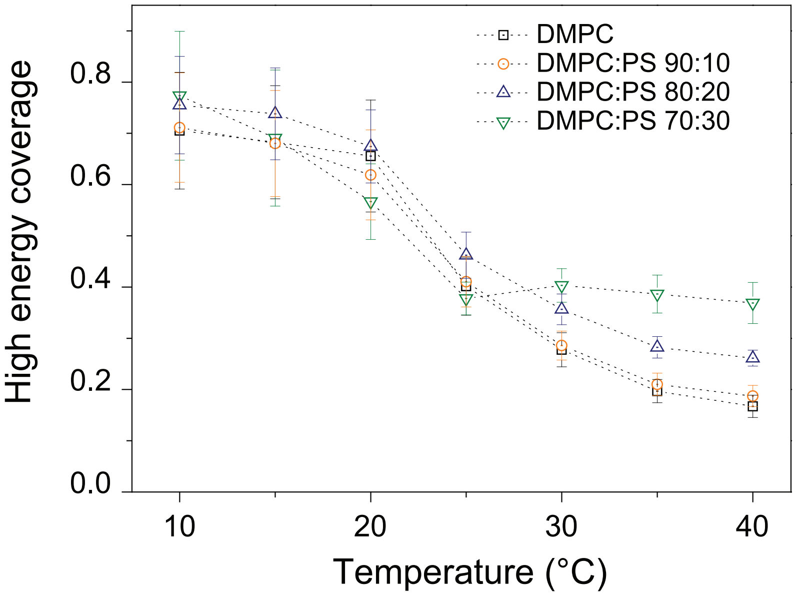

FIGURE A.7: Area fraction of 440 nm contribution in DMPC liposomes over temperature at 0% (black squares), 10% (orange circles), 20% (blue triangles) and 30% (green inverted triangles) polystyrene molar fraction.

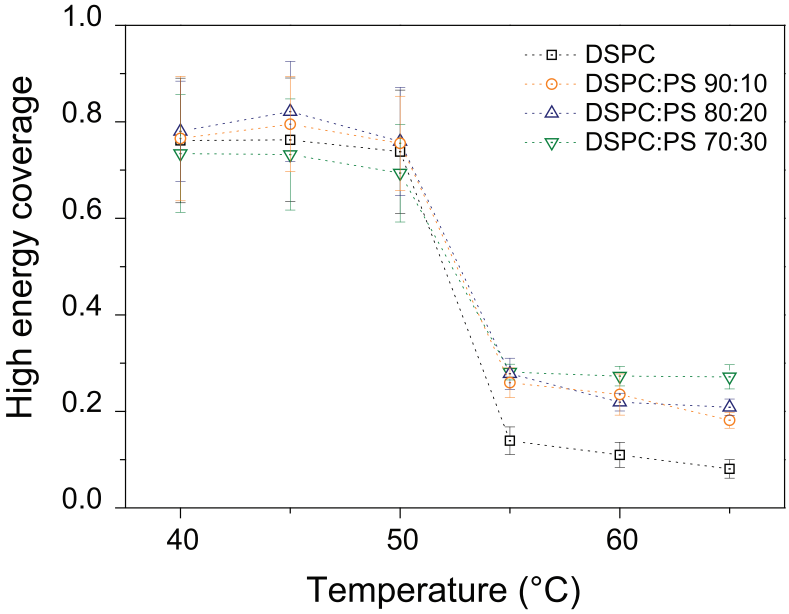

FIGURE A.8: Area fraction of 440 nm contribution in DSPC liposomes over temperature at 0% (black squares), 10% (orange circles), 20% (blue triangles) and 30% (green inverted triangles) polystyrene molar fraction.

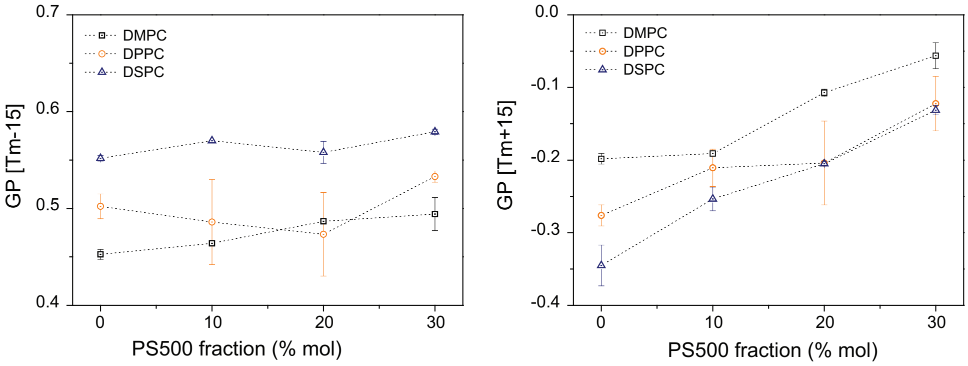

FIGURE A.9: (A) Values of general polarization at temperature $T_m - 15$ for DMPC (black squares), DPPC (orange circles) and DSPC (blue triangles) at different polystyrene molar fraction.(B) Values of general polarization at temperature $T_m + 15$ for DMPC (black squares), DPPC (orange circles) and DSPC (blue triangles) at different polystyrene molar fraction.

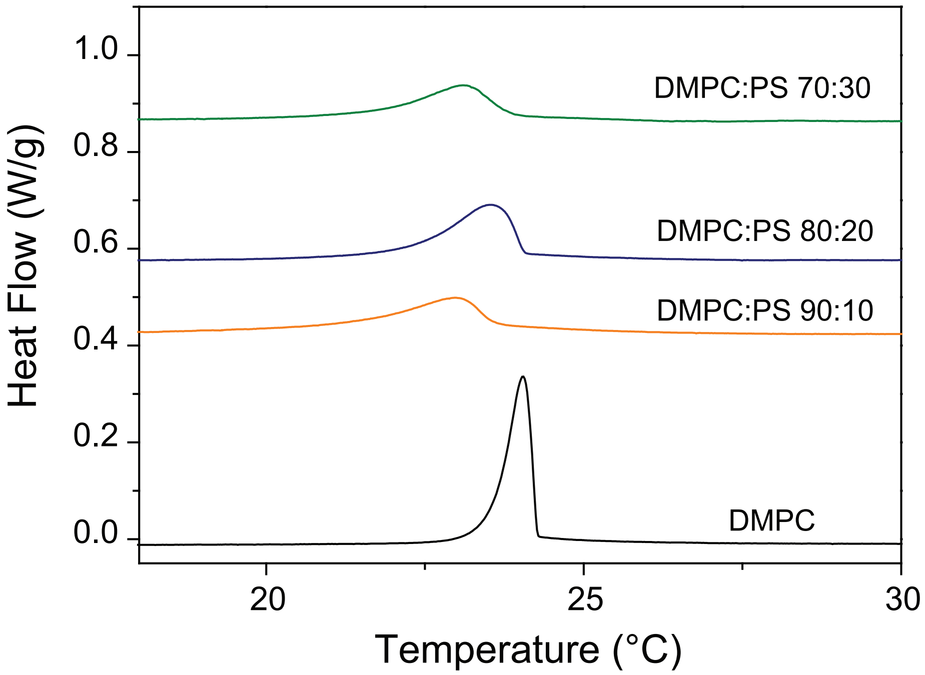

FIGURE A.10: DSC thermographs of DMPC liposomes containing increasing amount of polystyrene. Each curve represents the second thermographic signal from the full run experiment.

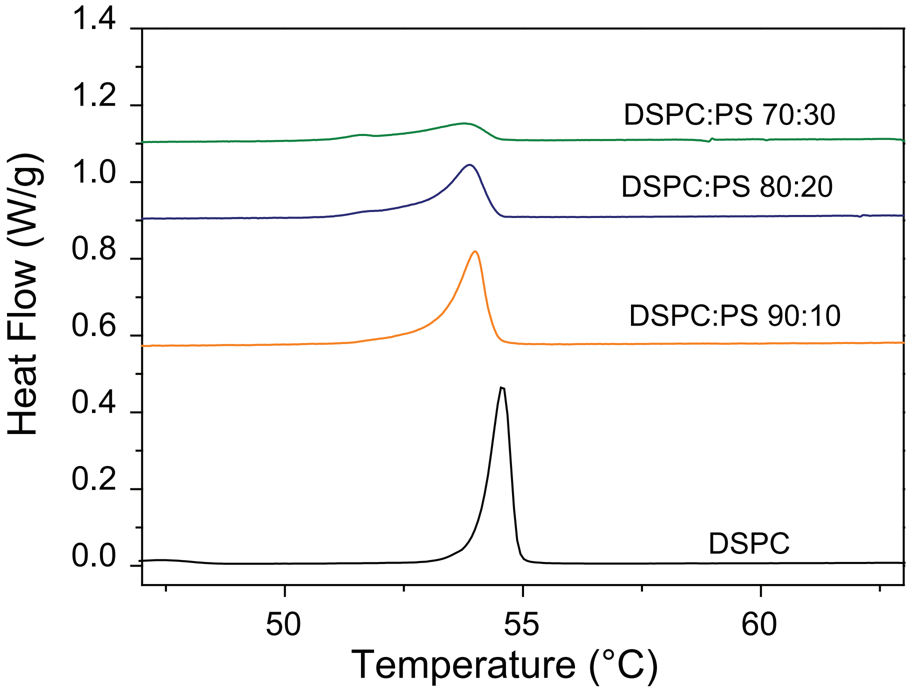

FIGURE A.11: DSC thermographs of DSPC liposomes containing increasing amount of polystyrene. Each curve represents the second thermographic signal from the full run experiment.

Polystyrene fraction [% mol]	ΔH kJ/mol	T_m °C	$T_{1/2}$ °C
0	26.3 ± 0.3	24.1 ± 0.1	0.19 ± 0.01
10	23.8 ± 0.5	23.8 ± 0.2	0.28 ± 0.01
20	22.8 ± 1.3	23.4 ± 0.4	0.53 ± 0.01
30	18.3 ± 1.2	23.3 ± 0.3	0.67 ± 0.01

TABLE A.1: Calculated ΔH, T_m and $T_{1/2}$ for DMPC with increasing molar fractions of polystyrene.

Polystyrene fraction [% mol]	ΔH kJ/mol	T_m °C	$T_{1/2}$ °C
0	43.1 ± 0.7	54.9 ± 0.3	0.23 ± 0.01
10	36.1 ± 0.8	54.4 ± 0.3	0.35 ± 0.01
20	24.1 ± 0.1	54.4 ± 0.7	0.47 ± 0.01
30	18.4 ± 0.5	54.1 ± 0.4	0.80 ± 0.01

TABLE A.2: Calculated ΔH, T_m and $T_{1/2}$ for DSPC with increasing molar fractions of polystyrene.

A.2 SANS disk model

This model calculates the form factor for a monodisperse right circular cylinder with uniform scattering length density. The form factor is normalized by the particle volume such that:

$$P(q) = \frac{scale}{V_{cyl}} \int_0^{\pi/2} f^2(q,\alpha) \sin\alpha d\alpha \tag{A.1}$$

where $V_{cyl} = \pi r^2 L$ is the volume of the cylinder, q is the scattering vector, α is defined as the angle between the cylinder axis and the scattering vector and the function f is defined as:

$$f(q,\alpha) = 2\Delta\pi V_{cyl} j_0(qH\cos\alpha)\frac{J_1(qr\sin\alpha)}{q^2}(qr\sin\alpha) \tag{A.2}$$

with $\Delta\rho$ the scattering length difference between the sample and the solvent, $j_0(x) = sin(x)/x$ and j_1 is the first order Bessel function. The integral over alpha averages the form factor over all possible orientations of the cylinder with respect to q.

A.3 SANS lamellar model

This model calculates the form factor from a lyotropic lamellar phase, assuming lamellae of uniform scattering length density that are randomly distributed in solution. No inter-lamellar structure factor is calculated. The scattering intensity $I(q)$ is:

$$I(q) = \frac{P(q)}{q^2}(\delta q^2) \tag{A.3}$$

where q is the scattering vector, δ is the bilayer thickness and $P(q)$ is the form factor defines as:

$$P(q) = 2\pi \frac{2\Delta\rho^2}{q^2}(1 - \cos(q\delta)) \tag{A.4}$$

with $\Delta\rho$ the scattering length difference between the sample and the solvent.

B

Changes in multi-component phase diagrams upon incorporation of polystyrene

B.1 Estimation of gel domains area coverage in GUV

To estimate the area fraction of S_o domains in liquid phase, we analyzed epifluorescence images of giant unilamellar vesicles. the area of solid domain was approximated to a circle of equivalent area. To correct for the sphericity of the vesicles, we tested two different approximations. For both approximations we obtained similar values of area coverage.

In case of vesicles presenting multiple domains or very elongated domains we subdivided the area covered by the solid phase into smaller approximated circles (Fig.).

B.1.1 Approximation A: determination of arc length

The area of the domain can be obtained by the measured diameter l (Fig B.1 A), which must be corrected to account for the sphericity of the GUV. To determine the real length of the domain, it is necessary to calculate the arc length γ spanned by a projected length l. Using a circular approximation (Fig B.1 B) yield that the arc length γ is equal to:

$$\gamma = \frac{\alpha}{\pi} \cdot 2\pi R \tag{B.1}$$

where α is the angle in radiants spanned by the length l. The angle α can be calculated by considering that

$$\frac{\alpha}{2} = \arccos(\frac{h}{R}) \tag{B.2}$$

where $h = \sqrt{R^2 - (l/2)^2}$ is the distance from the center of the projected l to the center of the circle.

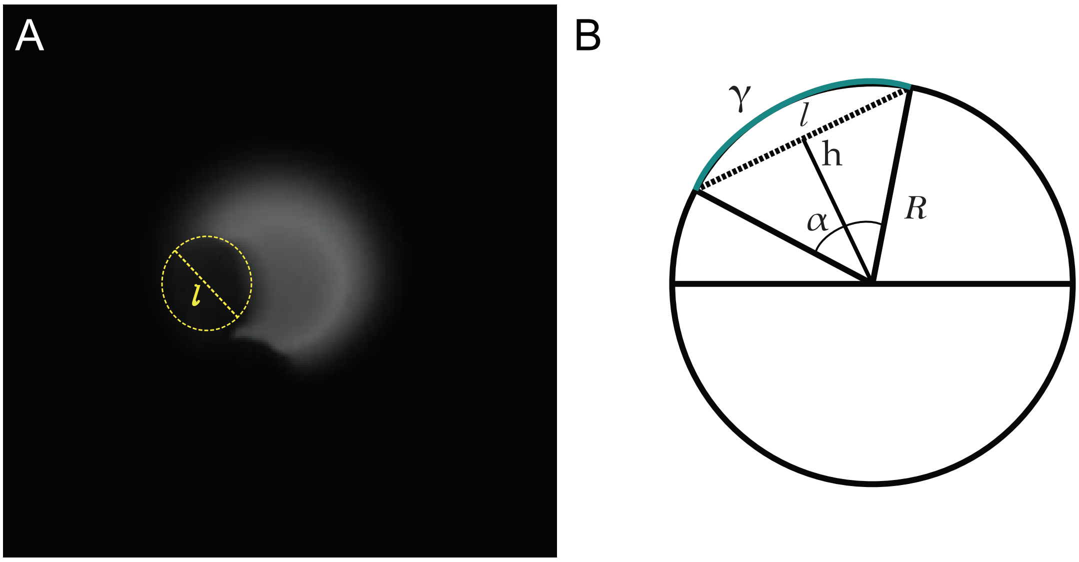

FIGURE B.1: (A) Image treatment for arc length approximation. (B) Schematics of the arc length estimation.

The fraction f of the solid area with respect to the area of the vesicle is defines as

$$f = \frac{S_g}{S_{GUV}} = \frac{2\pi(\gamma/2)^2}{4\pi R^2} = \frac{\gamma^2}{8R^2} \tag{B.3}$$

Therefore combining equation B.3, B.1 and B.2, we obtain

$$f = \frac{1}{2R} \cdot \arccos(\frac{\sqrt{R^2 - (l/2)^2}}{R}) \tag{B.4}$$

B.1.2 Approximation B: determination of solid angle

An alternative approach to measure the area spanned by a domain is to use spherical approximation (Fig. B.2). Unnder this approximation the area coverage f of a domain is

$$f = 1 - \cos\theta \tag{B.5}$$

where θ is the angle spanned by the circle of the domain. It is possible to determine θ by measuring the projected length l and calculate the angles spanned by the two projected points of l (Fig. B.2 B).

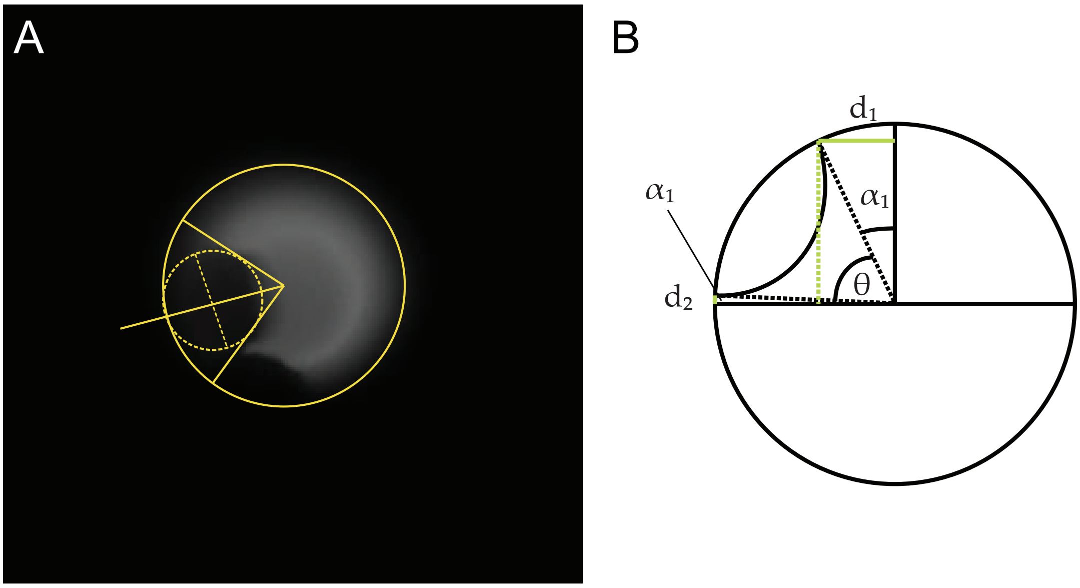
A
B
d_1
α_1
α_1
d_2
θ

FIGURE B.2: (A) Image treatment for solid angle approximation. (B) Schematics of the solid angle estimation.

Therefore θ can be written as:

$$\theta = \pi/2 - (\alpha_1 + \alpha_2) \tag{B.6}$$

C

Supplementary material for: DPPC bilayers in solution of high sucrose content

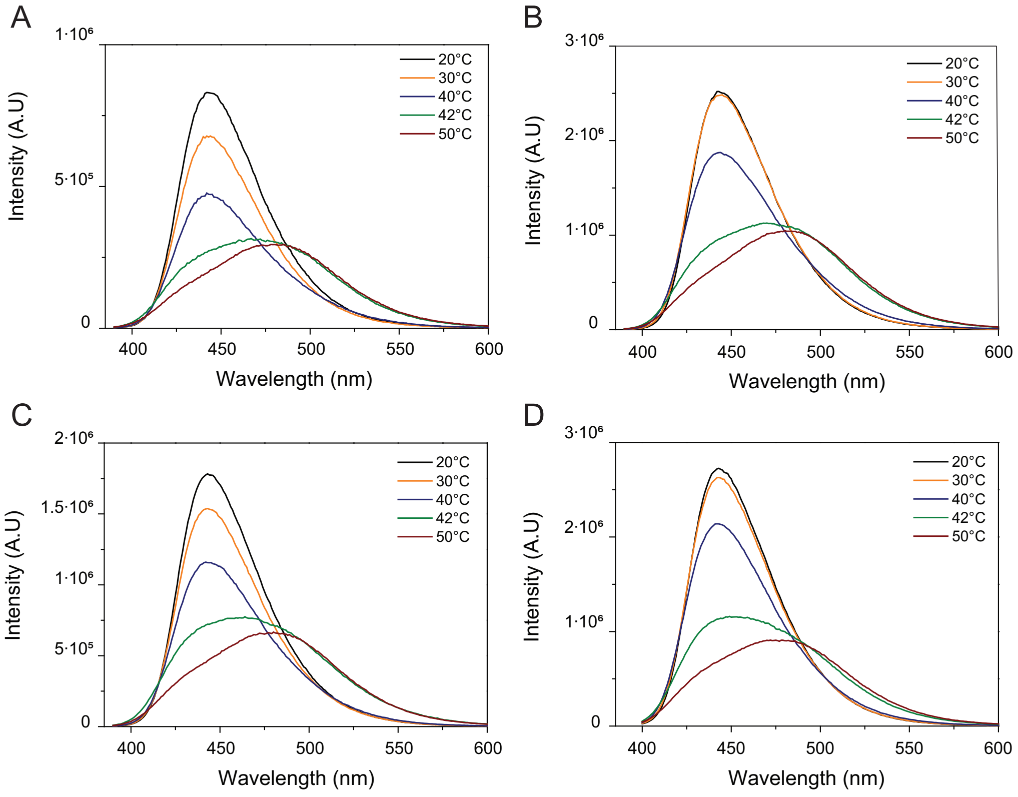

FIGURE C.1: Comparison of emission curves of Laurdan for DPPC MLVs formed in (A) water, (B) 0.12 M sucrose, (C) 0.7 M sucrose and (D) 1.5 M sucrose at 20°C (black line), 35°C (orange line), 42°C(blue line), 50°C(green line) and 60°C (red line).

C.1 Derivation of thermodynamics model for sucrose-lipid interaction

C.1.1 Cooperativity in the lipid main transition

It is assumed that two phases (gel and fluid) exchange their stability at a coexistence temperature T_m by means of a first order transition mechanism. Let us introduce the number of lipids N, the total Gibbs free-energies G_l, G_g, the enthalpies H_l, H_g and entropies S_l, S_g in the fluid and gel phases.

Molecular quantities are defined as $g_l = G_l/N$, $g_g = G_g/N$, $h_l = H_l/N$, $h_g = H_g/N$, $s_l = S_l/N$, $s_g = S_g/N$. Finally, we introduce the differences $\Delta g = g_l - g_g$, $\Delta h = h_l - h_g$, $\Delta s = s_l - s_g$ between the high and low temperature phases. We denote by T the absolute temperature, and $\beta = 1/(k_B T)$ the inverse temperature factor. The probability of occurrence of a phase is proportional to $\exp(-\beta G)$. As the Gibbs free-energy scales with the number of lipid, phases cannot coexist except but in a narrow temperature interval centered around T_m.

A standard thermodynamic relation states that

$$\frac{\mathrm{d}(\beta G)}{\mathrm{d}\beta} = G + \beta\frac{\mathrm{d}}{\mathrm{d}\beta}G = G - T\frac{\mathrm{d}}{\mathrm{d}T}G = G + TS = H. \tag{C.1}$$

On the other hand, at the coexistence temperature $\Delta G(T_m) = 0$. One can expand to first order in $T - T_m$ the difference in Gibbs free-energy

$$\beta\Delta G \simeq (\beta - \beta_m)\Delta H_m \simeq -\frac{T - T_m}{k_B T_m^2}\Delta H_m. \tag{C.2}$$

The probability of occurrence of the gel and liquid phases reads

$$\begin{aligned} p_l(N,\beta) &= \frac{e^{-\beta G_l}}{e^{-\beta G_l} + e^{-\beta G_g}} = \frac{1}{1 + e^{\beta N \Delta g}}; \\ p_g(N,\beta) &= \frac{e^{-\beta G_g}}{e^{-\beta G_l} + e^{-\beta G_g}} = \frac{1}{1 + e^{-\beta N \Delta g}}. \end{aligned} \tag{C.3}$$

The transition takes place on a temperature interval ΔT given by $\beta N \Delta g =$ $= N\Delta T \Delta h_m / k_B T_m^2 \sim 1$. It is inversely proportional to N.

To provide a phenomenological description of the melting transition, one introduces a cooperativity number N_c as the effective number of lipids that share the same internal state. The system is then treated as an assembly of N/N_c "bundles" changing state independently, with $N/N_c \gg 1$. The equilibrium enthalpy at temperature T is given by:

$$H(T) = N(p_l(N_c,T)h_l + p_g(N_c,T)h_g) = N(p_l(N_c,T)\Delta h + h_g). \tag{C.4}$$

where liquid-gel mismatch energy contributions are neglected and h_l and h_g are taken independent of temperature at the vicinity of the transition. Then

$$\begin{aligned} \frac{\mathrm{d}H}{\mathrm{d}T} &= N\Delta h \frac{\mathrm{d}p_l}{\mathrm{d}T}, \\ &= N\Delta h \frac{-e^{\beta N_c \Delta g}}{(1+e^{\beta N_c \Delta g})^2} \frac{\mathrm{d}\beta N_c \Delta g}{\mathrm{d}T}, \\ &= N N_c \frac{(\Delta h)^2}{k_B T^2} \frac{e^{\beta N_c \Delta g}}{(1+e^{\beta N_c \Delta g})^2}, \\ &= n N_c \frac{(\mathcal{N}_A \Delta h)^2}{4RT^2} \frac{1}{\mathrm{ch}(\beta N_c \Delta g/2)^2}, \end{aligned} \tag{C.5}$$

with $\mathcal{N}_A$ the Avogadro number, $\mathcal{N}_A \Delta h$ the molar enthalpy change at the transition, n the number of moles of lipids.

The peak maximum is at $\Delta g = 0$, $C_{p,max} = \mathrm{d}H/\mathrm{d}T|_{T=T_m} = nRN_c(\mathcal{N}_A\Delta h)^2/(4R^2T^2)$, from which N_c can be expressed in terms of molar quantities

$$N_c = \frac{C_{p,\mathrm{max}}}{n} \frac{4RT_m^2}{(\mathcal{N}_A \Delta h)^2} = 4\left(\frac{C_{p,max}}{nR}\right)\left(\frac{RT_m}{\mathcal{N}_A \Delta h}\right)^2. \tag{C.6}$$

C.2 Phenomenology of the lipid main transition

A simple insightful treatment of the lipid main transition was introduced by Doniach, and improved by several authors [178–180, 195–197]. It is based on a scalar order parameter showing two preferred values, one corresponding to the gel state, and the other to the fluid state. This statistical model can be implemented in practice by assigning binary variables (Ising spins) to the fixed vertices of a two dimensional lattice. Reference [178] presents in detail the historical development of the model.

In this approach, lipid molecules spontaneously adopt either a gel or a fluid conformation, depending on external thermodynamic conditions (temperature, but also isotropic pressure and membrane tension). In the Ising language, this is achieved by applying a uniform temperature (pressure, tension) dependent magnetic field that vanishes precisely at the coexistence temperature T_m, where fluid and gel are observed with equal probability. Additional nearest neighbour couplings (Js parameters) are introduced to enforce cooperativity. Above a critical J_c value, the system shows phase coexistence and metastability, with hysteretic thermal behavior upon heating and cooling cycles. Below the critical value, the system state evolves smoothly and reversibly with temperature. The latter case is therefore suitable to describe most experimental situations with a finite width, regular and reversible thermal capacitycurve determined *e.g.* in differential scanning calorimetry (DSC) experiments.

There is some freedom left in deciding whether the binary state is assigned to a whole lipid or just a lipid chain, or which lattice is most representative (the hexagonal lattice seeming the more appropriate), with all models in the end able to describe the observed behaviour [179]. Several Monte-Carlo studies were shown to successfully account for various situations of interest [197].

To explain the main features of sucrose induced changes in the DPPC melting transition, we implement one such model and solve it by means of a mean-field approximation. Each binary state takes a value 0 (gel) or 1 (fluid) and describe a single lipid molecule internal state. The average internal value is therefore a real number p comprised between 0 and 1, which is readily interpreted as the probability to find a lipid molecule in the fluid conformation. For a given microscopic configuration, one introduces a configurational energy

$$\Delta\mathcal{H} = N_l(\Delta h - T\Delta s) + JN_{gl}, \tag{C.7}$$

as the difference between the actual system state, and a reference state where all lipids would be in the gel state. N_l and N_{gl} are respectively the number of lipids in fluid state, and the number of lattice bonds linking lipids in a different state (state mismatch). J is the mismatch gel-fluid state penalty parameter. The quantity $\Delta\mathcal{H}$ determines the probability of the microscopic state, proportional to $\exp(-\beta\Delta\mathcal{H})$. Note that it is unusual to deal with temperature dependent "Hamiltonians" in statistical physics. The approach used here means that a coarse-graining step is performed by averaging over the inner conformations of each lipid molecule, while partitionning them into two broad classes (gel and fluid state). Eq. (C.7) is something of an intermediate quantity between the true (molecular) microscopic energy and the macroscopic Gibbs free-energy.

$\beta\Delta\mathcal{H}$ can be expanded around the coexistence temperature:

$$\beta\Delta\mathcal{H} = -\frac{\mathcal{N}_A\Delta h}{RT_m^2}(T - T_m)N_l + \frac{\mathcal{N}_A J}{RT_m}N_{gl}. \tag{C.8}$$

The Gibbs free-energy associated to the configurational energy above reads in the large N limit:

$$\beta\Delta G = \beta\langle\Delta\mathcal{H}\rangle - \mathcal{S}/k_B, \tag{C.9}$$

where appears the entropy $\mathcal{S}$ associated to the many internal gel-fluid microscopic configurations of the system. The above expression can be expressed at mean-field level by introducing the probability p of finding each lipid in the fluid state, and the average coordination z of a site in the lattice (average number of neighbouring lipid molecules, 6 for an hexagonal lattice). It reads

$$\beta\Delta G = -\frac{\mathcal{N}_A\Delta h}{RT_m^2}(T-T_m)Np+\frac{\mathcal{N}_A J}{RT_m}zNp(1-p)+N[p\ln(p)+(1-p)\ln(1-p)]. \quad \text{(C.10)}$$

The $\mathcal{S}/k_B = -N[p\ln(p)+(1-p)\ln(1-p)]$ expression is characteristic of the statistical entropy of N independent binary variables. The mean-field self-consistent equations result from minimizing $\beta\Delta G$ with respect to p, in order to find the best compromise between the number of configurations $\exp(\mathcal{S}/k_B)$ and the energy penalty $\langle\Delta\mathcal{H}\rangle$. One obtains

$$\ln(p)-\ln(1-p)+\frac{\mathcal{N}_A J}{RT_m}z(1-2p)-\frac{\mathcal{N}_A\Delta h}{RT_m^2}(T-T_m)=0, \quad \text{(C.11)}$$

or equivalently

$$\frac{p}{1-p}=\exp\left(\frac{\mathcal{N}_A\Delta h}{RT_m^2}(T-T_m)+\frac{\mathcal{N}_A J}{RT_m}z(2p-1)\right). \quad \text{(C.12)}$$

Self-consistent equations are trivially satisfied by

$$p(T)=\frac{\exp\left(\frac{\mathcal{N}_A\Delta h}{RT_m^2}(T-T_m)\right)}{1+\exp\left(\frac{\mathcal{N}_A\Delta h}{RT_m^2}(T-T_m)\right)} \quad \text{(C.13)}$$

at vanishing coupling $J=0$, and must be numerically solved in the general case.

There is freedom in deciding if the interaction term $-Jzp(1-p)$ is of enthalpic or entropic origin. Assuming that J is enthalpic and does not depend on temperature T, one derives the mean-field enthalpy difference

$$\Delta H(T)=Np(T)\Delta h+JzNp(T)(1-p(T)) \quad \text{(C.14)}$$

that can be compared with the experimental DSC thermograms once the solution of eq. (C.12) is obtained. Moreover, one observes that, irrespective of the choice done regarding the interaction term, the difference $\Delta H(p=1)-\Delta H(p=0)$ reaches the expected limit value $N\Delta h$, corresponding to the total latent heat upon melting completely the system from the gel to the fluid state.

Introducing the dimensionless coupling $\tilde{J}=\frac{\mathcal{N}_A J}{RT_m}z$, one finds that the critical value separating reversible and hysteretic temperature behaviour is $\tilde{J}_c=2$ in the mean-field approximation. A quite sharp specific heat peak can therefore be obtained with

$\tilde{J}_c \simeq 1.94$.

In the practical situation of a DPPC bilayer, when assigning binary variables to lipid molecules (not chains), treating lipids as basic degrees of freedom coupled with $\tilde{J}_c = 1.94$, and taking $\mathcal{N}_A \Delta h$ equal to the experimental value $38\ \mathrm{kJ} \cdot \mathrm{mol}^{-1}$ (9.1 kcal $\cdot\mathrm{mol}^{-1}$) leads to a non negligible amount of the minor component into the major component around the location of the phase transition. This means that the area under the peaked curve $\mathrm{d}\Delta H/\mathrm{d}T$ on a 10°C temperature interval centered around $T_m = 273.15 + 41.8 = 314.95$K gives a value 28 kJ$\cdot$mol^{-1}, smaller than the experimental one. This is inherent to the "Ising" like treatment of the internal degrees of freedom, and is also true for Monte-Carlo "exact" sampling of the configurations. To get around this shortcoming, one can decide on a phenomenological ground to assign a larger value to the constant $\mathcal{N}_A \Delta h$. We found that at mean field level, with $\tilde{J}_c = 1.94$, the correct $\Delta H(T_m + 5) - \Delta H(T_m - 5) = 38\ \mathrm{kJ} \cdot \mathrm{mol}^{-1}$ value is recovered for $\mathcal{N}_A \Delta h = 56\ \mathrm{kJ} \cdot \mathrm{mol}^{-1}$ (13.4 kcal$\cdot$mol^{-1}). There is then 16% of fluid lipid at $T_m - 5 = 36.8$°C and 84% at $T_m + 5 = 46.8$°C.

C.3 Influence of the sucrose on the gel transition

Increasing concentrations of sucrose in solution lead to a noticeable drop in latent heat (area under the specific heat curve) with only a tiny increase in the appearent melting temperature (of the order of 1K).

In first order phase transitions, the coexistence temperature T_m coincides with the ratio $\Delta h/\Delta s$. If the sucrose was only acting on changing the enthalpy jump $\Delta h'$, then keeping the melting temperature constant by 1 part in 300 would require a quasi-perfect matching of the entropy variation $\Delta s'$, with $T_m = \Delta h/\Delta s \simeq \Delta h'/\Delta s'$. On the other hand, it is well known that lipid melting temperature is extremely sensitive to molecular details. Perdeuteration of the DPPC alkyl chains, for instance, lowers the transition temperature by 4°C. Shifting one C16 fatty acid chain link with glycerol from *sn*-2 to *sn*-3 position has the same consequence. Going from *cis* to *trans* double bond insaturations raise the melting transition of DOPC by 60 K.

If one thinks of the action of sucrose as simply dehydrating the lipid headgroups, then a strong elevation of the melting transition temperature would be expected. Yet, the observed change goes in this direction, but in much weaker proportions. In addition, hydrophilic sucrose molecules are not really expected to interact with the bulk of hydrophobic alkyl chains region, which is where the largest part of the contribution to the enthalpy change Δh is expected to arise from.

Drops in latent heat at the transition can be alternatively explained by the presence of domains. If one assumes that in the presence of sucrose, lipids get separated into sucrose-depleted and sucrose enriched domains, and that only sucrose depleted domains melt as usual, with other domains remaining in the gel phase, then the result would also be a neat decrease in experimental latent heat. However, here is no clear reason for such domains to form, and this mechanism lacks experimental support.

We propose here an alternative mechanism where sucrose adsorbs indistinctly in the gel and fluid phases. Lipids that are in close contact with sucrose molecules are assumed to melt at a slightly higher temperature T'_m, and more importantly, to behave in a less cooperative way than in pure lipid water solutions. This could be justified for instance by saying that gel-fluid mismatch configurations are eased by surrounding sucrose molecules.

Adapting the previous model, the configurational energy becomes

$$\Delta\mathcal{H} = (\Delta h - T\Delta s)N_l + (\Delta h' - T\Delta s')N'_l + JN_{gl} + J'N'_{gl} + J''N''_{gl}, \tag{C.15}$$

with N_l the number of free lipids in fluid state, N'_l the number of lipid in fluid state in contact with sucrose, N_{gl} the number of unlike gel-fluid free lipid pairs, N'_{gl} the number of unlike gel-fluid lipid pairs, both in contact with sucrose and N''_{gl} the number of unlike gel-fluid pairs with one lipid free and one lipid in contact with sucrose, J, J', J'' being the corresponding mismatch penalties.

We assume now that the probability for a lipid to be in contact with sucrose is σ, that p is the average probability of finding free lipids in fluid state, and p' the average probabiliy of finding lipids in contact with sucrose in fluid state. The average configurational energy can be expressed in the mean-field limit.

$$\begin{aligned}\langle\beta\Delta\mathcal{H}\rangle &= -\frac{\mathcal{N}_A\Delta h}{RT_m^2}(T-T_m)(1-\sigma)Np - \frac{\mathcal{N}_A\Delta h}{RT_m^2}(T-T'_m)\sigma Np' \\ &\quad +N\tilde{J}(1-\sigma)^2p(1-p) + N\tilde{J}'\sigma^2p'(1-p') \\ &\quad +N\tilde{J}''\sigma(1-\sigma)[p(1-p')+p'(1-p)]\end{aligned} \tag{C.16}$$

where for simplicity we assume $\Delta h \simeq \Delta h'$, $T_m \simeq T'_m$ at the first order of the temperature expansion. The mean field configurational entropy then becomes:

$$\begin{aligned}
-\mathcal{S}/k_B &= N\Big[\sigma p' \ln(\sigma p') + \sigma(1-p')\ln[\sigma(1-p')] \\
&\quad +(1-\sigma)p\ln[(1-\sigma)p] + (1-\sigma)(1-p)\ln[(1-\sigma)(1-p)]\Big], \\
&= N\Big[\sigma\ln(\sigma) + (1-\sigma)\ln(1-\sigma) + \sigma[p'\ln(p') + (1-p')\ln(1-p')] \\
&\quad +(1-\sigma)[p\ln(p) + (1-p)\ln(1-p)]\Big]. \qquad \text{(C.17)}
\end{aligned}$$

The Gibbs free-energy $\beta\Delta G(p, p', \sigma, T) = \langle\beta\Delta\mathcal{H}\rangle - \mathcal{S}/k_B$ must now be minimised with respect to p and p'. We do not perform a minimisation over σ because we assume σ imposed by the sucrose molarity ([Sucrose]) of the hydrating solution.

The self-consistent equations become

$$\begin{aligned}
\ln\left(\frac{p}{1-p}\right) - \frac{\mathcal{N}_A\Delta h}{RT_m^2}(T-T_m) + \tilde{J}(1-\sigma)(1-2p) + \tilde{J}''\sigma(1-2p') &= 0; \\
\ln\left(\frac{p'}{1-p'}\right) - \frac{\mathcal{N}_A\Delta h}{RT_m^2}(T-T'_m) + \tilde{J}'\sigma(1-2p') + \tilde{J}''(1-\sigma)(1-2p) &= 0 \qquad \text{(C.18)}
\end{aligned}$$

With the numerical solution for $p(T), p'(T)$ determined, the temperature dependent enthalpy is readily obtained from eq. (C.16).

In practice, equations (C.18) are solved for each temperature T using the Newton-Raphson iteration scheme, starting initially from the exact solution at $\tilde{J} = \tilde{J}' = \tilde{J}'' = 0$, and iteratively converged for increasing values of the coupling constant. Below critical coupling $\tilde{J}_c = 2$, the method is fast and accurate.

An interesting behavior is obtained for the following choice of parameters:

- $T_m = 273.15 + 41.8\text{K}$, $T'_m = 273.15 + 41.8 + 5.0\text{K}$,
- $\tilde{J} = 1.94$; $\tilde{J}' = \tilde{J}'' = 0.97$,
- $\mathcal{N}_A\Delta h = \mathcal{N}_A\Delta h' = 56\ \text{kJ}\cdot\text{mol}^{-1}$.

The three graphs below explains how the decreased cooperativity mechanism works:

C.3.1 Connection with previous work and correspondence with the usual Ising model

Ising variables are usually binary variables s taking the values ±1. The order parameter $m = \langle s\rangle$ is a real number comprised between -1 and 1. The correspondence between p and m is

$$m = 2p - 1 \Leftrightarrow p = (1+m)/2. \qquad \text{(C.19)}$$

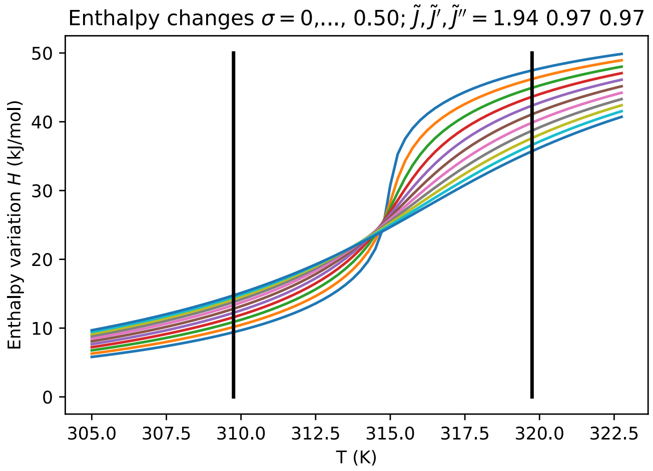

FIGURE C.2: Enthalpy variation with temperature as σ increases from 0 to 0.5. We integrate the area under the specific heat curve from $T_m - 5$ to $T_m + 5$.

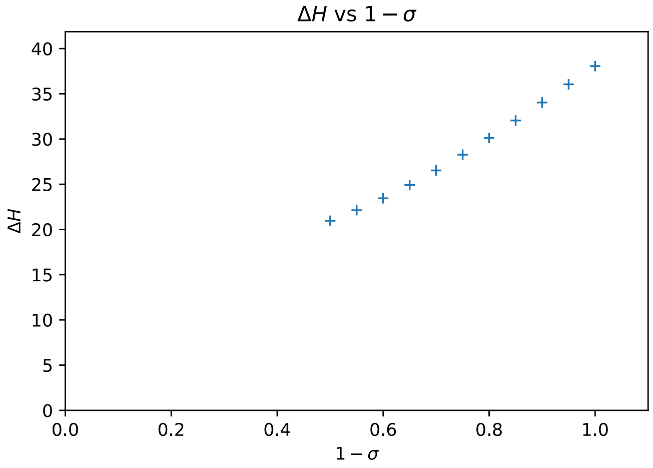

FIGURE C.3: Resulting enthalpy change vs $1 - \sigma$ (pure water at the right of the graph). We note that for the selected values, the ΔH curves seems initially to decrease linearly with $1 - \sigma$.

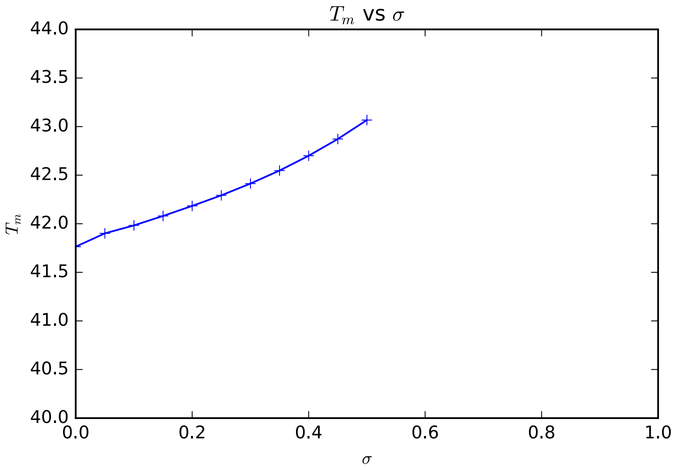

FIGURE C.4: Variation of the apparent melting temperature (inflexion point of $\Delta H(T)$)

At T_m, eq. (C.12) can be rewritten

$$\frac{1+m}{1-m} = \exp(\tilde{J}m), \tag{C.20}$$

which can be inverted as

$$m = \frac{e^{\tilde{J}m} - 1}{e^{\tilde{J}m} + 1} = \operatorname{th}(\tilde{J}m/2). \tag{C.21}$$

A comparison with the usual self-consistent Ising equation $m = \operatorname{th}(\beta J_{\text{Ising}} z m)$ shows that $J = 2J_{\text{Ising}}$. One could also have deduced it from the mismatch energy associated with two antiparallel spins around a bond ($2J_{\text{Ising}}$) which equals our mismatch energy J. Eq. (C.21) leads to the mean-field value $\beta J_{\text{Ising}} z = \tilde{J}/2 = 1$.

By comparison, the exact value of the critical point on a 2d hexagonal lattice Ising model is $\beta J_{\text{Ising}} = 0.2746\ldots$ (see [198], page 671). In our notations, this corresponds to $\tilde{J} = 0.5432$. Back to the original parameter J, one finds (with $z = 6$, and 1 cal=4.18 J):

- mean-field: $\mathcal{N}_A J = \frac{2}{z} R T_m = 860\ \mathrm{J} \cdot \mathrm{mol}^{-1} = 205\ \mathrm{cal} \cdot \mathrm{mol}^{-1}$,
- exact: $\mathcal{N}_A J = 2 \times 0.2746 \times R T_m = 1414\ \mathrm{J} \cdot \mathrm{mol}^{-1} = 338\ \mathrm{cal} \cdot \mathrm{mol}^{-1}$.

The mean-field approximation underestimates the magnitude of the coupling constant that is needed to correlate the spins to a given degree.

We can compare now the values used in this study to those of Jerala et al. [179]. In Jerela et al., the gel-fluid mismatch penalty is noted $\omega = J$. The proposed value for fitting the DSC curve of DPPC systems is $\omega = 282\ \mathrm{cal}$, when internal degrees of freedom are associated to whole lipids. This corresponds to a ratio $J/J_c = 282/338 = 0.8343$.

Transposed to the mean-field critical value $205\ \mathrm{cal} \cdot \mathrm{mol}^{-1}$, this would corresponds to a $J \simeq \omega \simeq 0.8343 \times 205 = 171\ \mathrm{cal} \cdot \mathrm{mol}^{-1}$ (715 J $\cdot$mol^{-1}). By comparison, we use in the above approach $J = 199\ \mathrm{cal} \cdot \mathrm{mol}^{-1}$ (830 J$\cdot$mol^{-1}) and $J' = J'' = 100\ \mathrm{cal} \cdot \mathrm{mol}^{-1}$ (415 J$\cdot$mol^{-1}). We therefore globally operate closer to the critical point.

Bibliography

[1] R. W. Gross, *Biochimica et Biophysica Acta (BBA) - Molecular and Cell Biology of Lipids* **2017**, *1862*, 731 –739.

[2] R. W. Gross, X. Han, *Chemistry and biology* **2011**, *18*, 284—291.

[3] D. Lingwood, K. Simons, *Science* **2010**, *327*, 46–50.

[4] D. M. Owen, A. Magenau, D. Williamson, K. Gaus, *BioEssays* **2012**, *34*, 739–747.

[5] Y.-H. Chan, S. Boxer, *Current opinion in chemical biology* **2008**, *11*, 581–7.

[6] J. D. Nickels et al., *Plos Biol* **2017**, *15*, e2002214.

[7] J. N. Israelachvili, D. Mitchell, B. W. Ninham, *Biochimica et Biophysica Acta (BBA) - Biomembranes* **1977**, *470*, 185 –201.

[8] D. E. Vance, J. E. Vance, *Biochemistry of Lipids, Lipoproteins and Membranes (Fifth Edition)*, Elsevier, **2008**.

[9] K. Simons, E. Ikonen, *Nature* **1997**, *387*, 569–572.

[10] A. Bangham, M. Standish, J. Watkins, *J Mol Biol* **1965**, *13*, 238–IN27.

[11] R. N. Lewis, Y.-P. Zhang, R. N. McElhaney, *Biochimica et Biophysica Acta (BBA) - Biomembranes* **2005**, *1668*, 203 –214.

[12] T. Parasassi, M. Di Stefano, M. Loiero, G. Ravagnan, E. Gratton, *Biophysical Journal* **1994**, *66*, 763—768.

[13] G. M'Baye, Y. Mély, G. Duportail, A. S. Klymchenko, *Biophysical journal* **2008**, *95 3*, 1217–25.

[14] M. I. Angelova, D. S. Dimitrov, *Faraday Discuss. Chem. Soc.* **1986**, *81*, 303–311.

[15] N. F. Morales-Penningston et al., *Biochimica et biophysica acta* **2010**, *1798 7*, 1324–32.

[16] N. Kahya, D. Scherfeld, K. Bacia, P. Schwille, *Journal of Structural Biology* **2004**, *147*, 77 –89.

[17] K. Olbrich, W. Rawicz, D. Needham, E. Evans, *Biophysical Journal* **2000**, *79*, 321 –327.

[18] W. Rawicz, K. Olbrich, T. McIntosh, D. Needham, E. Evans, *Biophysical Journal* **2000**, *79*, 328 –339.

[19] A. Lee, *Biochimica et Biophysica Acta (BBA) - Reviews on Biomembranes* **1977**, *472*, 237 –281.

[20] D. Marsh, *Handbook of lipid bilayers, second edition*, CRC Press, **2013**.

[21] N. Kučerka, S. Tristram-Nagle, J. F. Nagle, *The Journal of Membrane Biology* **2006**, *208*, 193–202.

[22] D. Marsh, *Biochemistry* **1980**, *19*, 1632–1637.

[23] S. Tristram-Nagle, R. Zhang, R. Suter, C. Worthington, W. Sun, J. Nagle, *Biophysical Journal* **1993**, *64*, 1097 –1109.

[24] N. Kučerka, M.-P. Nieh, J. Katsaras, *Biochimica et Biophysica Acta (BBA) - Biomembranes* **2011**, *1808*, 2761 –2771.

[25] P. F. F. Almeida, W. L. C. Vaz, T. E. Thompson, *Biochemistry* **1992**, *31*, 6739–6747.

[26] W. L. C. Vaz, R. M. Clegg, D. Hallmann, *Biochemistry* **1985**, *24*, 781–786.

[27] K. Tu, D. Tobias, M. Klein, *Biophysical Journal* **1995**, *69*, 2558 –2562.

[28] S. Leekumjorn, A. K. Sum, *Biochimica et Biophysica Acta (BBA) - Biomembranes* **2007**, *1768*, 354 –365.

[29] S. J. Marrink, J. Risselada, A. E. Mark, *Chemistry and Physics of Lipids* **2005**, *135*, 223 –244.

[30] O. Mouritsen, *Chemistry and Physics of Lipids* **1991**, *57*, 179 –194.

[31] J. F. Nagle, *Annual Review of Physical Chemistry* **1980**, *31*, 157–196.

[32] D. Uhríková, N. Kučerka, J. Teixeira, V. Gordeliy, P. Balgavý, *Chemistry and Physics of Lipids* **2008**, *155*, 80–89.

[33] K. Jacobson, D. Papahadjopoulos, *Biochemistry* **1975**, *14*, 152–161.

[34] A. Ulrich, M Sami, A Watts, *Biochimica et Biophysica Acta* **1994**, *1191*, 225–30.

[35] N. Markova, E. Sparr, L. Wadsö, H. Wennerström, *J. Phys. Chem. B* **2000**, *104*, 8053–8060.

[36] T. Heimburg, *Membrane Structure, in Thermal Biophysics of Membranes*, Wiley-VCH Verlag GmbH & Co. KGaA, **2007**.

[37] R. Koynova, M. Caffrey, *Chemistry and Physics of Lipids* **2002**, *115*, 107 –219.

[38] S. Mabrey, J. M. Sturtevant, *Proceedings of the National Academy of Sciences* **1976**, *73*, 3862–3866.

[39] H. Himeno, N. Shimokawa, S. Komura, D. Andelman, T. Hamada, M. Takagi, *Soft Matter* **2014**, *10*, 7959–7967.

[40] D. Haverstick, M Glaser, *Proceedings of the National Academy of Sciences of the United States of America* **1987**, *84*, 4475—4479.

[41] A. G. Lee, *Biochimica et Biophysica Acta (BBA) - Biomembranes* **2004**, *1666*, 62 –87.

[42] O. Mouritsen in *In Search of a New Biomembrane Model*, Biol. Skr. Dan. Vid. Selsk., **1998**.

[43] A. P. Demchenko, Y. Mély, G. Duportail, A. S. Klymchenko, *Biophysical Journal* **2009**, *96*, 3461 –3470.

[44] J. Korlach, P. Schwille, W. W. Webb, G. W. Feigenson, *Proceedings of the National Academy of Sciences* **1999**, *96*, 8461–8466.

[45] L. A. Bagatolli, E. Gratton, *Biophysical Journal* **2000**, *79*, 434 –447.

[46] O. G. Mouritsen, M. J. Zuckermann, *Lipids* **2004**, *39*, 1101–13.

[47] M. Hao, S. Mukherjee, F. R. Maxfield, *Proceedings of the National Academy of Sciences* **2001**, *98*, 13072–13077.

[48] M. R. Vist, J. H. Davis, *Biochemistry* **1990**, *29*, 451–464.

[49] S. Veatch, I. Polozov, K Gawrisch, S. Keller, *Biophysical Journal* **2004**, *86*, 2910—2922.

[50] J. Juhasz, F. J. Sharom, J. H. Davis, *Biochimica et Biophysica Acta (BBA) - Biomembranes* **2009**, *1788*, 2541 –2552.

[51] S. Bhattacharya, S. Haldar, *Biochimica et Biophysica Acta (BBA) - Biomembranes* **2000**, *1467*, 39 –53.

[52] R. F. de Almeida, A. Fedorov, M. Prieto, *Biophysical Journal* **2003**, *85*, 2406 – 2416.

[53] G. W. Stockton, C. F. Polnaszek, A. P. Tulloch, F. Hasan, I. C. P. Smith, *Biochemistry* **1976**, *15*, 954–966.

[54] S. Clejan, R. Bittman, P. W. Deroo, Y. A. Isaacson, A. F. Rosenthal, *Biochemistry* **1979**, *18*, 2118–2125.

[55] R. Demel, B. D. Kruyff, *Biochimica et Biophysica Acta (BBA) - Reviews on Biomembranes* **1976**, *457*, 109 –132.

[56] J. L. Rubenstein, B. A. Smith, H. M. McConnell, *Proceedings of the National Academy of Sciences* **1979**, *76*, 15–18.

[57] R. Demel, L. V. Deenen, B. Pethica, *Biochimica et Biophysica Acta (BBA) - Biomembranes* **1967**, *135*, 11 –19.

[58] R. Demel, P. Joos, *Chemistry and Physics of Lipids* **1968**, *2*, 35 –46.

[59] J. H. Ipsen, G. Karlström, O. Mouritsen, H. Wennerström, M. Zuckermann, *Biochimica et Biophysica Acta (BBA) - Biomembranes* **1987**, *905*, 162 –172.

[60] M. Nielsen, L. Miao, J. H. Ipsen, M. J. Zuckermann, *Physical Review E* **1999**.

[61] D. Marsh, *Biochimica et Biophysica Acta (BBA) - Biomembranes* **2010**, *1798*, 688 –699.

[62] Y. Wang, P. Gkeka, J. E. Fuchs, K. R. Liedl, Z. Cournia, *Biochimica et Biophysica Acta (BBA) - Biomembranes* **2016**, *1858*, 2846 –2857.

[63] Y.-W. Chiang, A. J. Costa-Filho, J. H. Freed, *The Journal of Physical Chemistry B* **2007**, *111*, 11260–11270.

[64] G. W. Feigenson, *Biochimica et Biophysica Acta (BBA) - Biomembranes* **2009**, *1788*, 47 –52.

[65] T. Baumgart, G. Hunt, E. R. Farkas, W. W. Webb, G. W. Feigenson, *Biochimica et Biophysica Acta (BBA) - Biomembranes* **2007**, *1768*, 2182 –2194.

[66] S. L. Veatch, S. L. Keller, *Biochimica et Biophysica Acta (BBA) - Molecular Cell Research* **2005**, *1746*, 172 –185.

[67] C. Dietrich et al., *Biophysical Journal* **2001**, *80*, 1417 –1428.

[68] S. L. Veatch, S. L. Keller, *Biophysical Journal* **2003**, *85*, 3074 –3083.

[69] C. Yuan, J. Furlong, P. Burgos, L. J. Johnston, *Biophysical Journal* **2002**, *82*, 2526 –2535.

[70] G. W. Feigenson, J. T. Buboltz, *Biophysical Journal* **2001**, *80*, 2775 –2788.

[71] J. R. Silvius, *Biophysical Journal* **2003**, *85*.

[72] T. M. Konyakhina, J. Wu, J. D. Mastroianni, F. A. Heberle, G. W. Feigenson, *Biochimica et Biophysica Acta (BBA) - Biomembranes* **2013**, *1828*, 2204 –2214.

[73] R. N.A. H. Lewis, D. A. Mannock, R. N. McElhaney in *Methods in Membrane Lipids*, (Ed.: A. M. Dopico), Humana Press, Totowa, NJ, **2007**, pp. 171–195.

[74] E. J. Prenner, R. N. Lewis, R. N. McElhaney, *Biochimica et Biophysica Acta (BBA) - Biomembranes* **1999**, *1462*, 201 –221.

[75] E. J. Prenner, R. N. Lewis, L. H. Kondejewski, R. S. Hodges, R. N. McElhaney, *Biochimica et Biophysica Acta (BBA) - Biomembranes* **1999**, *1417*, 211 –223.

[76] M. K. Jain, N. M. Wu, *The Journal of Membrane Biology* **1977**, *34*, 157–201.

[77] M. Fidorra, T. Heimburg, H. Seeger, *Biochimica et Biophysica Acta (BBA) - Biomembranes* **2009**, *1788*, 600 –607.

[78] B. Ladbrooke, R. Williams, D. Chapman, *Biochimica et Biophysica Acta (BBA) - Biomembranes* **1968**, *150*, 333 –340.

[79] H. Reinl, T. Brumm, T. M. Bayerl, *Biophysical Journal* **1992**, *61*, 1025 –1035.

[80] T. P. W. McMullen, R. N.A. H. Lewis, R. N. McElhaney, *Biochemistry* **1993**, *32*, 516–522.

[81] R. L. Biltonen, D. Lichtenberg, *Chemistry and Physics of Lipids* **1993**, *64*, 129 – 142.

[82] J. M. Sturtevant, *Annual Review of Physical Chemistry* **1987**, *38*, 463–488.

[83] *Neutron Scattering - Applications in Biology, Chemistry, and Materials Science*, (Eds.: F. Fernandez-Alonso, D. L. Price), Academic Press, **2013**.

[84] G. Weber, F. J. Farris, *Biochemistry* **1979**, *18*, 3075–3078.

[85] F. M. Harris, K. B. Best, J. D. Bell, *Biochimica et Biophysica Acta (BBA) - Biomembranes* **2002**, *1565*, 123 –128.

[86] S. Antollini, M. Soto, I. Boninideromanelli, C. Gutierrezmerino, P. Sotomayor, F. Barrantes, *Biophysical Journal* **1996**, *70*, 1275–1284.

[87] S. S. Antollini, F. J. Barrantes in *Methods in Membrane Lipids*, (Ed.: A. M. Dopico), Humana Press, Totowa, NJ, **2007**, pp. 531–542.

[88] A. D. Lúcio, C. C. Vequi-Suplicy, R. M. Fernandez, M. T. Lamy, *Journal of Fluorescence* **2010**, *20*, 473–482.

[89] K. Vijayan, D. E. Discher, J. Lal, P. Janmey, M. Goulian, *The Journal of Physical Chemistry B* **2005**, *109*, 14356–14364.

[90] C. Sanson, J.-F Le Meins, C. Schatz, A. A Soum, S. Lecommandoux, **2010**, *6*.

[91] S. A Sanchez, A. Tricerri, E. Gratton, **2012**, *109*, 7314–9.

[92] B. Valeur, M. N. Berberan-Santos in *Molecular Fluorescence*, Wiley-VCH Verlag GmbH & Co. KGaA, **2012**, pp. 181–212.

[93] T. Parasassi, G. D. Stasio, G. Ravagnan, R. Rusch, E. Gratton, *Biophysical Journal* **1991**, *60*, 179 –189.

[94] T. Parasassi, G. Ravagnan, R. M. Rusch, E. Gratton, *Photochemistry and Photobiology* **1993**, *57*, 403–410.

[95] L. Bagatolli, E. Gratton, G. Fidelio, *Biophysical Journal* **1998**, *75*, 331 –341.

[96] L. A. Bagatolli, B. Maggio, F. Aguilar, C. P. Sotomayor, G. D. Fidelio, *Biochimica et Biophysica Acta (BBA) - Biomembranes* **1997**, *1325*, 80 –90.

[97] T. Parasassi, M. D. Stefano, M. Loiero, G. Ravagnan, E. Gratton, *Biophysical Journal* **1994**, *66*, 120 –132.

[98] T. Parasassi, G. Ravagnan, R. M. Rusch, E. Gratton, *Photochemistry and Photobiology* **1993**, *57*, 403–410.

[99] M. Bacalum, B. Zorilă, M. Radu, *Analytical Biochemistry* **2013**, *440*, 123 –129.

[100] X. Zhao, R. Li, C. Lu, F. Baluška, Y. Wan, *Plant Physiology and Biochemistry* **2015**, *87*, 53 –60.

[101] D. Owen, C. Rentero, A. Magenau, A. Abu-Siniyeh, K. Gaus, *Nature protocols* **2011**, *7*, 24–35.

[102] E. Sezgin, T. Sadowski, K. Simons, *Langmuir* **2014**, *30*, PMID: 24905799, 8160–8166.

[103] J. Dinic, H. Biverståhl, L. Mäler, I. Parmryd, *Biochimica et Biophysica Acta (BBA) - Biomembranes* **2011**, *1808*, 298 –306.

[104] L. Jin et al., *Biophysical Journal* **2006**, *90*, 2563 –2575.

[105] M. Amaro, F. Reina, M. Hof, C. Eggeling, E. Sezgin, *Journal of Physics D: Applied Physics* **2017**, *50*, 134004.

[106] J. R. Jambeck et al., *Science* **2015**, *347*, 768–771.

[107] B. Gewert, M. M. Plassmann, M. MacLeod, *Environ. Sci.: Processes Impacts* **2015**, *17*, 1513–1521.

[108] M. Cole, P. Lindeque, C. Halsband, T. S. Galloway, *Marine Pollution Bulletin* **2011**, *62*, 2588 –2597.

[109] M. C. Fossi et al., *Marine Pollution Bulletin* **2012**, *64*, 2374 –2379.

[110] A. Collignon, J.-H. Hecq, F. Glagani, P. Voisin, F. Collard, A. Goffart, *Marine Pollution Bulletin* **2012**, *64*, 861 –864.

[111] Y. Lu, Y. Mei, R. Walker, M. Ballauff, M. Drechsler, *Polymer* **2006**, *47*, 4985 –4995.

[112] E. Bergami et al., *Ecotoxicology and Environmental Safety* **2016**, *123*, 6th Biannual ECOtoxicology MEeting (BECOME 2014) - Environmental emergencies: ecotoxicology as a management tool, 18 –25.

[113] M. A. Browne, A. Dissanayake, T. S. Galloway, D. M. Lowe, R. C. Thompson, *Environmental Science & Technology* **2008**, *42*, 5026–5031.

[114] G. Rossi, J. Barnoud, L. Monticelli, *The Journal of Physical Chemistry Letters* **2014**, *5*, PMID: 26276207, 241–246.

[115] D. Bochicchio, E. Panizon, L. Monticelli, G. Rossi, *Scientific Reports* **2017**, *7*, 6357.

[116] M. Jung et al., *Langmuir* **2000**, *16*, 968–979.

[117] E. Z. Radlinska et al., *Phys. Rev. Lett.* **1995**, *74*, 4237–4240.

[118] P. J. Flory, *Principles of Polymer Chemistry*, Cornell University Press, **1953**.

[119] I. Teraoka, *Polymer solutions: An introduction to physical properties*, John Wiley, **2002**.

[120] M. Kiselev, E. Zemlyanaya, V. Aswal, R. Neubert, *European biophysics journal : EBJ* **2006**, *35*, 477–93.

[121] J. F. Nagle, S. Tristram-Nagle, *Biochimica et Biophysica Acta (BBA) - Reviews on Biomembranes* **2000**, *1469*, 159 –195.

[122] T. P. T. Dao et al., *ACS Macro Letters* **2015**, *4*, 182–186.

[123] M. Jung, B. H. Robinson, D. C. Steytler, A. L. German, R. K. Heenan, *Langmuir* **2002**, 2873–2879.

[124] Q. D. Pham, D. Topgaard, E. Sparr, *Langmuir* **2015**, *31*, 11067–11077.

[125] A. G. Richter et al., *Langmuir* **2011**, *27*, 3792–3797.

[126] A. Rolland, A. Brzokewicz, B. Shroot, J. C. Jamoulle, *International Journal of Pharmaceutics* **1991**, *76*, 217–224.

[127] G. Albertini, C. Donati, R. Phadke, M. Ponzi Bossi, F. Rustichelli, *Chemistry and Physics of Lipids* **1990**, *55*, 331–337.

[128] H. Matsuki, E. Miyazaki, F. Sakano, N. Tamai, S. Kaneshina, *Biochimica et Biophysica Acta (BBA) - Biomembranes* **2007**, *1768*, 479 –489.

[129] A. M. Wolka, J. H. Rytting, B. L. Reed, B. C. Finnin, *International Journal of Pharmaceutics* **2004**, *271*, 5–10.

[130] F. Ollila, K. Halling, P. Vuorela, H. Vuorela, J. Slotte, *Archives of Biochemistry and Biophysics* **2002**, *399*, 103–108.

[131] C. Valenta, A. Steininger, B. G. Auner, *European Journal of Pharmaceutics and Biopharmaceutics* **2004**, *57*, 329–336.

[132] S. Borsacchi et al., *Phys. Chem. Chem. Phys.* **2016**, *18*, 15375–15383.

[133] R. Abboud, C. Charcosset, H. Greige-Gerges, *Journal of Membrane Biology* **2016**, *249*, 327–338.

[134] M. R. Preiss, A. Hart, C. Kitchens, G. D. Bothun, *Journal of Physical Chemistry B* **2017**, *121*, 5040–5047.

[135] G. D. Bothun, *Journal of Nanobiotechnology* **2008**, *6*, 13.

[136] L. Bagatolli, E Gratton, **1999**, *77*, 2090–101.

[137] L. S. Hirst, A. Ossowski, M. Fraser, J. Geng, J. V. Selinger, R. L. B. Selinger, *Proceedings of the National Academy of Sciences* **2013**, *110*, 3242–3247.

[138] A. S. Klymchenko, R. Kreder, *Chemistry & Biology* **2014**, *21*, 97 –113.

[139] A. J. Metso, H. Zhao, I. Tuunainen, P. K. Kinnunen, *Biochimica et Biophysica Acta (BBA) - Biomembranes* **2005**, *1713*, 83 –91.

[140] T. Parasassi, E. K. Krasnowska, L. Bagatolli, E. Gratton, *Journal of fluorescence* **1998**, *8*, 365–373.

[141] D. Brown, E. London, *The Journal of Membrane Biology* **1998**, *164*, 103–114.

[142] R. Phillips, T. Ursell, P. Wiggins, P. Sens, *Nature* **2009**, *459*, 379–385.

[143] D. Chen, M. M. Santore, *Proceedings of the National Academy of Sciences* **2014**, *111*, 179–184.

[144] J. Wolff, C. M. Marques, F. Thalmann, *Phys. Rev. Lett.* **2011**, *106*, 128104.

[145] O. S. Ostroumova, E. G. Chulkov, O. V. Stepanenko, L. V. Schagina, *Chemistry and Physics of Lipids* **2014**, *178*, 77 –83.

[146] M. Weinrich, H. Nanda, D. L. Worcester, C. F. Majkrzak, B. B. Maranville, S. M. Bezrukov, *Langmuir* **2012**, *28*, 4723–4728.

[147] E. Sezgin, T. Sadowski, K. Simons, *Langmuir* **2014**, *30*, 8160–8166.

[148] P. Yancey, M. Clark, S. Hand, R. Bowlus, G. Somero, *Science* **1982**, *217*, 1214–1222.

[149] L. M. Crowe, D. Reid, J. Crowe, **1996**, *71*, 2087–93.

[150] J. H. Crowe, L. M. Crowe, A. E. Oliver, N. Tsvetkova, W. Wolkers, F. Tablin, *Cryobiology* **2001**, *43*, 89–105.

[151] J. H. Crowe, L. M. Crowe, J. F. Carpenter, C Aurell Wistrom, *The Biochemical journal* **1987**, *242*, 1–10.

[152] M. d. C. Luzardo, F. Amalfa, A. Nuñez, S. Díaz, A. Biondi de Lopez, E. Disalvo, *Biophysical Journal* **2000**, *78*, 2452–2458.

[153] T. Lenné, C. J. Garvey, K. L. Koster, G. Bryant, *The journal of physical chemistry. B* **2009**, *113*, 2486–2491.

[154] H. G. Döbereiner, O. Selchow, R. Lipowsky, *European Biophysics Journal* **1999**, *28*, 174–178.

[155] J. Genova, A. Zheliaskova, M. D. Mitov, *Colloids and Surfaces A: Physicochemical and Engineering Aspects* **2006**, *282-283*, 420–422.

[156] V. Vitkova, J. Genova, M. D. Mitov, I. Bivas, *Molecular Crystals and Liquid Crystals* **2006**, *449*, 95–106.

[157] J. F. Nagle, M. S. Jablin, S. Tristram-Nagle, K. Akabori, *Chemistry and Physics of Lipids* **2015**, *185*, 3–10.

[158] J. F. Nagle, M. S. Jablin, S. Tristram-Nagle, *Chemistry and Physics of Lipids* **2016**, *196*, 76–80.

[159] D. Chapman, R. Williams, B. Ladbrooke, *Chemistry and Physics of Lipids* **1967**, *1*, 445–475.

[160] G. Strauss, P. Schurtenberger, H. Hauser, *BBA - Biomembranes* **1986**, *858*, 169–180.

[161] L. M. Crowe, J. H. Crowe, *BBA - Biomembranes* **1991**, *1064*, 267–274.

[162] C. C. De Vequi-Suplicy, C. R. Benatti, M. T. Lamy, *Journal of Fluorescence* **2006**, *16*, 431–439.

[163] K. A. Riske, R. P. Barroso, C. C. Vequi-Suplicy, R. Germano, V. B. Henriques, M. T. Lamy, *Biochimica et Biophysica Acta (BBA) - Biomembranes* **2009**, *1788*, 954 –963.

[164] C. Demetzos, *Journal of Liposome Research* **2008**, *18*, 159–173.

[165] D. Marsh, A. Watts, P. Knowles, *Biochimica et Biophysica Acta (BBA) - Biomembranes* **1977**, *465*, 500 –514.

[166] D. A. Mannock, R. N. Lewis, R. N. McElhaney, *Biophysical Journal* **2006**, *91*, 3327 –3340.

[167] B. Z. Chowdhry, G Lipka, J. M. Sturtevant, *Biophysical journal* **1984**, *46*, 419–22.

[168] C. Chen, D. Berns, *Biophysical Journal* **1981**, *36*, 359–367.

[169] K. B. Konov, D. V. Leonov, N. P. Isaev, K. Y. Fedotov, V. K. Voronkova, S. A. Dzuba, *Journal of Physical Chemistry B* **2015**, *119*, 10261–10266.

[170] J. Stunmpel, W. L. Vaz, D. Hallmann, *Biochim Biophys Acta* **1985**, *821*, 165–168.

[171] C. H.J. P. Fabrie, B. de Kruijff, J. de Gier, *BBA - Biomembranes* **1990**, *1024*, 380–384.

[172] C Grabielle-Madelmont, R Perron, *Journal of Colloid and Interface Science* **1983**, *95*, 471 –482.

[173] K. Jørgensen, O. Mouritsen, *Biophysical Journal* **1995**, *69*, 942 –954.

[174] J. H. Crowe, L. M. Crowe, D. Chapman, *Science* **1984**, *223*, 701–703.

[175] K. L. Koster, Y. P. Lei, M. Anderson, S. Martin, G. Bryant, *Biophysical Journal* **2000**, *78*, 1932 –1946.

[176] J. Wolfe, G. Bryant, *Cryobiology* **1999**, *39*, 103 –129.

[177] T. Lenné, C. Garvey, K. Koster, G. Bryant, *Chemistry and physics of lipids* **2009**, *163*, 236–42.

[178] T. Heimburg, R. Biltonen, *Biophysical Journal* **1996**, *70*, 84 –96.

[179] R. Jerala, P. Almeida, R. Biltonen, *Biophysical journal* **1996**, *71*, 609–15.

[180] R. E. Goldstein, S. Leibler, *Physical review. A* **1989**, *40*, 1025–1035.

[181] S. Zalba, T. L. ten Hagen, *Cancer Treatment Reviews* **2017**, *52*, 48 –57.

[182] P. V. Escribá, *Trends in Molecular Medicine* **2006**, *12*, 34 –43.

[183] B. P. Head, H. H. Patel, P. A. Insel, *Biochimica et Biophysica Acta (BBA) - Biomembranes* **2014**, *1838*, 532 –545.

[184] A. Hryniewicz-Jankowska, K. Augoff, A. Biernatowska, J. Podkalicka, A. F. Sikorski, *Biochimica et Biophysica Acta (BBA) - Reviews on Cancer* **2014**, *1845*, 155 –165.

[185] E. L. Niero et al., *Journal of Experimental & Clinical Cancer Research* **2014**, *33*, 37.

[186] K. Charalambous et al., *Journal of the American Chemical Society* **2012**, *134*, 5746–5749.

[187] H. Khandelia, J. H. Ipsen, O. G. Mouritsen, *Biochimica et Biophysica Acta (BBA) - Biomembranes* **2008**, *1778*, 1528 –1536.

[188] J. A. Lundbaek, P. Birn, J. Girshman, A. J. Hansen, O. S. Andersen, *Biochemistry* **1996**, *35*, 3825–3830.

[189] D. Marsh, *Biochimica et Biophysica Acta (BBA) - Biomembranes* **2008**, *1778*, 1545 –1575.

[190] E. Bastiaanse, K. M Hold, A. van der Laarse, *Cardiovascular Research* **1997**, *33*.

[191] R. Chen, M. E. Eccleston, Z. Yue, N. K. H. Slater, *J. Mater. Chem.* **2009**, *19*, 4217–4224.

[192] V. H. Ho, N. K. Slater, R. Chen, *Biomaterials* **2011**, *32*, 2953 –2958.

[193] S. Khormaee et al., *Advanced Functional Materials* **2013**, *23*, 565–574.

[194] A. Weinberger et al., *Biophysical journal* **2013**, *105*, 154–64.

[195] S. Doniach, *The Journal of Chemical Physics* **1978**, *68*, 4912–4916.

[196] R. E. Goldstein, S. Leibler, *Phys. Rev. Lett.* **1988**, *61*, 2213–2216.

[197] V. P. Ivanova, T. Heimburg, *Physical review. E Statistical nonlinear and soft matter physics* **2001**, *63*, 041914.

[198] M. E. Fisher, *Reports on Progress in Physics* **1967**, *30*, 615.

Mattia MORANDI

Disruption of model membranes' phase behavior upon interaction with hydrophilic/hydrophobic molecules

Résumé

Ce travail concerne l'altération du comportement de phase de membranes lipidiques lors de leur interaction avec des molécules hydrophiles ou hydrophobes. L'utilisation de sondes moléculaires de fluorescence sensibles à leur micro-environnement constitue un aspect majeur de ce travail. Les techniques de spectroscopie de fluorescence et de microscopie confocale ont été mises à profit pour l'étude du comportement de ces sondes, donnant accès au degré de compacité et d'ordre dans les membranes.

Nos résultats montrent que le polystyrène, un plastique rencontré de façon commune dans les régions polluées des océans, présente la capacité de modifier le comportement de phase des membranes lipidiques, entrant notamment en compétition avec le cholestérol.

Nous avons montré que la présence élevée de sucres, tel que l'on peut le rencontrer dans certaines situations relevant de la bio-préservation, a pour effet de rompre la qualité de compaction des lipides, et nous avons proposé un nouveau modèle thermodynamique pour interpréter nos résultats.

Enfin, les effets sur la membrane de l'incorporation d'un polymère amphiphile comportant un cholestérol greffé ont été étudiés, dans le cadre de l'élaboration de nouvelles stratégies thérapeutiques à base de lipides.

Membranes modèles de lipides ; Transition de phase ; Coexistence de phase ; Polystyrène ; Cholesterol ; Saccharose ; Microscopie confocal ; Laurdan

Résumé en anglais

This work focuses on the alterations of lipid membrane phase behavior upon interaction with hydrophobic and hydophilic molecules. One major aspect of this thesis is the employement of environment sensitive probes to obtain information on the lipid bilayer packing by means of confocal spectral imaging and fluorescence spectroscopy.

Our results show that polystyrene, a commonly found plastic in ocean wastes, has the ability to disrupt the lipid bilayer phase behavior and has a competitive interaction with cholesterol.

The presence of high concentration of sugars, relevant in the field of biopreservation, has been found to alter the lipid bilayer packing and a new thermodynamics model has been proposed to complement the experimental results.

Finally, the effects of an amphiphilic cholesterol-grafted polymer on model membrane was investigated, providing insight into potential new lipid therapeutic strategies.

Lipid model membrane ; Phase transition ; Phase coexistence ; Polystyrene ; Cholesterol ; Sucrose ; Confocal microscopy ; Laurdan